

IN-18  
153705  
P.128

NASA Technical Memorandum 104764

# Impact Experiments into Multiple-Mesh Targets: Concept Development of a Lightweight Collisional Bumper

Friedrich Hörz, Mark J. Cintala

Ronald P. Bernhard, Frank Cardenas, William Davidson, Gerald Haynes,  
Thomas H. See, Jerry Winkler

Barry Gray

(NASA-TM-104764) IMPACT EXPERIMENTS INTO MULTIPLE-MESH TARGETS: CONCEPT DEVELOPMENT OF A LIGHTWEIGHT COLLISIONAL BUMPER  
 (NASA) ~~128 P~~ N93-23247  
 Unclas  
 495135 234p G3/18 0153705

March 1993



ORIGINAL CONTAINS  
COLOR ILLUSTRATIONS

NASA Technical Memorandum 104764

## Impact Experiments into Multiple-Mesh Targets: Concept Development of a Lightweight Collisional Bumper

Friedrich Hörz, Mark J. Cintala  
*Solar System Exploration Division  
Lyndon B. Johnson Space Center  
Houston, Texas*

Ronald P. Bernhard, Frank Cardenas, William Davidson, Gerald Haynes,  
Thomas H. See, Jerry Winkler  
*Solar System Exploration Department  
Lockheed Engineering and Sciences Company  
Houston, Texas*

Barry Gray  
*Physics Department  
Clear Lake High School  
Houston, Texas*

National Aeronautics and Space Administration  
Lyndon B. Johnson Space Center  
Houston, Texas  
March 1993

# Table of Contents

List of Figures and Tables	v
Abstract	vii
Introduction	1
Experiment Description	3
Objectives	3
Physical Set Up and Procedures	4
Experimental Variables and Their Significance	7
Results	12
Photo-Documentation	12
Penetration-Hole Diameters	13
Effects of Impact Velocity	19
Effects of Separation Distance	20
Effects of Specific Bumper Mass	20
Effects of Mesh Opening	21
Effects of Mixed Meshes	21
Effects of Projectile Species	22
Comparison with Multiple-Stacked Foils	22
Total Bumper Damage	23
Witness-Plate Observations	27
Mass Considerations	53
Specific Areal Bumper Mass (SM)	53
Total Bumper Mass Lost ( $M_t$ )	53
Mass of Recovered Particulates	57
Discussion	63
Summary and Recommendations	64
References	71
Appendix	73


Preceding Page Blank

## List of Figures and Tables

Figure 1	1
Figure 2	5
Figure 3	9
Figure 4	16-17
Figure 5	25
Figure 6	30
Figure 7	31
Figure 8	33
Figure 9	38
Figure 10	39
Figure 11	44
Figure 12	45
Figure 13	50
Figure 14	51
Figure 15	55
Figure 16	59
Figure 17	61
Table 1a	66-67
Table 1b	68-69

Preceding Page Blank

v

 INTENTIONALLY BLANK

PRECEDING PAGE BLANK NOT FILMED

## ABSTRACT

This study explores the utility of multiple-mesh targets as potential lightweight shields to protect spacecraft in low-Earth orbit against collisional damage. Earlier studies revealed that single meshes comminute hypervelocity impactors with efficiencies comparable to contiguous targets. Multiple interaction of projectile fragments with any number of meshes should lead to increased comminution, deceleration and dispersion of the projectile, such that all debris exiting the mesh stack possesses low specific energies (ergs/cm<sup>2</sup>) that would readily be tolerated by many flight systems.

The study is conceptual exploring the sensitivity of major variables such as impact velocity, the specific areal mass (g/cm<sup>2</sup>) of the total mesh stack (SM), and the separation distance (S) between individual meshes. Most experiments employed five or ten meshes with total SM typically <0.5 the specific mass of the impactor, and silicate glass impactors rather than metal projectiles.

While projectile comminution increases with increasing impact velocity due to progressively higher shock stresses, encounters with multiple-meshes at low velocity (1-2 km/s) already lead to significant disruption of the glass impactors, with the resulting fragments being additionally decelerated and dispersed by subsequent meshes, and, unlike most contiguous single-plate bumpers, leading to respectable performance at low velocity. Total specific bumper mass must be the subject of careful trade-off studies; relatively massive bumpers will generate too much debris being dislodged from the bumper itself, while exceptionally lightweight designs will not cause sufficient comminution, deceleration or dispersion of the impactor. Separation distance was found to be a crucial design parameter, as it controls the dispersion of the fragment cloud. Substantial mass savings could result if maximum separation distances were employed. The total mass of debris dislodged by multiple-mesh stacks is modestly smaller than that of single, contiguous-membrane shields. The cumulative surface area of all penetration holes in multiple-mesh stacks is an order of magnitude smaller than that in analog multiple-foil shields, suggesting good long-term performance of the mesh designs. Due to different experimental conditions, direct and quantitative comparison with other lightweight shields is not possible at present.

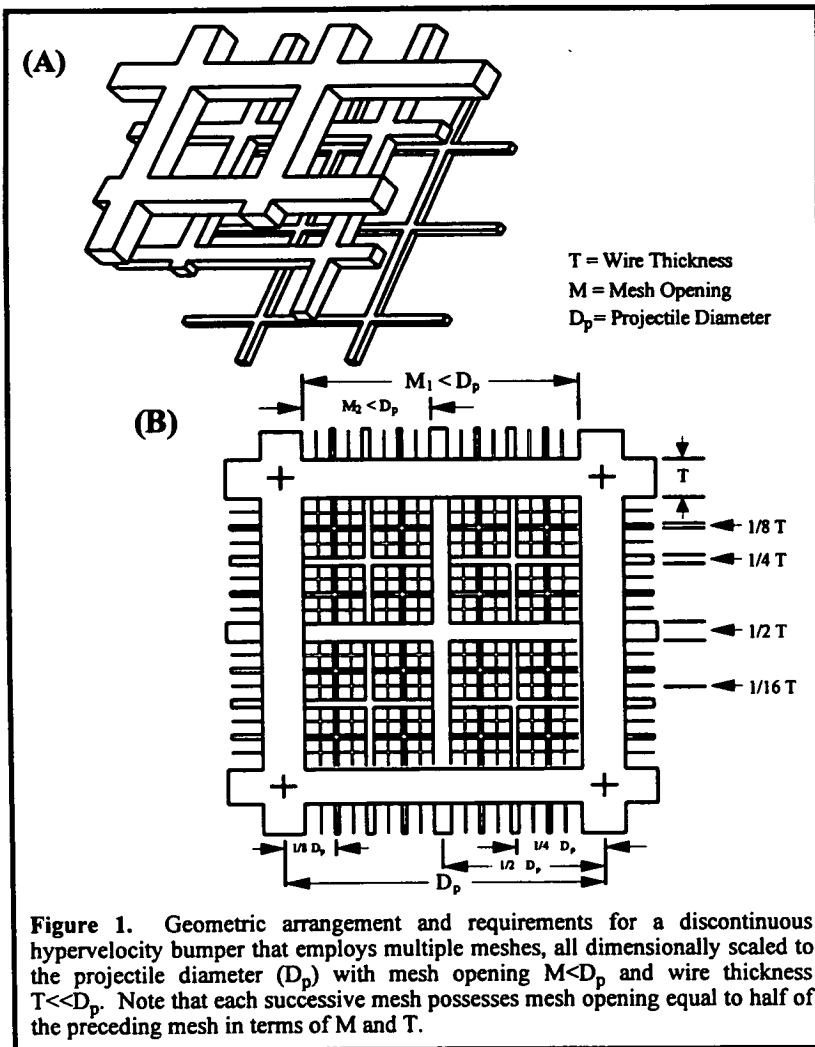
Preceding Page Blank

PRECEDING PAGE BLANK NOT FILMED

## INTRODUCTION

The growing population of man-made orbital debris, in combination with natural micrometeoroids, is a major collisional hazard to flight systems in low-Earth orbit (LEO). As a consequence, substantial technology development was initiated to effectively protect such systems with hypervelocity "bumpers" that were first conceptualized by Whipple (1958). Such bumpers are passive shields, typically membranes or sheet-like structures, mounted at some standoff distance from the flight system. Very thick bumpers will terminate the threat from hypervelocity projectiles in cratering events, while relatively thin shields will be penetrated, causing various degrees of projectile vaporization, melting and collisional fragmentation, the degree and extent of which is highly dependent on the specific areal bumper mass (SM;  $g/cm^2$ ). This specific mass not only controls collisional outcomes, but it also drives the total launch mass of any practical shield, thereby affecting payload mass and launch costs. Because of the significance of these factors a substantial technology development effort is being pursued to produce lightweight collisional bumpers (e.g., Anderson, 1987, 1990; or Christiansen, 1990; 1992).

Previously, we have presented experimental evidence that mesh-like structures, possessing a high degree of transparency (Figure 1), will collisionally fragment impactors with efficiencies similar to those of continuous sheets (Hörz *et al.*, 1992a). Other than substantial material-dependent effects, the crucial parameter is the specific bumper mass encountered by the projectile. In principle, any mesh that has openings smaller than the diameter of the projectile ( $D_p$ ), and that is constructed from sufficiently thick materials (*i.e.*, wire) may collisionally fragment the projectile in a manner similar to a continuous bumper (*i.e.*, sheet) of identical thickness  $T$ , assuming both mesh and contiguous membrane are constructed from the same material. Hörz *et al.* (1992a, 1992b) also presented evidence



that  $T$  can be small, relative to the projectile diameter (e.g.,  $D_p/T = 10$ ), and still disrupt

the projectile diameter (e.g.,  $D_p/T = 10$ ), and still disrupt millimeter-sized glass projectiles with great efficiency when encountering Al-foils or aluminum-wire meshes.

The basic idea of a lightweight multiple-mesh bumper, as illustrated in Figure 1, seems to be substantiated by the above experiments: a series of meshes, all dimensionally scaled to a modeled  $D_p$ , should be able to efficiently comminute the entire projectile. The fragments generated by the first mesh will be further comminuted by the second and third mesh, each successive mesh being dimensioned such that it will interact with and destroy a fragment half the size of that which collided with the preceding mesh. Progressive comminution may be accomplished by such a succession of meshes, with the  $n^{th}$  mesh controlling the smallest fragment that is permitted to exit the stack and which, presumably, can be tolerated by the flight system behind the meshes. In addition, it is expected that the multiple collisions will lead to a substantial deceleration of the projectile, since each encounter will dissipate some finite amount of the projectile's kinetic energy. These principles and expectations are based on bumper designs employing multiple contiguous membranes (e.g., Gehring, 1970; Richardson, 1970; Dickinson *et al.*, 1987). Furthermore, following Cour-Palais and Crews (1990), multiple collisions will lead to successive entropy changes and thus, enhanced thermal effects compared to single collisions, which should aid in promoting further disaggregation of the impactor.

This report on multiple-mesh experiments is an extension of the single-mesh penetration studies of Hörz *et al.*, (1992a). All meshes were dimensionally scaled to the projectiles used (*i.e.*, had mesh openings  $<D_p$ ), yet variable wire thicknesses. Most of the experimental mesh stacks had a specific areal mass (SM) smaller than that of the projectile. Consider the following: the "ballistic limit" defines a minimum bumper thickness that will prevent physical penetration by hypervelocity impactors. This thickness for a single aluminum sheet is typically a factor of 3-5 times larger than  $D_p$  at  $\sim 6-7$  km/s. For example, for our 3.17 mm diameter soda-lime glass impactors, the ballistic limit thickness for aluminum 1100 is  $\sim 11$  mm at 6 km/s projectile velocities (e.g., Hörz *et al.*, 1992a or Cour-Palais, 1987). This thickness corresponds to a specific bumper mass of essentially 3 g/cm<sup>2</sup>. Many of the multiple-mesh experiments in this study possess SM values of  $\sim 0.2$  g/cm<sup>2</sup> (*i.e.*, an order of magnitude less total mass than in the ballistic-limit case of single plates). Thus, most of our experiments explored "lightweight" bumpers, compared to single sheets.

However, based on the above, it is to be expected that many of our bumpers will be physically penetrated, albeit only by fragments. It is important to note that the experimental focus was not to prevent such penetrations, but to efficiently comminute the projectile and disperse the fragment cloud such that only fragments of low specific energies (ergs/g) exited the bumper to potentially impinge upon a flight system. A significant number of flight systems, especially structural components, can readily tolerate some modest, superficial damage by such fragment clouds. Such flight systems were simulated by placing "witness plates" of sufficient thickness (*i.e.*, to respond as infinite half-space targets for these fragments) behind the mesh stack.

While we set out to explore the effects of some of the variables perceived as potentially important, such as specific bumper mass (SM) or separation distance (S) between individual meshes, this effort was an exploratory study of limited scope. Our primary objectives were to

establish the sensitivity of diverse variables. As a consequence, some individual variables are often addressed by only 2-4 experiments. Those variables that were found to have particularly beneficial effects were frequently incorporated into subsequent target configurations, fully realizing that this procedure would somewhat disturb the intended, systematic nature of an experimental matrix. We simply desired to identify trends, with the minimum number of experiments, that seem important for future studies aimed at further development of the most suitable, optimum bumper design. It is for these reasons that the parametric matrix underlying this report cannot be as complete as desirable. Furthermore, investigation of a fair number of variables made presentation of the results in concise and clear fashion a somewhat difficult task.

## EXPERIMENT DESCRIPTION

### OBJECTIVES

The primary performance criterion of any bumper arrangement is its ability to dissipate sufficient kinetic energy of the impactor such that the specific energy (ergs/unit surface area) of the resulting debris cloud is below the value that can be tolerated by a flight-system. This value varies from system to system. If the threshold value is 0, a totally opaque bumper is required that must employ contiguous components. For all finite threshold values, fragments below some critical size, velocity or kinetic energy will principally be permitted to exit the bumper. The question then becomes one of partitioning sufficient energy into the impactor and the bumper itself to assure that the ensuing debris cloud does not exceed these critical threshold values. Many experimental studies attest to the complexity of this debris cloud and to the technical difficulties in characterizing, via in-situ measurements, such parameters as fragment-size distribution, the widely variable velocities, and the spatial distribution and dispersion of the cloud (e.g., Piekutowsky, 1990). The witness plates to the target's rear, as used in this study, faithfully record these conditions, yet their interpretation is difficult, highly empirical and possibly somewhat subjective on occasion. However, they are highly suitable to delineate first-order trends in largely parametric inquiries, such as the present study as described by e.g., Piekutowsky (1987, 1990) Dickinson *et al.* (1987), Stilp *et al.* (1990), Schonburg and Taylor (1990), Cour-Palais and Crews (1990), and many others.

While efficient energy deposition into the bumper is a desirable design goal it will have the detrimental effect of physically dislodging material, possibly at very high speeds, from the bumper itself. This dislodged mass contributes to the damage of a flight system. Indeed, it can be the dominating effect because it exceeds projectile mass for a wide range of impact conditions. Consequently, trade-offs must be made between efficient energy partitioning and total mass dislodged. Massive bumpers shed too much mass, while lightweight designs may not decelerate the impactor sufficiently; obviously an "intermediate" mass that represents a compromise between potentially beneficial and detrimental effects seems to be indicated. This is the reason why the specific bumper mass was carefully determined and varied in the experiments discussed below, why each mesh was weighed before and after an experiment, and why we collected and weighed loose particulates.



## PHYSICAL SET UP AND PROCEDURES

As illustrated in Figure 2, we enclosed the entire target in a sealed box that not only permitted efficient bench-top assembly and disassembly of the entire targets, but that also allowed physical recovery and subsequent weighing of loose particulates. Note that this box was subdivided by a massive plate that served to mount the very first target mesh. Therefore, it always defined the plane of the primary impact and loose material in the "up-range" compartment could be recovered separately from the debris in the "downrange" compartment. The latter are termed somewhat simplistically "ejecta" mass (" $m_e$ ,"; up-range) and "spall" mass (" $m_s$ ,"; downrange), respectively. These particulates constitute debris that is apt to become space borne, thereby contributing to the growing orbital-debris population. It seems self evident that this dislodged mass should be kept at a minimum and that it may serve as a discriminator among diverse bumper designs.

Note that throughout this report we distinguish the mass of the physically recovered particulates ( $m_e$  and  $m_s$ ; their sum is defined as "dislodged" mass;  $m_d$ ) and the mass loss of the bumper itself ( $M_t$ ), derived from the summation of the weight difference of individual stack members before and after an experiment. The term " $M_t$ " describes all displaced mass, whereas  $m_e$ ,  $m_s$  and  $m_d$  refer only to those fractions that were physically recovered, the latter including -- in addition -- any materials potentially dislodged from the witness plate.

Also illustrated in Figure 2 are the five types of meshes used in this study. As described by Hörz *et al.*, (1992a), the three most massive meshes were manufactured from aluminum (alloy 5365) welding rods of thicknesses 1.59 mm (0.0625" or 0.5  $D_p$ ), 0.76 mm (0.030" or 0.24  $D_p$ ) and 0.58 mm (0.023" or 0.18  $D_p$ ). These rods were placed through machined holes in a mesh ring and held in place with set screws. The center-to-center distance of the rods was 3.175 mm, (*i.e.*, equal to the exact projectile diameter; see Figure 1). The two finest meshes were commercial screen materials, available in rolled stock, also made from aluminum wires. One had center-to-center distances of 3.175 mm (equal to  $D_p$ ) and consisted of a double strand of two wires, each 0.25 mm (0.01" or 0.08  $D_p$ ) thick, in one direction, whereas the orthogonal single strand wire had a diameter of 0.3 mm (0.012" or 0.01  $D_p$ ). The other commercial screen had center-to-center distances of 1.59 mm (1/2  $D_p$ ) and employed a single wire of 0.25 mm thick (0.010" or 0.08  $D_p$ ). The specific masses of these various meshes were 0.3421, 0.0776, 0.0456, 0.016 and 0.018 g/cm<sup>2</sup>, respectively, for the five meshes made from 1.59, 0.76, 0.58, 0.30/0.25 and 0.25 mm thick wires. The total specific mass of the entire target stack was termed "Stack Mass" (SM; g/cm<sup>2</sup>). Most experiments employed the commercial meshes, consistent with our objectives to explore lightweight bumper designs, because custom manufacture of the more massive bumpers was very time consuming and costly, as each mesh consisted of 90 wires and two set screws per wire. Each mesh ring contained three holes (Figure 2) that matched continuously threaded rods that were used to stack the individual mesh rings. Suitable spacers provided the desired separation distances (S) between individual meshes (Figure 2). The "standoff" distance (L) refers to the distance of the witness plate from the last mesh; L varied somewhat because of the different S values, and the variable numbers of meshes that had to be accommodated inside a box of fixed geometry.

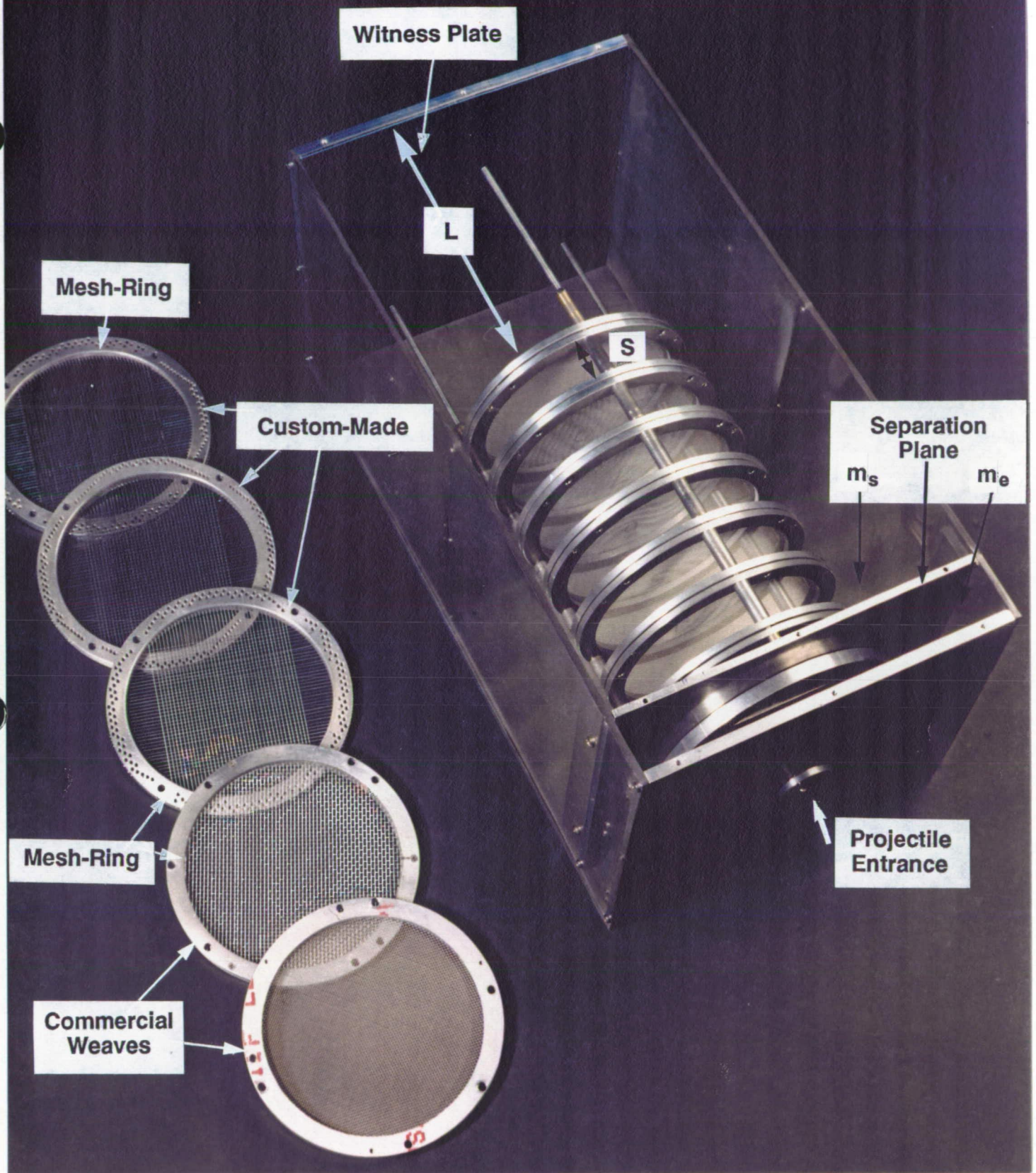


**Figure 2.** Top view of target container with the cover plate removed. The dimensions of the box are ~30 x 30 x 60 cm. Included in this view are examples of the five different mesh types employed throughout this study. The commercial meshes were clamped between the two halves of the the aluminum holders, while the man-made meshes were assembled wire-by-wire, each wire being held in place by set screws. The meshes were held in place at the desired separation (S) and standoff (L) distance by the three standoff rods. Note the aluminum plate associated with mesh 1 which sperated the target container into "uprange" and "downrange" compartments permitting the collection of loose ejecta ( $m_e$ ) and spall ( $m_s$ ) debris, respectively. The projectile enters the box in the front through a 12 mm diameter hole.

No effort was made to systematically align and "register" the orthogonal wire directions of successive grids when using the commercial meshes, which were randomly mounted into the mesh rings. In contrast, the custom-made meshes had similar orientations of the two wire directions, yet modest lateral displacement among successive grids was permitted. Thus, no concerted effort was made to register the meshes precisely. Each mesh was simply marked, at a fixed place, after assembly to preserve the relative orientation(s) of all meshes. The 1<sup>st</sup> mesh ring was always smaller than the subsequent meshes because (1) it had to sustain a relatively small projectile entrance hole and (2) it was part of the massive separation plate described above. All other mesh rings or clamps were relatively massive, potentially blocking most of the laterally dispersing debris, making the use of cylindrical witness plates impractical in this study. Based on Hörz *et al.*, (1992b) such debris is negligible for the thin targets employed in this study because the dispersion angles are generally small ( $<90^\circ$ ). Even after numerous shots using the lightweight meshes, no major debris interactions with the mesh rings were observed. Therefore, the witness plates should reflect the character of the respective debris clouds. However, modest ring damage did occur with time, when employing the massive, custom-made meshes (see also Hörz *et al.*, 1992a).

The actual tests employed both a horizontal 5 mm light-gas gun and a vertical 8 mm powder-propellant gun within the Experimental Impact Facility at the Johnson Space Center in Houston, Texas. The light-gas gun velocities were limited to  $<6$  km/s because of the accelerated degradation of gun hardware which results at higher velocities. Velocity measurements were generally accurate to within 1%, based on redundant laser/photo-diode occultations, as well as detection of light flashes generated during sabot and projectile impacts. All shot numbers  $<3000$  refer to the light-gas gun experiments, while all shot numbers  $>3000$  refer to experiments conducted on the powder gun; the numerical sequence corresponds to the chronological sequence.

## EXPERIMENTAL VARIABLES AND THEIR SIGNIFICANCE

Figure 3 schematically presents the experimental matrix investigated in this study. Table 1 details additional initial conditions (and results). It is obvious that impact velocity, specific bumper mass, number of meshes, separation distance and projectile material represent the major variables, all poorly constrained or unknown for multiple-mesh penetrations. The experimental focus was to gain some understanding of the relative role(s) of these variables. As a result, only a few experiments were needed to isolate any specific parameter, at otherwise identical conditions. The scope of this study was neither intended to, nor did it permit detailed characterization of all variables. We deliberately explored a fair number of variables with a minimum number of experiments.

For convenience, related experiments are combined into Groups A through I in Figure 3 and throughout this report. Some experiments fit the detailed objectives of more than one Group and are repeated, where applicable. Much of the general matrix was preconceived, yet refinements were developed during the course of this study and, if warranted, were included in subsequent

Preceding Page Blank



experiments as detailed below. The various Groups had the following primary and secondary objectives:

GROUP A -- Based on a few precursor tests (Table 1; Experiment Numbers 813, 822 and 822; see Hörz *et al.*, 1992a) we started with commercially available screen stock and assembled stacks of five meshes, separated by 25.4 mm. The selected mesh possessed openings which were comparable to the projectile diameter ( $M = D_p = 3.17$  mm). The objective was to explore the effects of impact velocity. While substantial comminution was prevalent, considerable kinetic energy still seemed to reside in the debris cloud based on witness-plate observations. Therefore, we decided to increase the number of meshes within the stack to ten.

GROUP B -- This group was a repeat of the Group A experiments, albeit with ten meshes, effectively duplicating the total shield mass of the Group A experiments. Again, the major objective was to explore the effects of impact velocity. The effects of having twice as many meshes were noticeable resulting in substantially less mass of a finer grain size reaching the witness plate.

GROUP C -- These experiments were designed to test the effects of the mesh opening and used the commercial screen of  $M = 0.5 D_p = 1.59$  mm. Specific areal shield mass is (fortuitously) nearly constant relative to Groups A and B. For all practical purposes this series was a duplicate of Group B, aside from employing a finer mesh. Three experiments at varying impact velocity were conducted. The first-order result was that this screen appeared to be superior to the coarser screen, and is the reason why many subsequent experiments employed only the fine mesh.

GROUP D -- Utilizing ten-member stacks of the fine mesh, this series was intended to delineate the effects of separation distance at constant velocity. We explored separation distances of 12.7, 25.4 and 50.8 mm (*e.g.*, 1/2", 1" and 2") at otherwise identical conditions. Additionally, we utilized a separation distance of 101 mm (4"), but do to the size of our target box we could only accommodate a five-member stacks with such a larger separations distance. The effects of separation distance were more substantial than those associated with velocity. Therefore, as best as possible, we accounted for this effect in many subsequent experiments and introduced 50.8 mm (2") as the optimum separation distance for ten-member targets in many of the subsequent experiments.

GROUP E -- The ten-member stack, separated by 50.8 mm, seemed to be the superior arrangement. We also performed low-velocity experiments with this configuration to address the effects of large velocity variations on such stacks.

GROUP F -- The purpose of this group of experiments was to explore the role of total bumper mass. To this end, we employed the more massive, custom-made meshes produced from welding rods. The total number of meshes was limited to five because the total mass rapidly exceeded that of Groups A-E, which had already been judged to yield satisfactory results. Two identical targets sets composed the Group F experiments. One set was impacted at  $\sim 2$  km/s ( $F_a$ ), while the other was impacted at  $\sim 5.9$  km/s ( $F_b$ ), in order to explore the effects of impact velocity on massive-mesh bumpers.

GROUP G -- These experiments come close to the idealized concept of Figure 1 because they employed a mixture of meshes, each differing in specific areal mass. Details of these stacks were driven by the two commercial screens which always acted as the last two stack member; the custom-made screens of increasingly higher masses were added at the front side of the stack one at a time, thus leading to stacks totaling 3, 4 or 5 meshes (see Table 1). As was the case with the Group F series, one set of experiments refers to low-velocity ( $G_a$ ) experiments, while the other refers to high-velocity ( $G_b$ ) experiments. Note that these targets do not exactly duplicate the concept illustrated in Figure 1, except for the very last screen, because all other meshes had constant mesh openings (*i.e.*,  $M = D_p = 3.17$  mm). We were unable to secure suitably dimensioned meshes ( $M < D_p$ ) made from aluminum wires  $<< 250 \mu\text{m}$  ( $<< 10/1000$ "") thick.

GROUP H -- Thus far, all experiments (Groups A-G) were conducted with soda-lime glass projectiles. This group employed aluminum and stainless steel projectiles in order to explore the effects of physical properties of the impactors, specifically of silicates versus metals. These experiments employed the target configuration of the Group D experiments, which had provided the best results for the soda-lime projectiles.

GROUP I -- This final group of experiments employed multiple, contiguous aluminum foils (75  $\mu\text{m}$  thick) that closely resembled the specific areal mass ( $SM = 0.02 \text{ g/cm}^2$ ) of the finest commercial mesh ( $SM = 0.18 \text{ g/cm}^2$ ), and employed the previously determined most favorable separation distance of 50.8 mm. This group includes low- and high-velocity shots with glass projectiles, and one 2 km/s experiment that employed an aluminum impactor. These experiments were intended to permit first order comparison of multiple continuous versus discontinuous bumpers.

## RESULTS

### PHOTO-DOCUMENTATION

A detailed pictorial summary of each experiment is presented in Appendix, which documents the physical penetration and deformation phenomena of each individual mesh, combined with a photograph of the associated witness plate. Figure 3, and all subsequent Figures, should assist the reader in evaluating the relationship(s) among the various groups and the major variables, while numerical ordering of experiments in the Appendix and in Table I should assist in locating specific initial conditions and results for any given experiment. Regardless, the large number of individual target components, and associated measurements, makes concise presentation of the results somewhat cumbersome, yet we encourage the reader to consult the Appendix and Table I for details.

The rationale for the detailed photo-documentation is to convey to the reader some appreciation of the experimental products, many of which defy quantification at present, yet which contain and convey substantial information and unequivocal trends in pictorial form. In particular, the witness plates are difficult to analyze, as detailed by Hörz *et al.*, 1992a (and others).

Referring to Appendix, all meshes for a given experiment are arranged in an internally consistent orientation that preserves and portrays the proper relative position of each stack-member during the actual impact event(s). Note that successive penetration holes may frequently have dramatically different orientations of their longest axis (*e.g.*, 979) or the holes may develop aspect ratios that have little resemblance to the preceding holes (*e.g.*, 982). Such effects are real and not a matter of erroneous mesh orientation during preparation of the figures. Most likely they relate to the chance collision of massive fragments producing somewhat lumpy mass distribution of the debris cloud as described by Hörz *et al.* (1992a).

While the term "penetration hole" is used throughout this report, it must be made clear that much of the actual opening is caused by the bending and deformation of individual wires. This implies that the "hole diameter" and the associated surface area, as used in this report, is a measure of the damage rendered to individual meshes. In an operational sense it defines a fraction of the bumper surface that is rendered non-operational during subsequent collisions. After summing individual holes within a single stack-target we refer to the cumulative surface area of all holes as the "internal shield damage". Note that there may not necessarily be a direct relationship between "hole size" and any measure of displaced mass.

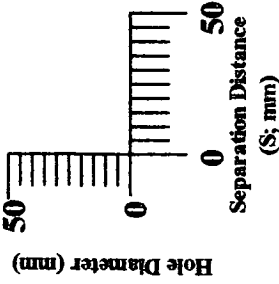
#### PENETRATION-HOLE DIAMETERS

Measurements of all hole diameters are illustrated in Figure 4, which displays the initial dispersion of an energetic debris cloud through a number of meshes, in particular for Groups A-E that employed the low-weight, commercial screens. The maximum hole diameter is typically found in mesh five or six. A comparatively rapid restriction of this debris cone seems to occur for the subsequent meshes, as their penetration holes decrease rapidly over a few meshes. These observations suggest that it is predominantly the peripheral part of the debris cloud that is being terminated upon collision with successive meshes, while the central portions of the cloud tend to contain high specific energies that enable deep penetration of the targets. This further suggests that the projectile is fragmented, yet not thoroughly dispersed by the first layer, consistent with the small target thickness ( $D_p/T \sim 10$ ) that produces central clusters of projectile fragments as described by Hörz *et al.* (1992b). In essence, this central cluster contains relatively large fragments that will penetrate further, and that require repetitive encounters with successive meshes to be sufficiently comminuted. Once this is accomplished, relatively rapid termination of the fine-grained debris seems to take place.

As is evidenced by a number of experimental configurations (*e.g.*, the Group D and E experiments), individual meshes toward the rear of the mesh stack may not display macroscopic deformation and are considered undamaged, as documented in detail in Appendix (*e.g.*, 982 or 990). Clearly, this is a highly desirable result for any collisional shield. Nevertheless, the mesh stacks have some finite transparency and debris reached the witness plate in all cases, including those stacks containing undamaged meshes. Without exception, this debris was fine grained and highly dispersed.

**No V SM**

975; 5.89; 0.08  
 977; 5.25; 0.08  
 976; 4.28; 0.08



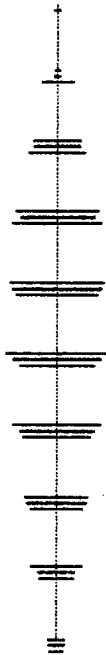
**(A)**

979; 5.86; 0.16  
 980; 5.12; 0.16  
 981; 4.41; 0.16



**(B)**

982; 5.74; 0.18  
 983; 5.14; 0.18  
 988; 4.16; 0.18



**(C)**

997; 5.93; 0.09  
 990; 5.97; 0.18  
 982; 5.74; 0.18  
 989; 5.81; 0.18



**(D)**

990; 5.97; 0.18  
 3423; 1.95; 0.18  
 3422; 1.02; 0.18



**(E)**

14, 15.



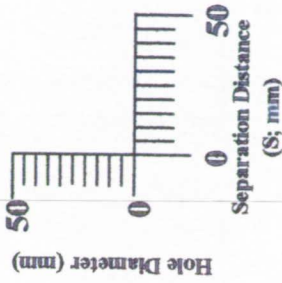
No V SM

**a** 3435; 1.91; 1.69  
 3434; 2.00; 0.39  
 3433; 1.98; 0.23



No V SM

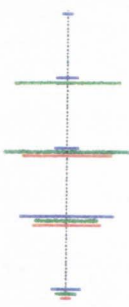
**b** 1008; 5.94; 1.69  
 1007; 5.83; 0.39  
 1006; 5.80; 0.23  
 975; 5.89; 0.08



**a** 3432; 2.00; .050  
 3431; 1.95; 0.16  
 3428; 1.94; 0.08



**b** 1004; 5.80; 0.50  
 1003; 5.91; 0.16  
 1002; 5.87; 0.08



993; 5.76; 0.18  
 995; 4.59; 0.18  
 3425; 1.95; 0.18  
 3424; 0.99; 0.18



998; 5.86; 0.10  
 999; 6.03; 0.20  
 3426; 2.00; 0.20  
 3427; 1.97; 0.20



**Figure 4.** Measurements of the average penetration-hole diameter in each individual mesh. Note that the separation distance (horizontal dimension) and hole diameter (vertical dimension) are to identical scales for all experiments, permitting a direct comparison of absolute and relative hole sizes (the actual vertical and horizontal scales are slightly different). The impact point is to the left at the first mesh. Note the gradual increase to a maximum hole diameter and the comparatively rapid closure over a few meshes towards the rear of the stack (e.g., Group B). Also note the relatively large holes produced in the contiguous foils of Group I. For a detailed discussion and interpretations see text.

In comparing the mesh experiments with those employing multiple foils (Group I) we note that the witness plates associated with the Group I experiments are substantially less damaged or not damaged at all. However, the penetration holes are factors of 2-3 times larger in the foils (see Figure 4) because they interacted with the highly dispersed debris and failed (principally by a few major tears) over a substantial surface area (e.g., 999).

Data from both target configurations indicates that multiple interactions are an especially effective means of comminuting and decelerating hypervelocity projectiles, as previously suggested by many (e.g., Dickinson *et al.*, 1987; Cour-Palais and Crews, 1990; Christiansen, 1992). The foil stacks comminuted/decelerated the 3.17 mm impactors into fragments that ultimately failed to penetrate foils as thin as 76  $\mu\text{m}$ , and the mesh stacks produced witness-plate damage that is only consistent with extremely fine-grained, low-velocity particles.

### Effects of Impact Velocity

The Group A experiments, intended to explore the effects of velocity, do suggest such a dependence, as do all other tests performed at variable velocity under otherwise identical conditions (*i.e.*, Groups B, C and E). However, these differences are relatively subtle to the degree that (unavoidable) idiosyncrasies of specific experiments, even of individual meshes within an individual stack, may deviate from the general trends. Nevertheless, the higher velocity impactors, generally display modestly wider dispersion angles on the first few meshes (e.g., Group A), and typically resulted in the maximum penetration hole residing in meshes 5-7 for the Group B experiments. The penetration holes in the meshes behind the mesh containing the maximum penetration-hole diameter tend to rapidly decrease in size, especially at higher velocities. These observations suggest that the high-velocity impactor initially produces a more widely dispersed debris plume that seems to have possessed sufficient kinetic energy to expand and penetrate through a few meshes. Most likely these are also relatively fine-grained plumes that rapidly lose energy during a small number of subsequent mesh encounters. The extreme case of such a scenario is illustrated by the Group C experiments, yet the trend is very general. Examination of the Group E experiments seems to indicate that the lower velocity (<2 km/s) projectiles produce relatively small holes, and that the debris is being comminuted/terminated by <10 meshes. Substantially smaller penetration holes are also produced in the massive-grid bumpers (Groups F and G) at 2 km/s compared to 6 km/s cases. We conclude that the high-velocity impactors comminute and diverge much more readily than the low-velocity projectiles. On the other hand, the central portions of the debris clouds seem to have comparable penetration power, because the low-velocity clouds consist of many large, barely dispersed fragments. These interpretations rely heavily on observations made in association with single foil penetrations (Hörz *et al.*, 1992b) and the penetration of single meshes (Hörz *et al.*, 1992a), which provide constraints on, and insights into comminution of the projectile and the ensuing debris clouds that is generated by the primary impact on the first member of our target-stacks.

It seems significant that low- and high-velocity (glass) impactors are effectively decelerated and comminuted by most experiments that employed ten, relatively thin meshes that contained less cumulative specific mass (SM = 0.18 and 0.16 g/cm<sup>2</sup>, respectively) than the projectile itself (0.48

g/cm<sup>2</sup>), and order of magnitude less mass than that represented by the contiguous, single-sheet, ballistic limit shield. As described by many (*e.g.*, Hohler *et al.*, 1975 or Orphal *et al.*, 1992) the target thickness at the ballistic limit is highly sensitive to impact velocity because it must be viewed as a truncated cratering event (Hörz *et al.*, 1992b). Our mesh stacks seem to display a comparatively modest velocity dependence, a highly favorable property, and are significantly different from the contiguous single-sheet bumpers in this respect.

### **Effects of Separation Distance**

The Group D experiments were configured to test the effects of separation distance (S) on identical meshes; the projectile velocity was essentially constant, while the four S values were 12.7, 25.4, 50.8 and 101.6 mm. Note that the experiment 989, which employed the smallest S, produced a substantial sized exit hole in the 10<sup>th</sup> mesh. In contrast, the 10<sup>th</sup> mesh was undamaged in experiment 982 which utilized an S of 25.4 mm, while meshes 8, 9 and 10 of 990 (S = 50.8 mm) were unaffected. In 997 (S = 101.6) mesh five of the stack was essentially intact (note that 997 is an exact duplicate of 996, thereby attesting to reproducibility of these experiments).

Obviously, it helps to permit the debris cloud to disperse freely such that its energy (ergs/cm<sup>2</sup>) is substantially lower by the time the debris cloud encounters the second, and subsequent grids. Assuming that the first mesh produces a nearly identical debris cloud for each experiment, it is important to note that the hole dimensions of the second mesh (and successive meshes) do not correspond to simple line-of-sight geometry. Note the relatively small holes in the second mesh of 990 and 996/997 compared to those of 982 and 989. This observation strongly suggests that the outer fringes of the debris cloud have particularly low specific energies that are effectively unable to proceed to subsequent meshes. The wider the separation distance, the larger the peripheral fraction of the cloud that can be terminated by only a few meshes. Therefore, separation distance is of crucial significance in any multiple-encounter bumper design, and the largest practical separation distances should be sought. These results indicate the need for further studies designed to investigate the trade-offs between S, and the number and thickness of individual meshes that would result in optimum bumper performance at minimal mass.

### **Effects of Specific Bumper Mass**

Group F experiments were primarily intended to address the effects of bumper mass at both low and high projectile velocities. This group employed the most massive targets within our experimental matrix, some having a specific areal mass of 1.69 g/cm<sup>2</sup>, essentially four times that of the impactor (0.47 g/cm<sup>2</sup>). Not surprisingly, the most massive stacks were penetrated the least, and penetration power -- as judged by the state of deformation of posterior meshes -- is systematically decreased with increasing mesh mass. Clearly, the meshes in the experiments with the smallest specific mass suffered substantially more damage than those utilizing more massive shielding. Note that all of the custom-made, massive meshes exhibited penetration holes that were much smaller than those observed within the commercial lightweight screens (975). In addition, substantially smaller holes resulted with low-velocity projectiles (Group F<sub>a</sub>) compared to their high-velocity counterparts (Group F<sub>b</sub>).

## Effects of Mesh Opening

Identical, total bumper masses can be designed by varying the wire thickness and mesh openings, while maintaining  $M < D_p$ . The commercial weaves that were selected possessed mesh openings of 3.175 and 1.59 mm, with wires of different thicknesses, resulting in nearly identical specific areal masses of 0.016 and 0.018 g/cm<sup>2</sup>, respectively. Therefore, Group B and C experiments may be viewed as evaluating the effects of mesh size. Note that the finer meshes (Group C) produces modestly smaller penetration holes in the first few meshes (e.g., meshes 3 and 4), and especially in those meshes located towards the rear of the stack (e.g., mesh 6). We suggest that the finer meshes provide more interactions with the debris, thus comminuting, decelerating and dispersing the debris more readily. Also note that the hole sizes are modestly smaller for the Group C experiments compared to Group B, again suggesting that the peripheries of the debris cloud are particularly affected. These results suggest that finer meshes are to be preferred, as long as they possess sufficient mass to induce substantial projectile fragmentation. Clearly, some threshold value for wire thickness must exist below which the projectile is not fragmented efficiently, if at all.

## Effects of Mixed Meshes

The Group G experiments most closely resemble the bumper configuration depicted in Figure 1; experiments in Group G<sub>a</sub> were conducted with projectile velocities of ~2 km/s, while those in Group G<sub>b</sub> employed projectile velocities of ~6 km/s. The most massive mesh of each stack was located on the projectile-entrance side of the stack box, followed by meshes of systematically decreasing SM. However, the mesh openings were not scaled to half that of the previous mesh as depicted in Figure 1. Only the last mesh layer possessed a mesh opening that was half that of all preceding meshes. As expected, the more massive first grid substantially affected the results leading to minimal deformation of the last mesh(es). Note that many of the Group G bumpers possess substantially higher specific masses than those characterizing the Group A-E experiments. They appear to be more massive than is required, suggesting the need for experiments utilizing suitably scaled, less-massive meshes. The damage to meshes four or five (e.g., 1003) approach or exceed the damage observed in the commercial lightweight screens. This increased damage seems to be caused by relatively large fragments dislodged from the preceding, massive mesh. Obviously, fragments are being dislodged from the first mesh that add to the damage caused by the projectile. As a consequence, the Group G arrangements did not perform well; they simply seem too massive. On the other hand, the present observations could well reflect a general detrimental characteristic of the concept illustrated in Figure 1 because there will always be a relatively massive member at the entrance side that may shed materials capable of inducing damage to the successively more lightweight and delicate meshes.

In general, the specific mass or wire thickness composing the first mesh of the Group A-E tests sufficed to break up the projectile into many fragments, as previous documented in the single-mesh experiments (Hörz *et al.*, 1992a), or the foil-penetration experiments (Hörz *et al.*, 1992b). Consequently, wires that are only 1/20<sup>th</sup> to 1/50<sup>th</sup> that of typical projectile dimensions may suffice to disintegrate millimeter-sized impactors. Unfortunately, the scope of this effort

prevented acquisition or manufacture of meshes that employed aluminum wires with diameters of <0.25 mm (0.01") to test mixed mesh stacks composed of truly thin wires, consistent with the concept illustrated in Figure 1.

### **Effects of Projectile Species**

The standard projectiles utilized in this concept study were soda-lime glass spheres to make a direct comparison with the earlier experiments (Hörz *et al.*, 1992a and 1992b) possible. In an effort to provide some cursory insight as to how silicate projectiles compare to metal impactors, a few (ten-mesh stack,  $S = 50.8$  mm) experiments employing aluminum (2024) and stainless-steel (304) projectiles were carried out. These experiments comprise Group H. The aluminum projectile traveling at 5.76 km/s were substantially fragmented, resulting in mesh damage akin to that produced by the glass projectiles. However, at low velocities the aluminum impactors remained intact and penetrated the entire stack without fragmentation, unlike the silicate spheres. Obviously, the peak stresses stayed below the aluminum's tensile strength at low velocities. A single, stainless-steel projectile (4.6 km/s) experiment was conducted that resulted in the projectile remaining intact through the entire ten-mesh stack; this is not unexpected in a general sense, and especially in view of the fact that the entire stack contained a specific areal mass of only  $\sim 1/10^{\text{th}}$  that of the steel projectile.

None of these results are surprising. The few Group H experiments employing metal impactors are not detrimental to the intrinsic merits of multiple-mesh shield. The increased tensile strengths of metal projectiles, relative to silicates, are germane to all shield developments. Collision protection from high-density, high-strength metal impactors simply demands more shield mass, regardless of the specific shield design. We note, nevertheless, that even the current aluminum meshes are capable of substantially disintegrating and melting aluminum projectiles at 6 km/s. We also note that our use of aluminum meshes/wires was largely one of convenience in this parametric study. Mesh wires from materials of more suitable dynamic properties can be envisioned, such as ceramic fiber bundles, high-density, high tensile-strength metals, etc.

### **Comparison with Multiple-Stacked Foils**

A few experiments, Group I in Figure 4, were conducted with multiple, contiguous aluminum foils for comparison with the multiple-mesh stacks; the Group E experiments are the most direct analogs. As Figure 4 is to scale, it is immediately apparent that substantially larger penetration holes resulted in the foils, typically factors of 2-3 times larger than those produced in the mesh bumpers. The actual size of the foil holes is controlled by a few large tears and cracks, which cause large flaps of relatively pristine foil to be folded rearwards. The mesh targets do not permit the propagation of such long cracks and/or tears.

Experiments 998 and 999 employed five and ten foils, respectively, duplicating the separation distances ( $S = 101.6$  mm and 50.8 mm, respectively) associated with 987 and 990 of Group D. For the ten-foil stack, the last three foils remained essentially pristine, and no debris reached the witness plate. This differs from the transparent mesh stacks that permitted transmission of fine-grained debris to the witness plate. This observation suggests that a single, relatively thin,

contiguous foil may be placed at the rear of any mesh stack, thereby rendering it opaque and preventing most (all) mass from reaching the witness plate (flight system, if the latter mandates such a high degree of protection).

The trends displayed by the low-velocity mesh shots are also maintained within the foil series (*i.e.*, relatively small penetration holes compared to those produced by the high-velocity collisions). Again, the absolute hole diameters in the foil series (*e.g.*, 3426; Group I) are substantially larger than those produced in the low-velocity meshes experiments (*e.g.*, 3423; Group E). However, meshes nine and ten remained pristine in 3423, whereas all ten foils were penetrated by the 2 km/s projectile. This modestly superior performance at low velocities of mesh bumpers -- if verified by additional experiments -- is most likely caused by the fact that the actual mesh wires (for equivalent specific bumper masses) are simply thicker than the corresponding foils and cause increased projectile fragmentation.

A single experiment (3427) was conducted with a foil stack and an aluminum projectile. The intact projectile penetrated the entire stack and impacted the witness plate, while the witness plate on the mesh analog (3426; Group H) indicated modest disruption of the projectile by the mesh stack. Again, the mesh-stack performance seems modestly superior at low velocities. Consult Appendix and note the difference in the crater morphologies between 3427 and 3426.

## TOTAL BUMPER DAMAGE

Using the average diameter of the penetration holes (Figure 4 and Table 1) we calculated the surface area for each hole, and then summed all penetration-hole areas for a given stack to generate a cumulative surface-area parameter. This single value greatly facilitates the comparison of the individual tests, as it is a measure of the total damage sustained by the entire target. Operationally, this value is a measure of the bumper's transparency for subsequent collisions. Smaller values are obviously desirable, because they imply improved preservation of the bumper's integrity. Obviously, modification of the physical transparency relates to the long-term performance of any shield design. The total surface area rendered inoperative by a collision is a discriminator for bumper designs that otherwise have similar/identical bumper performance against the immediate threat posed by a single collision.

These cumulative surface areas are illustrated in Figure 5. Note that the total specific bumper mass is the dominant factor. The more massive bumpers (*e.g.*, Groups F and G) suffered less cumulative damage than did the majority of the commercial screen targets (Groups A-E). The Group A experiments only employed five meshes, while the Group B experiments used ten.

Furthermore, the low-velocity experiments ( $< 2$  km/s), without exception, sustained substantially less damage than their high-velocity equivalents (*e.g.*, Groups E or I - also compare Group F<sub>a</sub> and G<sub>a</sub> with Groups F<sub>b</sub> and G<sub>b</sub>). Some velocity dependence is also observed within the individual groups at light-gas gun velocities (*e.g.*, Groups A and C); the higher velocity experiments produced more cumulative damage. Group B seems at odds with this statement, yet we presently ascribe this to experiment idiosyncrasy. We summarize from these observations that

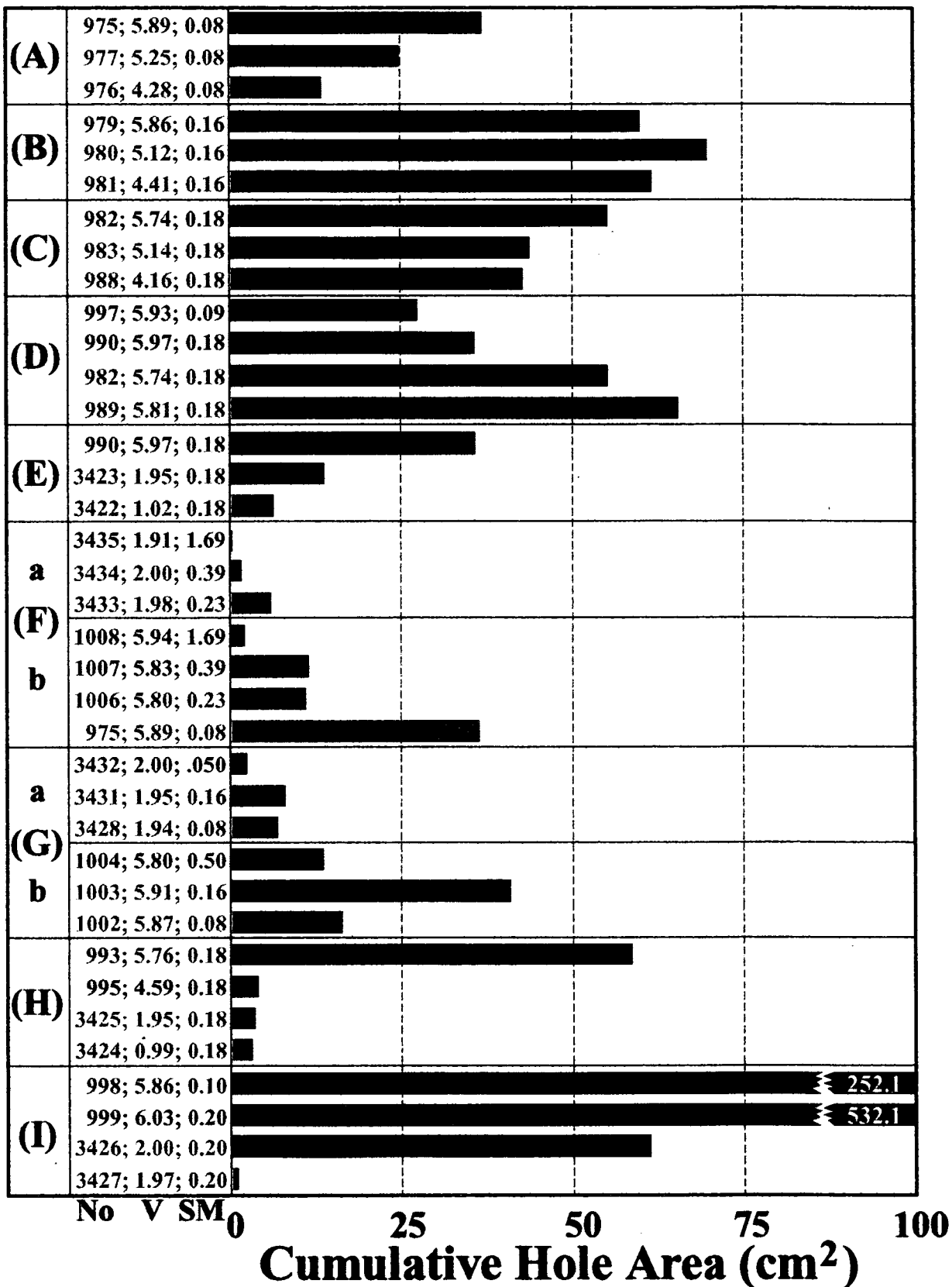


Figure 5. Sum of the surface area represented by all hole diameters illustrated in Figure 4 and listed in Table 1. The surface area is a measure of the total, internal damage suffered by a specific bumper, and it has implications for a shield's long-term performance and integrity. Note the large surface area destroyed during the contiguous-foil experiments (Group I). For a detailed discussion refer to text.

24 INTENTIONALLY BLANK

significantly less damage to the mesh bumper results from projectiles traveling at  $< 2$  km/s compared to the damage resulting from projectiles traveling at  $> 4$  km/s; most, but not all, experiments between 4 and 6 km/s exhibited modest velocity dependence as well.

Referring to the Group D experiments in which we varied the separation distance at constant bumper mass -- except for 996/997 with five meshes as opposed to the ten meshes of all others -- and essentially constant velocity, we observe significant effects in this cumulative damage parameter. The larger the separation distance, the smaller the cumulative surface area damaged. This observation substantiates -- in a cumulative sense -- the interpretations offered in association with Figure 4 that the total damage suffered is not related to a constant dispersion geometry of the debris cloud, but only to its energetic, central portion. Increasingly larger fractions of the peripheral cloud are being progressively dispersed with increasing separation distance, to the effect that they can be terminated by very lightweight stack members.

Not surprisingly, the metallic impactors (Group H) produce relatively little damage, except for the high-velocity aluminum projectile (993) which generated a similar degree of total bumper damage as did the glass projectiles. In fact, the aluminum impactor produced modestly more damage ( $58.7 \text{ cm}^2$ ) than the most appropriate glass-analog experiment (990), which destroyed  $36.1 \text{ cm}^2$  of the mesh surface.

As was evident from Figure 4 and the photo-documentation in Appendix, the multiple, contiguous-foil experiments (Group I) are poor performers by this cumulative-damage criterion. The surface area destroyed in the foil series can be an order of magnitude larger when compared to meshes of identical specific mass.

### WITNESS-PLATE OBSERVATIONS

In this section we present a series of photographic plates that illustrates the nature of the debris clouds which exited the mesh stacks and that best serve to compare the diverse experimental conditions. Note that high resolution images of the individual witness plates are part of Appendix, and that considerable detail may have been lost during the production of the illustrations that follow.

All witness-plates were made of annealed, 1100-series aluminum that were  $\sim 30 \text{ cm} \times \sim 30 \text{ cm} \times 3.17 \text{ mm}$  thick; the dimensions may serve as a scale in all witness-plate renditions. The standoff distance (L; the distance from the last mesh or foils to the witness plate) varied (see Table 1); although it remained constant within any experimental group. Therefore, inferences regarding relative dispersion angles derived from inspection of the debris-spray pattern diameter are essentially correct within any given experimental group, yet not necessarily among groups. The plates were blued with water-based ink, a procedure that does not modify the physical properties of the surfaces, and that is vastly superior to traditional paints which tend to chip, delaminate and spall. Obviously, colored surfaces reveal substantially more detail than unpainted, metallic plates. Experiment identification, for possible comparison with the more detailed Appendix illustrations, is given by the number in the upper left-hand corner of each frame.



# Effects of Specific Bumper Mass (SM)

N = Variable  
at  $\approx 5.9$  km/s

N



1  
SM = 0.016

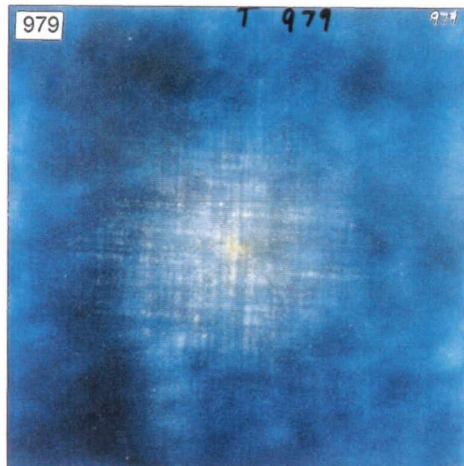


N

5  
SM = 0.08



2  
SM = 0.032



10  
SM = 0.16



3  
SM = 0.048



10  
SM = 0.18

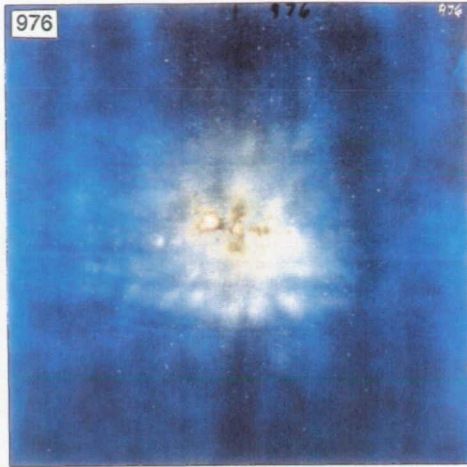
**Figure 6.** Witness-plate spray and damage patterns obtained by stacking an increased number of identical meshes; targets were impacted with soda-lime projectiles at constant velocity. The number in the upper left-hand corner of each frame is the experiment number (See Table 1 or Figure 3 for details). Note as the number of meshes increase from N=1 to N=10 that the degree of projectile comminution increases, while the amount of damage to the witness plate decreases. Experiments 813, 822 and 823 were described by Hörz *et al.* (1992a) and employed cylindrical witness plates, the reason for the ring-like termination of the spray patterns.

# 5 Versus 10 Member Stacks

(Group A)  
 N = 5  
 S = 25.4 mm  
 SM = 0.08 g/cm<sup>2</sup>

(Group B)  
 N = 10  
 S = 25.4 mm  
 SM = 0.16 g/cm<sup>2</sup>

km/s



km/s

4.28

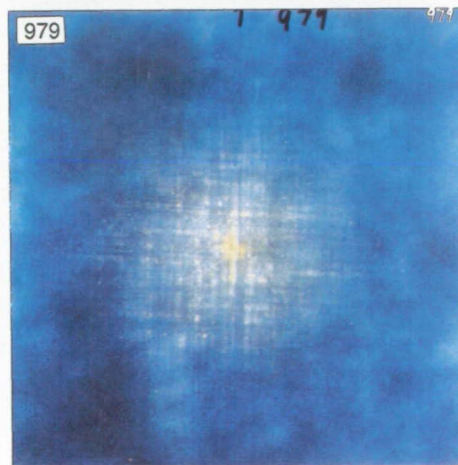
4.41

5.25



5.12

5.89



5.86

**Figure 7.** Comparison of five- and ten-member mesh stacks, at otherwise identical impact conditions, except projectile velocities. Note the increased comminution of the projectile by the ten-member bumpers. Note also the progressively higher comminution efficiency with increasing velocity.

# Effects of Mesh-Opening

**(Group B)**  
 M = 3.17 mm  
 N = 10  
 S = 25.4 mm  
 SM = 0.16 g/cm<sup>2</sup>

**(Group C)**  
 M = 1.59 mm  
 N = 10  
 S = 25.4 mm  
 SM = 0.18 g/cm<sup>2</sup>

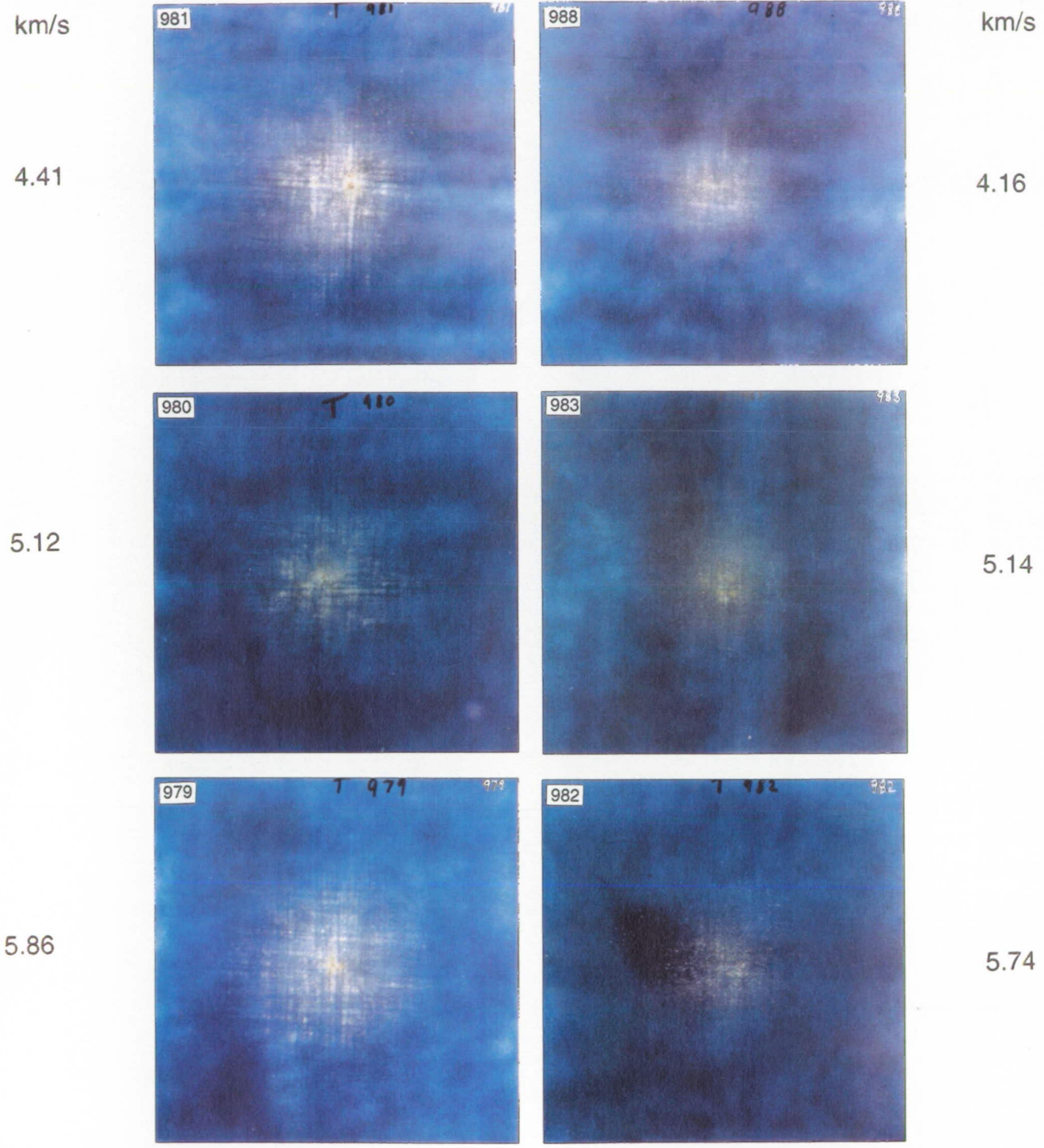


**Figure 8.** Illustration showing the effects of mesh opening at three different velocities. Note that less mass is reaching the witness plate for all Group C experiments, which employed the finer commercial mesh of M=1.59 mm (0.5 D<sub>p</sub>). The Group C experiments also generated finer-grained debris.

Figure 6 presents an overview of what happens when increasingly larger numbers of meshes are stacked, with all other conditions remaining constant ( $S = 25.4$  mm). Not surprisingly, the increasing numbers of interactions with subsequent meshes result in systematically progressive comminution of the debris cloud. Furthermore, the mass asymmetries of the actual (random) impact point on the first mesh are systematically homogenized by the subsequent mesh interactions, yielding debris clouds that have progressively more homogeneous fragment-size, mass and energy distributions. The unfavorable, local energy concentrations and lumpy nature of the debris cloud produced during the impact with a single mesh progress toward the desirable conditions of a relatively homogeneous cloud. Note that the total specific bumper mass (SM) in all experiments is substantially smaller than that of the glass projectile ( $0.467$  g/cm<sup>2</sup>). Thus, these are indeed lightweight bumpers.

Experiments 979 and 982 (Figure 6) employed the two different commercial meshes (see Figure 3 or Table 1) that differ primarily in mesh size ( $M_{979} = 1.0 D_p$  and  $M_{982} = 0.5 D_p$ ) at nearly identical specific areal mass. It can be seen that the larger number of interactions afforded by the finer mesh results in superior performance. Note in Appendix that meshes nine and ten are essentially undamaged in 982.

Following the overview presented in Figure 6, we now return to the experimental matrix to systematically present the effects of the major variables that characterize Groups A-I. Figure 7 illustrates the results of the Group A and B experiments, Group A utilizing five-mesh stacks, while Group B employed ten-mesh stacks. It is apparent that the ten-member stacks permitted the passage of fewer particles of less mass, attesting to the increased debris comminution by the ten-member stack. Note the occasional large crater and the local clustering of craters in the Group A experiments, which was substantially reduced by the ten-member stacks. Although these patterns are difficult to quantify, there is no question -- from inspection of the original witness plates -- that less mass exited the ten-mesh stacks compared to the five-member stacks; this is true at all three velocities. Compare these experiments with 813 of Figure 6 to gain some appreciation about the efficiency of comminution due to multiple-mesh interactions.

Figure 8 compares the witness plates of the Group B experiments with those from Group C; the major difference being the mesh opening (M). Note that the finer-weave meshes resulted in still finer-grained debris particles and that significantly less mass exited the target stack. Again, somewhat finer and less widely dispersed debris clouds characterize the high-velocity experiments. [Photographic procedures are responsible for an artifact in the 5.1 km/s frames that portrays less widely dispersed ejecta relative to either the lower- or higher-velocity experiments. Detailed inspection of the original plates negates this impression and results in fairly similar dispersion angles within a specific group.] Group C experiments systematically produce smaller footprints than the Group B experiments. As the specific bumper mass is similar for the Group B and C experiments, we conclude that most of the observed differences are caused by the finer meshes. These finer meshes offer substantially more interactions with the expanding debris cloud. Recall from Figure 4 that meshes nine and ten were only minimally damaged, if at all, for the Group C experiments. Consequently, the witness-plate damage largely reflects the stack's physical transparency to fine-grained particles. Undoubtedly, the finer meshes outperformed their coarser counterparts.

Figure 9 displays the witness plates associated with the Group D experiments, all employing the fine meshes that were intended to explore the effects of separation distance (S) at essentially constant velocity (~5.8 km/s). The shortest separation distance (S = 12.7 mm) resulted in distinctly lumpy crater clusters that are less prominent at intermediate S values (982) and which completely disappear for S = 50.8 mm (990). Recall that experiment 996/997 that used the largest S (101.8 mm) only contained five meshes. Nevertheless, it is important to note that the 5<sup>th</sup> and last meshes was barely damaged (see Figure 4 and Appendix) during the experiment, whereas the 10<sup>th</sup> mesh of experiment 989 possessed a substantial penetration hole. Experiment 990 represents what should be considered as an ideal result in that the latter meshes (*i.e.*, 8, 9 and 10) remained essentially undamaged, only transmitting an extremely fine-grained, widely dispersed debris cloud to the witness plate. This resulted in the highly desirable condition of low specific energy (ergs/cm<sup>2</sup>) having to be absorbed by the witness plate (flight system). It seems clear that the separation distance is the *most* crucial parameter for any collisional bumper that employs multiple-target members at otherwise constant conditions.

The effects of projectile velocity are illustrated in Figure 10, which shows the witness plates associated with the Group E experiments that employed the superior target configuration, as defined by this study (*i.e.*, fine meshes, S = 50.8 mm, and ten-member stacks). Experiment 990 is reintroduced and compared to experiments conducted at velocities of ~1 and 2 km/s. As previously mentioned, higher velocities result in more comminution and fragmentation. However, the substantial disintegration of the entire projectile at all velocities reinforces our earlier conclusion that multiple-mesh stacks perform extremely well over a wide range of velocities. The performance of these multiple-mesh bumpers over a wide velocity range, yet specifically at low velocities, seems excellent, at least for silicate impactors.

Figure 11 portrays the Group F experiments where each target was composed of five custom-made, identical meshes per stack so that the wire thickness (and therefore, SM) and the impact velocity are the major variables. Because of the substantially increased bumper mass, five-member stacks were deemed sufficient for these experiments; separation distance of 25.4 mm was used in order to permit comparison with the Group A experiments, the latter representing the lowest areal mass (975). As can be seen in this figure, the bumper mass can become so large as to effectively result in an opaque bumper (3435 and 1008) that prevents fragments from reaching the witness plate. The actual value of SM for such cases (1.688 g/cm<sup>2</sup>) converts into a single, continuous aluminum sheet ~6.2 mm thick that would have readily been penetrated by the high-velocity projectile resulting in some damage of the witness plate (see corresponding witness plates in Hörz *et al.*, 1992a; Figure 6). This comparison suggests that even relatively massive multiple-mesh stacks significantly outperform equally massive, continuous single bumpers. While a modest velocity dependence is undeniable, multiple-mesh bumpers are less sensitive to impact velocity than continuous bumpers, and perform particularly well at low velocities, at least for silicate impactors. Furthermore, massive mesh stacks can be non-transparent at specific masses that are smaller than those characterizing the ballistic limits of single membranes.

Nevertheless, the most significant conclusion we reach when comparing the Group F experiments with those of Groups A-E is that very massive-mesh bumpers do not necessarily



# Effects of Separation Distance (S)

(Group D)

$V \approx 5/8 \text{ km/s}$

$N = 10$

$SM = 0.18 \text{ g/cm}^2$

S  
(mm)

12.7



S  
(mm)

25.4

50.8



101.6

$N = 5$   
 $SM = 0.09$

**Figure 9.** Illustration of the effects of separation distance (S), at otherwise constant impact conditions (except for experiment 996 that only employed five meshes). Note that 990 resulted in an almost opaque stack, as evidenced by the minimal damage to the witness plate. Experiment 990 resulted in the best overall performance among all experimental configurations in this study.

# Effects of Velocity

(Group E)  
N = 10  
S = 50.8 mm  
SM = 0.18 g/cm<sup>2</sup>

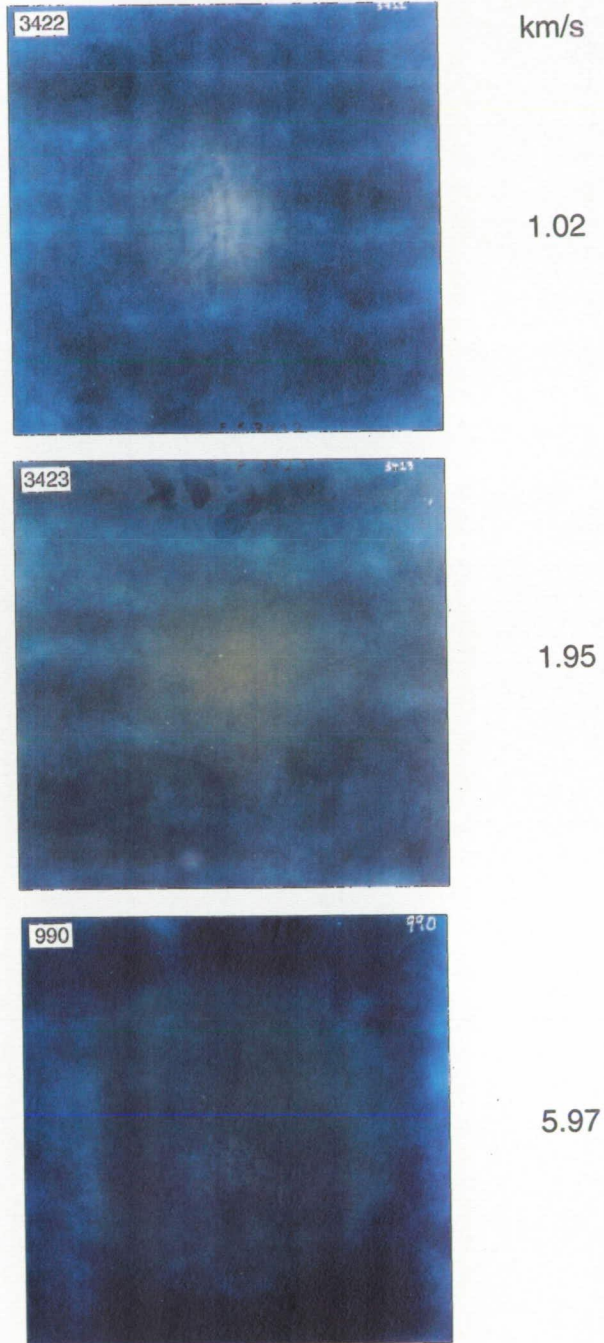


**Figure 10.** The effects of velocity at otherwise constant target and impact conditions employing ten-member, identical mesh stacks. Note that the soda-lime glass spheres are substantially disintegrated at low velocity, suggesting the stacks may be particularly attractive bumpers at low encounter velocities.



result in the most superior bumpers, except for the extreme, totally opaque case. The five-member stack experiments employing the lightweight, commercial meshes already lead to qualitatively similar projectile comminution and witness plate damage (e.g., Figure 6 and 7, or 996 in Figure 9). More importantly, many of the ten-mesh experiments, all containing less bumper mass than each of the Group F experiments, result in superior performance. Most notably, experiment 990 (see Figure 9) resulted in a nearly opaque bumper at some factor of nine less mass compared to 1008 (Figure 11), and at ~12 times less mass than that characterizing the ballistic limit of single sheets. We concur with previous studies (e.g., Dickinson, 1987; Cour-Palais and Crews, 1990 or Christiansen, 1990; 1992) that it is not necessary to employ massive continuous or discontinuous target components, if multiple collisions are permitted. Relatively modest material thicknesses will suffice to accomplish significant fragmentation, dispersion and deceleration of the projectile.

Figure 12 contains photographs of the witness plates resulting from the Group G experiments which employed a mixture of different meshes, similar, yet not identical, to those conceptualized in Figure 1. Again, a separation distance of 25.4 mm was utilized to facilitate direct comparison with the Group F experiments. By and large, the mixed-mesh experiments exhibited a relatively poor performance compared to all other experiments, yet they were still superior to single-plate bumpers of equivalent mass (Hörz *et al.*, 1992a). As evidenced by the occasional large-fragment impact at radial ranges beyond the major spray pattern (e.g., 3428 or 1004), and especially from the size and nature of the penetration holes (see Appendix), we postulate that the primary impact into the initial massive grid produces a number of relatively large fragments that are capable of penetrating the remaining, more delicate meshes and reaching the witness plate. This process may also have affected the witness plates of the Group F experiments illustrates in Figure 11. The mass dislodged by collisions with single meshes or contiguous membranes may well exceed the initial impactor's mass, as described by many (Hohler *et al.*, 1975; Cour-Palais, 1987). For a direct comparison with analog experiments consult Hörz *et al.* (1992a). Thick targets tend to shed debris of sufficient size and frequency to produce noticeable witness-plate damage. Indeed, bumper-derived debris dominates the witness plates in most cases where the bumper mass is larger than the specific mass of the impactor. Consequently, optimum bumper designs demand careful and deliberate trade-offs between the degree of projectile comminution and the total mass displaced from the bumper itself. Relatively thin targets suffice to severely disrupt the impactors.

The Group H and I experiments were conceived to initiate comparison of the present experiments with the ongoing collisional-bumper developments by others. The number of experiments performed during this phase of our investigation is small, rendering such comparisons as incomplete and tentative at best.

The Group H experiments employed projectiles other than our standard soda-lime glass spheres. Most traditional bumper developments utilize metal impactors, in particular aluminum. We justify the use of silicate projectiles for two reasons: (1) Natural silicate impactors are still the dominant projectile species in LEO for particle sizes <1 mm, with the possible exception of very small (<10  $\mu\text{m}$ ) particles, a conclusion that is based on direct compositional analysis of impactor fragments or melts in microcraters retrieved from space (e.g., Bernhard *et al.*, 1992). (b) A substantial database of continuous thin-film penetrations by soda-lime glass projectiles exists





# Effects of Specific Bumper Mass (SM)

(Group F)  
N = 5

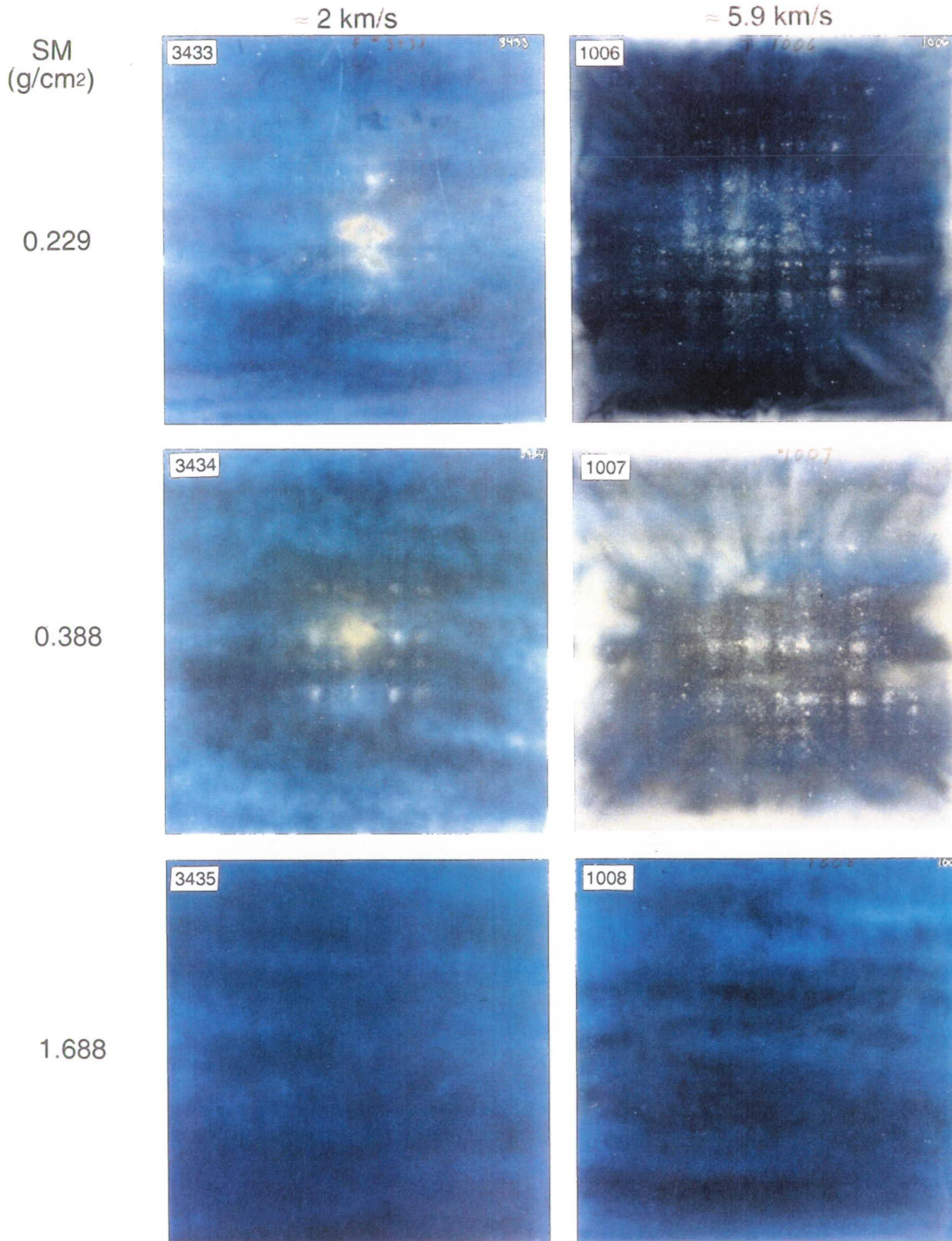


**Figure 11.** Illustrates the results of impacts at 2 and 5.9 km/s into five-member stacks of substantially different specific mass (SM). Note that the more massive stacks (SM=1.688 g/cm<sup>2</sup>) effectively resulted in opaque shields (*i.e.*, little or no damage to the witness plate). Note also that the low-velocity experiments resulted in respectable comminution and deceleration of the soda-lime projectiles, suggesting less dependence on velocity than those reported from ballistic limit studies of contiguous, single bumpers.

42, 43

# Mixed Mesh Experiments

(Group G)

N = Variable

S = 25.4 mm

≈ 2 km/s

≈ 5.9 km/s

SM  
(g/cm<sup>2</sup>)



0.0799  
N = 3



SM  
(g/cm<sup>2</sup>)

0.0799  
N = 3

0.1579  
N = 4



0.1579  
N = 4

0.4951  
N = 5



0.4951  
N = 5

**Figure 12.** Illustrates the results of impacts at 2 and 5.9 km/s into *mixed-mesh* stacks; each stack consisted of a different number of meshes of very different specific mass resulting in a wide range of total cumulative bumper mass (SM). It is clear that more fragments and mass exit the low-mass designs compared to the more massive, five-member stacks. Note that numerous bumper fragments must have reached the witness plates compared to the commercial mesh experiments (e.g., 990), indicating that more massive bumpers are not necessarily advantageous.

(Hörz *et al.*, 1992b), offering internal consistency and direct comparison among diverse target configurations. Unquestionably, the physical properties of the impactors are significant, and extensive experiments with mesh stacks and metal impactors will have to be performed in the future.

The witness plates associated with the three aluminum and one stainless-steel projectile experiments can be seen in Figure 13. All projectiles were 3.17 mm (1/8") in diameter, the same as the soda-lime glass spheres. The target configuration used in these experiments was the same as the one that provided the best results from the various glass-projectile experiments (*i.e.*, the finest mesh and S of 50.8 mm; same as Group E). At low velocities (3424 and 3425), the aluminum projectiles completely penetrated the mesh stack without undergoing significant fragmentation. Nevertheless, the witness-plate crater in the 2 km/s experiment does indicate some degree of projectile fragmentation; the resulting crater diameter is larger, and the crater depth is shallower than that associated with the "normal" crater case of 3424. Note, however, that the high-velocity experiment (993) resulted in the total destruction of the aluminum projectile and a thin deposit of aluminum on the witness plate. The witness plate indicates that the aluminum projectile was completely molten at conditions where the glass projectiles still contained some discernible particulates, either melt droplets or solids. Examination of the witness plates in Figure 13 reveals that the ten-mesh stack performed as an effect bumper for aluminum projectiles at 5.8 km/s impact velocities. In contrast, the 4.6 km/s steel projectile (995) passed through the stack while generating only a few small fragments.

These four experiments graphically demonstrate the substantial difference in the collisional fragmentation behavior of silicates and diverse metals, especially at low velocities and low-peak stresses. We are neither surprised by these results, nor do we perceive them as greatly detrimental to the concept of multiple-mesh shielding. The observed trends are germane to all bumper developments. For the sake of internal consistency, we employed only one target material (aluminum), yet we do not wish to imply that aluminum is the best material for the manufacture of mesh bumpers. An important part of the ongoing, contiguous-shield development relates to the identification of particularly suited materials; similar efforts to identify the most suitable wire materials for mesh bumpers should be initiated as well.

The Group I experiments, illustrated in Figure 14, were carried out in order to permit first-order comparisons with multiple-foil shields like those investigated by Dickinson *et al.* (1987) or Cour-Palais and Crews (1990), for example. As best as was possible using commercial products, we scaled the specific mass of the foils to that of the meshes by choosing 75  $\mu\text{m}$  thick aluminum foils (1100 series; not as good a choice as 6061 series), each foil having a specific mass of 0.02  $\text{g}/\text{cm}^2$ , which is slightly more than our finest mesh (0.018  $\text{g}/\text{cm}^2$ ). Foil experiment 3426 is equivalent to mesh experiment 3423 (Figure 10). In both cases, little mass reached the witness plate, although the meshes appeared to have done better at dispersing the debris cloud. Although the area damaged on the witness plate was smaller for the multiple-foil case, the severity of that damage was much greater. The high-velocity experiment (999) is the foil analog to mesh experiment 990 (Figure 9). As can be seen in Figure 14, the 999 witness plate is totally devoid of any damage; in fact, foils 8, 9 and 10 were not penetrated, rendering the entire stack opaque. While mesh experiment 990 resulted in no damage to meshes 8, 9 and 10, it did permit the







# Metal Impactors

(Group H)

N = 10

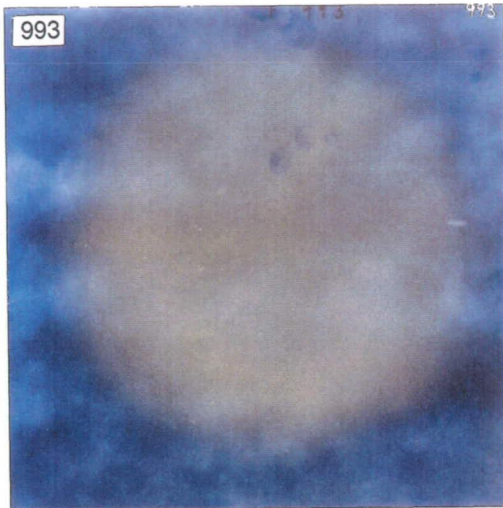
S = 25.4 mm

SM = 0.18 g/cm<sup>2</sup>

Aluminum  
0.99 km/s



Aluminum  
5.76 km/s



Aluminum  
1.95 km/s



Steel  
4.59 km/s



**Figure 13.** Witness plate damage produced by aluminum and stainless-steel projectiles that interacted with ten-member stacks identical to that of experiment 990, which result in the best performance for the soda-lime glass projectiles. Note that at low velocity, only minor fragmentation of the aluminum impactor occurred, while at higher velocities (5.76 km/s) the aluminum projectiles seems to have completely atomized resulting in a prominent deposit of vaporized or molten material on the witness plate. The stainless-steel projectile plowed through the entire ten-member stack remaining virtually intact, and exited with sufficient energy to penetrate the 3.17 mm thick aluminum witness plate.

48, 49

# Multiple Foil Experiments

(Group I)  
S = 50.8 mm

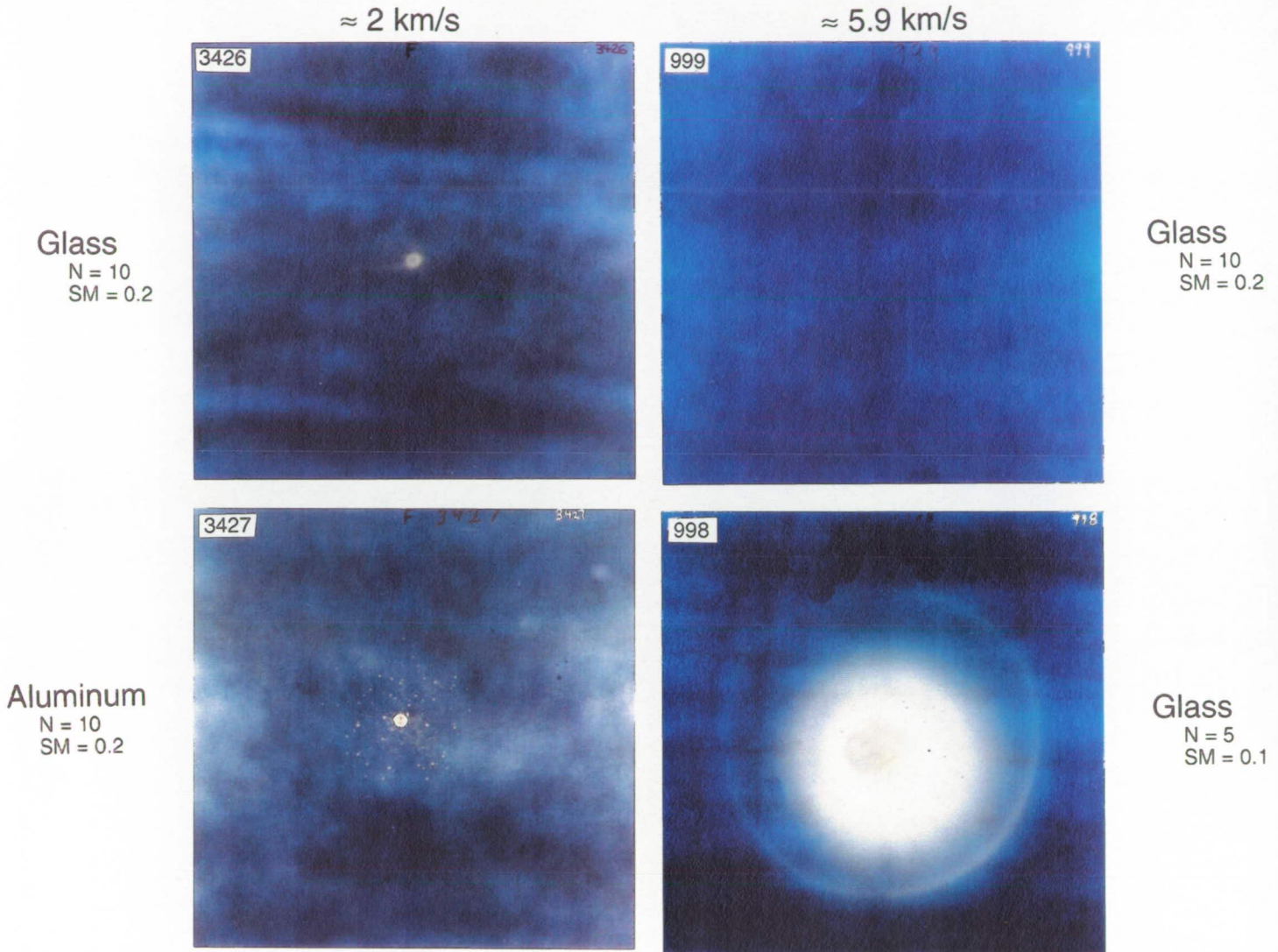


**Figure 14.** Witness plates documenting the debris generated by ten-member, contiguous (aluminum) foil stacks that possessed comparable specific mass ( $0.2 \text{ g/cm}^2$ ) to many of the mesh stacks ( $0.16 - 0.18 \text{ g/cm}^2$ ). Clearly, the contiguous foils terminate the peripheral parts of the debris cloud with higher efficiency reducing the total damage to the witness plate (e.g., 3426) or totally eliminating the witness-plate damage (e.g., 999), resulting from glass impactors. Compare witness plates 3422 and 990 (Figure 10) with witness plate 3427 and note that there is no significant difference between the discontinuous and continuous designs regarding the comminution efficiency of low-velocity aluminum projectiles. Experiment 996 (Figure 9) is the analog for experiment 998. Contiguous foil targets lead to massive deposits of vaporized or molten materials that impinged upon the witness plate with high specific energies causing substantial erosion and mass removal, as evidenced by the central depression within the witness plate. Experiment 998 employed an S of 101.8 mm.

passage of very fine-grained debris. Foil experiment 998 is the equivalent of mesh experiment 996/997 (Figure 9), both employing the largest separation distance ( $S = 101$  mm) and only five target members in each stack. The most striking phenomenon on the 998 foil witness plate is the deposition of aluminum melts/vapors, and only a few, widely dispersed, small craters. Although it is not discernible in the photograph, witness plate 998 possesses a central area that is noticeably eroded and of greater relief than the initial surface. The clear impression is that the deposition process was energetic.

In Figure 14, experiment 3426 is the glass-analog experiment to the low-velocity ( $\sim 2$  km/s), aluminum-projectile, ten-foil experiment (3427), while experiment 3423 (Figure 1) is its mesh equivalent. Examination of witness-plate 3427 shows that the foils did not fragment the low-velocity aluminum projectile, unlike experiments 3426 and 3423. This comparison illuminates the substantial difference in the collisional behavior of silicates and metals at low velocities more than the performance of different bumper designs.

## MASS CONSIDERATIONS

The results of all weight measurements are summarized in Figure 15. The data refer to the entire mesh stack, with detailed measurements pertaining to individual meshes, where applicable, contained in Table 1. We deliberately present absolute masses, rather than values normalized to the impactor's mass ( $M_p$ ); the latter was 0.037 g for the soda-lime glass spheres.

### SPECIFIC AREAL BUMPER MASS (SM)

As some of the interpretations and implications relate to the total specific areal mass (SM), we plotted this parameter in the first column; the specific areal mass for the glass impactors was  $0.467$  g/cm<sup>2</sup>. Examination of SM in Figure 15 illustrates that most of the target configurations contained  $<50\%$  the mass of the associated projectiles. Only two experiments (3432 and 1004) possess SM values similar to that of the impactor, while two additional experiments (3435 and 1008) had larger masses; none approached specific masses that are typical for the ballistic limit of single aluminum plates (*i.e.*,  $\sim 3$  g/cm<sup>2</sup> at 6 km/s). Note that attempts were made to perform the majority of experiments at constant SM, between  $0.16$  and  $0.2$  g/cm<sup>2</sup>, so that other variables could be isolated and addressed.

### TOTAL BUMPER MASS LOST ( $M_t$ )

This parameter represents the total mass that was physically removed (*i.e.*, lost) from the entire target stack; it is the sum of the weight difference (the mass before impact minus the mass after impact) before and after an experiment, for all bumper elements. Typical values of  $M_t$  for the lightweight stacks range between  $0.15$  and  $0.25$  g, which constitutes  $\sim 4$  to  $7$  times the projectile mass. These values are smaller than those typical for craters or single-sheet penetrations close to the ballistic limit (Hörz *et al.*, 1992a).

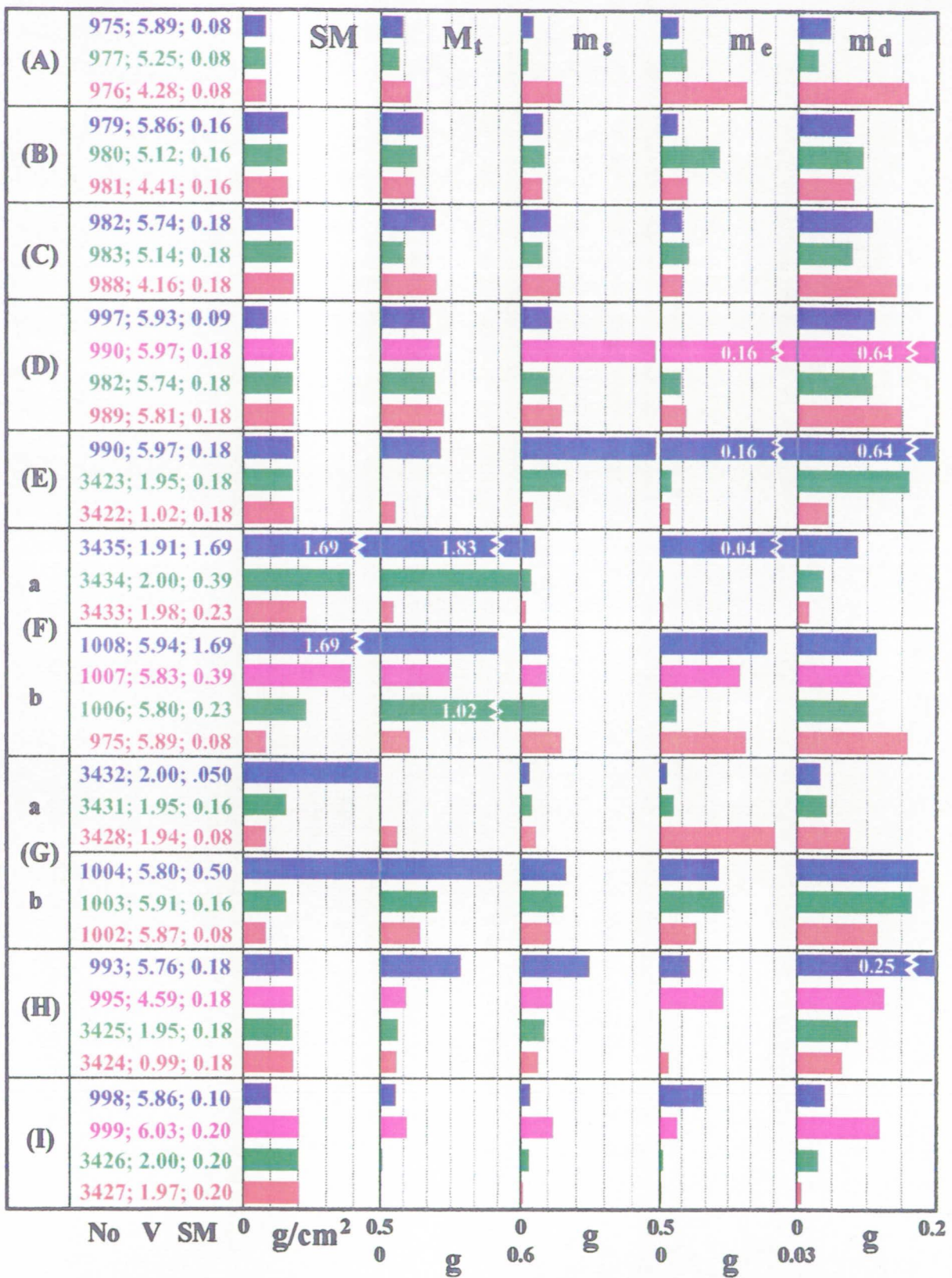


Figure 15. Summary of all mass measurements. The initial bumper mass (SM) is plotted to illustrate its relationship with certain mass-related results.  $M_t$  is the total mass loss of the entire stack as determined by weight difference. Note that  $M_t$  for the commercial mesh stacks (Groups A-E) equals between 5 to 7 times the mass of the projectile (0.037 g). Columns  $m_s$  and  $m_e$  refer to the recovered spall and ejecta particulates, respectively, while  $m_d$  equals the sum of  $m_s$  and  $m_e$ . Note the different scales at the bottom, especially for  $m_s$  and  $m_e$ , which illustrates the dominance of particles generated by collisions with the multiple meshes, whereas the ejecta are largely derived from the first mesh.  $m_d$  was typically 4 to 6 times larger than the projectile mass for Groups A-E, suggesting relatively good performance of multiple stacks compared to single bumper designs (Hörz *et al.*, 1992b).

Examination of  $M_t$  for Group A and B suggests that the removed mass relates to the specific bumper mass, an observation that was expected from, and that is totally consistent with single-mesh and foil penetrations (Hörz *et al.*, 1992a and 1992b). This observation is also corroborated by the massive Group F and G targets, although we do not understand the unusually large mass loss of experiment 1006, which perturbs otherwise systematic trends within Group F. The low-velocity experiments do not yield good  $M_t$  values, because substantial mass from powder-combustion products, and possibly from vaporized sabot material can enter the impact chamber and be deposited onto the targets. In fact, there were a few cases where such deposits lead to an apparent mass increase for some meshes, which is obviously a misleading result and the reason why some experiments do not have an entry for  $M_t$  (*e.g.*, 3423). The interior of the light-gas gun in the Experimental Impact Facility at JSC is exceptionally clean, and the masses are not affected by any undesirable contamination. Despite these differences, the 2 km/s impacts typically exhibited less mass losses than the >4 km/s cases, yet no clear cut velocity dependence of  $M_t$  can be extracted between 4 and 6 km/s (*i.e.*, see the Group A, B and D experiments at constant bumper mass). In addition, there is no apparent trend for  $M_t$  in those experiments where the separation distance (Group D) was varied. Of significance is the lower mass loss associated with the contiguous-foil experiments (Group I), when compared to the mesh experiments of comparable bumper mass, despite the gapping penetration holes within the foils.

The above observations, especially those relating to contiguous foils, serve to emphasize that there is not a systematic relationship between the physically displaced mass and the size of penetration holes in our experiments. We initiated these mass measurements in support of the dimensional-hole analyses, expecting that such a relationship exists and that it could be quantified. This expectation was based on the systematic relationships between crater diameter and displaced volume or mass (Holsapple and Schmidt, 1987). In any case, our penetration holes are dominated by an expanding debris plume that encountered relatively thin targets which largely responded by plastic and/or brittle deformation, with minimal mass loss. As a result, we do not presently believe  $M_t$  to be an important criterion when evaluating the performance of bumpers; the cumulative hole area (Figure 4) seems more significant.

#### MASS OF RECOVERED PARTICULATES

The columns headed with  $m_s$  (*i.e.*, downrange spall products) and  $m_e$ , (*i.e.*, up-range ejecta products) represent the total particulate mass that was recovered from the rear and front compartments of the target box, respectively (see Figure 2). The parameter  $m_d$  represents the sum of  $m_s$  and  $m_e$ , or the total mass of particulates that may be reintroduced into the space environment as potentially hazardous orbital debris. Note the different absolute-mass scales for  $m_s$ , and  $m_e$ . The following trends are observed: (1)  $m_s$  is much larger than  $m_e$ , generally by an order of magnitude; (2) the total recovered mass ( $m_d$ ) is typically <0.2 g (*i.e.*, generally between 2-5 times the mass of the projectile). The latter values are akin to the those obtained for single-plate and mesh penetrations close to the ballistic limit (see Figure 27 and 28 in Hörz *et al.*, 1992a).

In detail, a modest velocity dependence is suggested by comparing Groups  $F_a$  and  $G_a$  with Groups  $F_b$  and  $G_b$ , or within the Group E experiments. These experiments indicate that less mass

will be liberated at lower impact velocities. Unfortunately, this trend is contradicted by the Group A and -- to an extent -- Group B experiments. Furthermore, there does not appear to be a systematic relationship between  $m_d$  and SM, except in the case of the Group G experiments, where the SM-dependent trends for the low-velocity group ( $G_a$ ) are opposite to those associated with the high-velocity group ( $G_b$ ).

Experiment 990 is an exception as far as liberated mass is concerned. Earlier, experiment 990 was singled out as representing the best initial conditions for our multiple-mesh experiments, resulting in minimal damage to the witness plate. It is exceptional in both  $m_s$  and  $m_e$ , the reason we accept the results as correct. Nevertheless, a repeat experiment is needed to verify the anomalously high  $m_s$  and  $m_e$ . On the other hand, the maximum comminution (witness-plate evidence) associated with this experiment is certainly suggestive of unusually intense interactions with the meshes that apparently liberated an unusually large number of particles from the bumper itself.

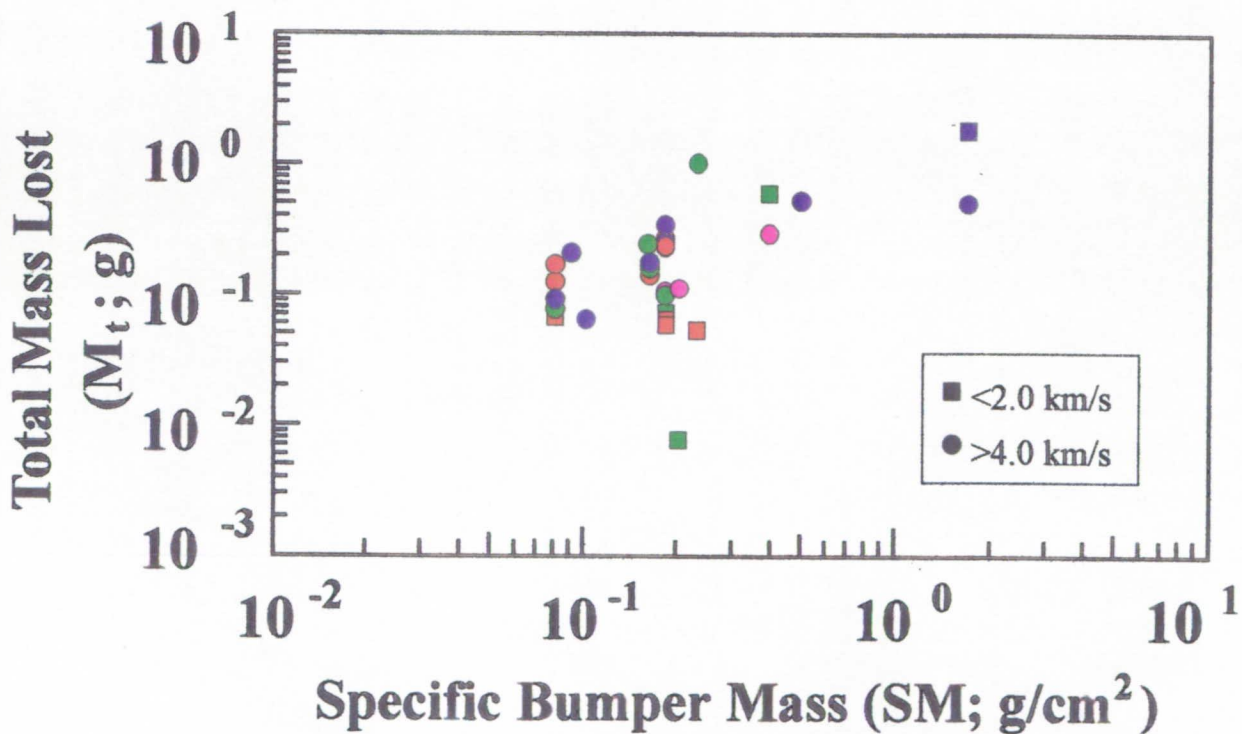


Figure 16. Total mass lost from the entire stack plotted as a function of specific bumper mass. Note that the loss can be kept constant by design, within reason, despite substantial variation in the total bumper mass. Data point colors and shapes can be utilized to determine associated experiment number in previous plots (*i.e.*, Figures 4, 5 and 15).

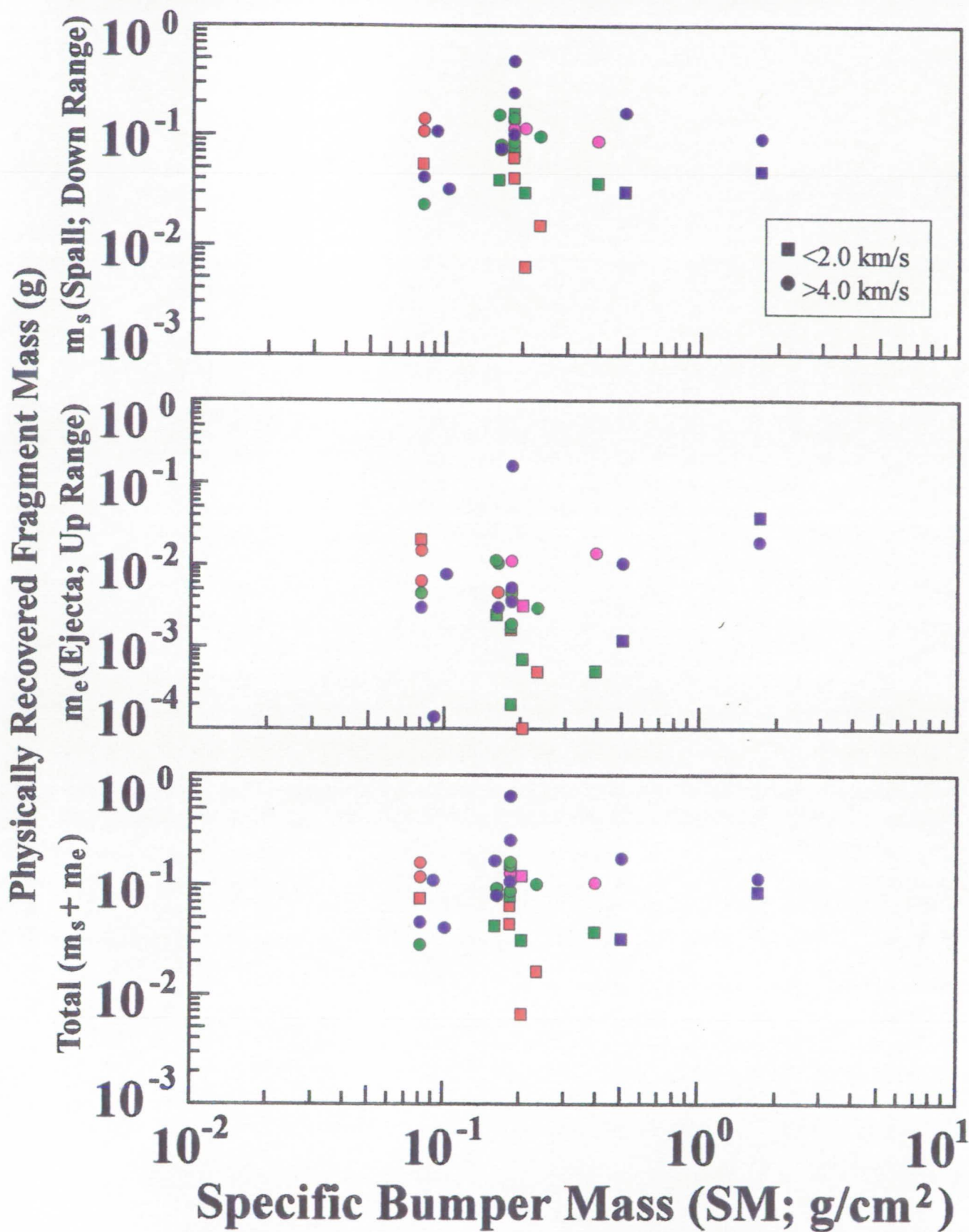


Figure 17. Specific bumper mass versus displaced spall mass ( $m_s$ ), ejecta mass ( $m_e$ ) and the sum of  $m_s$  and  $m_e$  (*i.e.*,  $m_d$ ). Again, note a relatively constant displaced mass seems possible for a wide range of absolute bumper masses. Data point colors and shapes can be utilized to determine associated experiment number in previous plots (*i.e.*, Figures 4, 5, and 15).

The set of mass data contained in Figure 15 is re-plotted in Figures 16 and 17 for ease of comparison with identical plots (*i.e.*, Figure 25, 26 and 27) of Hörz *et al.*, 1992a. Because the present data scatter widely, and because it is difficult to track each datum, only a few general comments are offered. Figure 16 illustrates that any fitting procedure to the data set would result in some modest dependency of total mass lost ( $M_t$ ) to the specific bumper mass (SM). The slope of such a fit would be shallower than that characterizing specific sets of closely related experiments, as illustrated in Figure 15 or Figure 25 of Hörz *et al.* (1992a). We conclude from Figure 16 that  $M_t$  modestly depends on the total shield mass, yet little on the specific bumper design. Conversely, Figure 16 suggests that the total mass lost may be held constant (possibly at minimum -- by design) over a significant range of specific bumper masses. Furthermore, the relative masses ( $M_t/m_p$ ) of the multiple-stack experiments are not dramatically different from those of single-plate or mesh penetrations (see Figure 25 of Hörz *et al.*, 1992a).

Comparing Figure 17 with Figures 26 and 27 from our previous report we again note that no dramatic and unexpected increases occurred for spall ( $m_s$ ), ejecta mass ( $m_e$ ) and their combined total ( $m_d$ ). Nevertheless, the dislodged masses for multiple-stack designs are less sensitively related to SM than are the single-foil or mesh penetrations. We ascribe this to numerous collisions by predominantly small impactor fragments. The lowest displaced mass ( $m_d = 5 \times 10^{-3}$  at SM = 0.2) is associated with low-velocity experiment 3427, while the largest displaced mass ( $m_d = 0.64$ ) is associated with experiment 990. This relative insensitivity of liberated mass to shield mass entails -- in practical terms -- that one can design multiple-collision shields over a wide range of specific mass without too much concern for the amount liberated particulates. The corollary conclusion is equally valid from Figure 17, that a variety of options exist to reduce the amount of liberated particulates at constant shield mass.

## DISCUSSION

The purpose of this concept study was to determine the usefulness of multiple-meshes bumpers in comminuting, dispersing and decelerating glass projectiles traveling at velocities of 1 to 6 km/s. The respective roles of impact speed (V), mesh opening (M), separation distance (S), wire thickness (T) and associated specific areal bumper mass (SM) were investigated. Criteria to evaluate the performance of specific designs, in order of significance, focused on an assessment of the damage suffered by massive witness plates (*i.e.*, simulated flight-systems), the measurement of total mass displaced from the test article, and the total damage suffered by the mesh stack determined from diameter measurements of successive penetration holes. The purpose of this report is to document the experimental products and some first-order results. Where appropriate, we offered interpretations and defined general trends during the description of these experiments; the latter will not be summarized here. The purpose of this discussion is to compare the current findings with other lightweight collisional bumpers and to establish the basic utility of multiple-mesh stacks.

Leading candidates for lightweight collisional shields also employ multiple bumper elements. Such bumpers have demonstrated that successive penetrations of relatively thin membranes are especially beneficial, because successive shocks in the projectile and its fragments produce more



efficient comminution, dispersion and deceleration of the debris clouds compared to single-sheet penetrations. The leading candidates are designated "MS" (Multiple Shock; Cour-Palais and Crews, 1990) and "MDB" (Mesh-Double Bumper; Christiansen, 1990) shields; note that the latter contains a single mesh at the projectile entrance side. Fully developed and optimized versions of these designs, including ballistic limit curves, are presented in Christiansen (1993, MS designs) and Christiansen and Kerr (1993; MDB design). These designs provide completely opaque shields at specific areal masses of  $\sim 0.32 \text{ g/cm}^2$  (MDB) and  $0.31 \text{ g/cm}^2$  (MS) for 3.175 mm diameter projectiles of aluminum at  $\sim 6 \text{ km/s}$ . Complete opaqueness is largely accomplished by relatively thick, contiguous "rear" walls that terminate all fragments exiting the preceding bumper. This rear wall typically weighs some  $0.135 \text{ g/cm}^2$ , thus leaving masses for the bumper only component that are akin to those used in the present mesh stacks. The primary criterion to judge bumper performance during the development of the MS and MDB designs related to the degree of deformation, especially prospective perforation, of the rear wall. This makes comparison with our "massive" witness plates somewhat conjectural, as one must translate crater size on an infinite halfspace witness plate into a penetration event of the MS and MDB rear walls, which were typically about 0.5 mm thick. There is little doubt that some of the debris clouds generated by our mesh stacks would *not* have penetrated this rear wall (e.g., experiment 990).

It is important to note that the overall depth of current MS and MDB designs is substantially smaller, typically some  $30 D_p$ , compared to typical stack depths of 70 to  $150 D_p$  used in the present experiments. This substantially affects the separation distance (S), and the MS and MDB designs are distinctly more compact than the majority of our mesh experiments, a possible advantage in the engineering and implementation of bumpers. On the other hand, the MS and MDB designs -- unlike the current mesh stacks -- fully utilize and substantially rely on lightweight, nonmetallic materials, selected for highly favorable dynamic properties per unit mass. If meshes were to be fabricated from such specialized materials, substantial mass savings could be realized relative to the aluminum wires and commercial window screens employed in this (low-cost) concept study.

The above descriptions and comparisons serve to illustrate that quantitative comparison between the present experiments and the more fully developed MS and MDB shields is inhibited due to different experimental arrangements and conditions. Nevertheless, we note that substantial comminution, dispersion and deceleration of the ensuing debris cloud was accomplished in the present experiments that employed a bumper system of cumulative mass properties comparable to that of the MS and MDB designs. Therefore, we conclude that the current concept studies demonstrate the basic utility of multiple meshes as potential lightweight, collisional shields.

## SUMMARY AND RECOMMENDATIONS

We experimented with multiple meshes as possible collisional bumpers. Direct comparisons with equivalent experiments into single, contiguous bumper plates (Hörz *et al.*, 1992b) and into single-mesh targets (Hörz *et al.*, 1992a) indicates substantial mass savings at equivalent bumper performance. Unfortunately, direct comparison with the multi-shock concepts employing

contiguous membranes (*i.e.*, Cour-Palais and Crews, 1990) and the mesh double-bumper concept (*i.e.*, Christiansen and Kerr, 1993) is not possible because of substantially different experimental set-ups and criteria of evaluation. The limited scope of this effort did not permit experimentation that would make direct comparisons with these concepts possible. We strongly urge that such a quantitative comparison be made. We still maintain that meshes, at equivalent specific bumper mass, can afford thicker bumper elements (*i.e.*, wires) than contiguous foils, potentially affording more thorough comminution, dispersion and deceleration of the impactor. Meshes constructed from Nextel, a ceramic fiber, seem particularly promising and should be explored.

Furthermore, we recommend that future MS and MDB developments include the measurement of hole diameters in the diverse target components, and the collection and measurement of displaced masses. Without question, the damage suffered by the rear wall, currently the exclusive focus of the SM and MDB studies, is the criterion of utmost importance and the deciding factor whether a specific design exhibits acceptable performance characteristics. We documented the displaced mass because it may become a secondary criterion in discriminating between shield designs of equivalent performance; all other things equal one would certainly pick the bumper that generates the least number of displaced particulates. The hole-diameter measurements constitute a minor criteria by comparison. Nevertheless, it may be used to determine the long-term integrity of specific shields.

Lastly, favorable features of the MS, MDB and multiple-mesh stack designs could possibly be combined. It seems simple to replace the last mesh with a contiguous foil in order to render the entire stack as opaque as contiguous shield concepts. Note that this would preserve the favorable property of relatively small, internal shield damage, while providing complete opacity, the potentially most favorable aspect of MS or MDB. In a sense, the MDB design is already such a mixture, and additional hybrids are described by Christiansen (1993).

Clearly, the MS and MDB concepts share with our multiple-mesh stacks the crucial and favorable characteristic of multiple shock interactions (*e.g.*, Gehring, 1970; Richardson, 1970). Such multiple interactions cause increased impactor comminution, and effective dispersion and deceleration. Unquestionably, multiple-collision shields are to be preferred over single-bumper plates.

Table 1a. Light-Gas Gun Experiments.

GROUP	A	A/F <sub>b</sub>	A	B	B	B	C/D	C	C	D	E	H	H	R	D	I	I	G <sub>b</sub>	G <sub>b</sub>	G <sub>b</sub>	F <sub>b</sub>	F <sub>b</sub>	F <sub>b</sub>	F <sub>b</sub>		
EXPERIMENT NUMBER	813	823	823	823	823	823	823	823	823	823	823	823	823	823	823	823	823	823	823	823	823	823	823	823	823	
PROJECTILE																										
Diameter (mm)	3.175	3.175	3.175	3.175	3.175	3.175	3.175	3.175	3.175	3.175	3.175	3.175	3.175	3.175	3.175	3.175	3.175	3.175	3.175	3.175	3.175	3.175	3.175	3.175	3.175	
Specific Mass (g)	0.037	0.037	0.037	0.037	0.037	0.037	0.037	0.037	0.037	0.037	0.037	0.046	0.047	0.130	0.037	0.037	0.037	0.037	0.037	0.037	0.037	0.037	0.037	0.037	0.037	
Material <sup>1</sup>	SL	SL	SL	SL	SL	SL	SL	SL	SL	SL	SL	SL	SL	SL	SL	SL	SL	SL	SL	SL	SL	SL	SL	SL	SL	
Velocity (km/sec)	5.96	6.07	5.77	5.89	5.89	4.28	5.25	5.86	5.12	4.41	5.74	5.14	4.16	5.81	5.97	5.90	5.76	4.59	5.86	6.03	5.87	5.91	5.80	5.83	5.94	
TARGET																										
Arial Mass (g/cm <sup>2</sup> )																										
MESH 1																										
Mesh Opening (mm)	3.175	3.175	3.175	3.175	3.175	3.175	3.175	3.175	3.175	3.175	3.175	3.175	3.175	3.175	3.175	3.175	3.175	3.175	3.175	3.175	3.175	3.175	3.175	3.175	3.175	
Wire Diameter (mm)	0.305	0.305	0.305	0.305	0.305	0.305	0.305	0.305	0.305	0.305	0.305	0.305	0.305	0.305	0.305	0.305	0.305	0.305	0.305	0.305	0.305	0.305	0.305	0.305	0.305	
Mass (loss; g)	0.0014	0.0005	0.0003	0.0013	0.0024	0.0011	0.0008	0.0015	0.0034	0.0025	0.0029	0.0015	0.0016	0.0018	0.0018	0.0039	0.0070	0.0088	0.0010	0.0022	0.0016	0.0013	0.0041	0.0070	0.0094	
Hole Diameter (mm)	3.46	4.51	2.80	6.19	6.19	3.44	5.67	8.24	9.14	11.87	6.51	6.42	6.10	7.14	6.28	6.21	5.33	3.08	3.53	3.67	7.55	11.52	3.18	4.51	11.73	
Shield Mass (g/cm <sup>2</sup> )	0.016	0.016	0.016	0.016	0.016	0.016	0.016	0.016	0.016	0.016	0.016	0.018	0.018	0.018	0.018	0.018	0.018	0.018	0.018	0.018	0.018	0.018	0.018	0.018	0.018	
MESH 2																										
Mesh Opening (mm)	3.175	3.175	3.175	3.175	3.175	3.175	3.175	3.175	3.175	3.175	3.175	3.175	3.175	3.175	3.175	3.175	3.175	3.175	3.175	3.175	3.175	3.175	3.175	3.175	3.175	
Wire Diameter (mm)	0.305	0.305	0.305	0.305	0.305	0.305	0.305	0.305	0.305	0.305	0.305	0.305	0.305	0.305	0.305	0.305	0.305	0.305	0.305	0.305	0.305	0.305	0.305	0.305	0.305	
Mass (loss; g)	0.0329	0.0197	0.0161	0.0161	0.0107	0.0108	0.0056	0.0085	0.0066	0.0211	0.0150	0.0126	0.0131	0.0725	0.0304	0.0269	0.0109	0.0517	0.0477	0.0203	0.0122	0.0635	0.0519	0.2602	0.5522	
Hole Diameter (mm)	25.87	22.58	22.14	22.14	9.69	16.64	13.43	21.50	15.19	21.36	14.48	14.07	13.32	20.02	27.78	23.45	7.21	25.73	19.62	19.32	14.94	27.27	25.05	37.96	18.73	32.65
Shield Mass (g/cm <sup>2</sup> )	0.016	0.016	0.016	0.016	0.016	0.016	0.016	0.016	0.016	0.018	0.018	0.018	0.018	0.018	0.018	0.018	0.018	0.018	0.018	0.020	0.020	0.016	0.046	0.078	0.046	
Separation (M1 to M2; mm)	25.4	25.4	25.4	25.4	25.4	25.4	25.4	25.4	25.4	25.4	25.4	25.4	25.4	25.4	25.4	25.4	25.4	25.4	25.4	25.4	25.4	25.4	25.4	25.4	25.4	
MESH 3																										
Mesh Opening (mm)	3.175	3.175	3.175	3.175	3.175	3.175	3.175	3.175	3.175	3.175	3.175	3.175	3.175	3.175	3.175	3.175	3.175	3.175	3.175	3.175	3.175	3.175	3.175	3.175	3.175	
Wire Diameter (mm)	0.305	0.305	0.305	0.305	0.305	0.305	0.305	0.305	0.305	0.305	0.305	0.305	0.305	0.305	0.305	0.305	0.305	0.305	0.305	0.305	0.305	0.305	0.305	0.305	0.305	
Mass (loss; g)	0.0474	0.0263	0.0263	0.0200	0.0177	0.0170	0.0182	0.0184	0.0337	0.0369	0.0294	0.0206	0.0725	0.0635	0.0696	0.0094	0.1026	0.0862	0.0748	0.0345	0.1026	0.1026	0.0887	0.1185	0.2962	
Hole Diameter (mm)	31.70	31.91	31.91	31.91	22.51	22.06	25.05	35.39	25.87	24.23	20.99	20.57	35.63	28.27	34.33	9.36	52.37	38.89	112.98	71.98	36.32	51.44	8.96	28.03	18.61	
Shield Mass (g/cm <sup>2</sup> )	0.016	0.016	0.016	0.016	0.016	0.016	0.016	0.016	0.016	0.018	0.018	0.018	0.018	0.018	0.018	0.018	0.018	0.018	0.018	0.020	0.020	0.016	0.046	0.078	0.046	
Separation (M2 to M3; mm)	25.4	25.4	25.4	25.4	25.4	25.4	25.4	25.4	25.4	25.4	25.4	25.4	25.4	25.4	25.4	25.4	25.4	25.4	25.4	25.4	25.4	25.4	25.4	25.4	25.4	
MESH 4																										
Mesh Opening (mm)	3.175	3.175	3.175	3.175	3.175	3.175	3.175	3.175	3.175	3.175	3.175	3.175	3.175	3.175	3.175	3.175	3.175	3.175	3.175	3.175	3.175	3.175	3.175	3.175	3.175	
Wire Diameter (mm)	0.305	0.305	0.305	0.305	0.305	0.305	0.305	0.305	0.305	0.305	0.305	0.305	0.305	0.305	0.305	0.305	0.305	0.305	0.305	0.305	0.305	0.305	0.305	0.305	0.305	
Mass (loss; g)	0.0394	0.0251	0.0269	0.0336	0.0291	0.0305	0.0416	0.0381	0.0400	0.0367	0.0456	0.1062	0.0941	0.0091	0.0174	0.0604	0.0134	0.0650	0.0134	0.0650	0.0134	0.0650	0.0134	0.0650	0.0134	
Hole Diameter (mm)	34.84	34.84	22.21	31.41	35.74	31.46	27.28	35.84	30.26	27.41	28.57	41.56	38.13	6.46	30.39	40.26	137.66	125.53	43.30	8.18	15.97	5.75	0.1279	0.1279	0.1279	
Shield Mass (g/cm <sup>2</sup> )	0.016	0.016	0.016	0.016	0.016	0.016	0.016	0.016	0.016	0.018	0.018	0.018	0.018	0.018	0.018	0.018	0.018	0.018	0.018	0.020	0.020	0.016	0.046	0.078	0.046	
Separation (M3 to M4; mm)	25.4	25.4	25.4	25.4	25.4	25.4	25.4	25.4	25.4	25.4	25.4	25.4	25.4	25.4	25.4	25.4	25.4	25.4	25.4	25.4	25.4	25.4	25.4	25.4	25.4	

GROUP	EXPERIMENT NUMBER	813	822	823	975	976	977	979	980	981	982	983	988	989	990	991	993	995	996	997	998	999	1002	1003	1004	1006	1007	1008	F <sub>b</sub>	F <sub>b</sub>	F <sub>b</sub>	F <sub>b</sub>						
MESH 5					3.175	3.175	3.175	3.175	3.175	3.175	3.175	1.590	1.590	1.590	1.590	1.590	1.590	1.590	1.590	1.590	1.590				1.590	3.175	3.175	3.175										
Mesh Opening (mm)					0.305	0.305	0.305	0.305	0.305	0.305	0.305	0.254	0.254	0.254	0.254	0.254	0.254	0.254	0.254	0.254	0.254	0.076	0.076		0.254	0.384	0.762	1.590										
Wire Diameter (mm)					0.0415	0.0199	0.0363	0.0475	0.0288	0.0325	0.0472	0.0385	0.0391	0.0318	0.0318	0.0836	0.0952	0.1044	0.0069	0.0143	0.0699	0.0699			0.0150	0.3068	0.0010	0.0854										
Mass (loss; g)					43.20	43.20	25.33	36.37	45.79	41.27	36.57	41.76	35.73	30.32	31.85	30.16	39.77	51.76	8.89	3.93	0.78	119.22	119.22			3.83	2.78	1.11										
Hole Diameter (mm)					0.016	0.016	0.016	0.016	0.016	0.016	0.016	0.018	0.018	0.018	0.018	0.018	0.018	0.018	0.018	0.018	0.018	0.020	0.020		0.018	0.046	0.078	0.338										
Shield Mass (g/cm <sup>2</sup> )					25.4	25.4	25.4	25.4	25.4	25.4	25.4	25.4	25.4	25.4	25.4	25.4	25.4	25.4	25.4	25.4	25.4	50.8	50.8		25.4	25.4	25.4	25.4										
Separation (M4 to M5; mm)																																						
MESHES 6 - 10																																						
Mesh Opening (mm)					3.175	3.175	3.175	3.175	3.175	3.175	3.175	1.590	1.590	1.590	1.590	1.590	1.590	1.590	1.590	1.590																		
Wire Diameter (mm)					0.305	0.305	0.305	0.305	0.305	0.305	0.305	0.254	0.254	0.254	0.254	0.254	0.254	0.254	0.254	0.254	0.076	0.076																
Mass (loss; g)					0.0516	0.0333	0.0272	0.0515	0.0387	0.0410	0.0374	0.0237	0.0412	0.0135																								
Hole Diameter (mm)					41.37	42.24	37.47	37.47	36.52	33.56	35.07	13.48	33.93	38.43	6.17																							
Mass (loss; g)					0.0182	0.0301	0.0309	0.0304	0.0182	0.0322	0.0379	0.0030	0.0093	0.0095	0.0107																							
Hole Diameter (mm)					33.45	40.94	37.53	33.67	30.16	36.50	36.63	7.09	3.71	8.04	4.91																							
Mass (loss; g)					0.0051	0.0076	0.0164	0.0085	0.0089	0.0142	0.0392	0.0017		0.0088																								
Hole Diameter (mm)					20.35	28.35	28.09	19.04	18.69	22.48	38.83	0.70	2.91	3.38	7.73																							
Mass (loss; g)					10.48	20.95	16.30	1.80	2.35	12.87	32.92	0.62	2.79	4.20	7.62																							
Hole Diameter (mm)					0.880	16.220	15.260																															
TOTAL TARGET																																						
Mass Loss (absolute; g)					0.0014	0.0334	0.0674	0.1246	0.1246	0.0781	0.0928	0.1775	0.1587	0.1409	0.2326	0.0994	0.2351	0.2681	0.2533	0.3192	0.3426	0.1069	0.1796	0.2108	0.0651	0.1113	0.1702	0.2457	0.5209	1.0214	0.2964	0.5036						
Total Shield Mass (g/cm <sup>2</sup> )					0.016	0.032	0.048	0.080	0.080	0.080	0.160	0.160	0.160	0.180	0.180	0.180	0.180	0.180	0.180	0.180	0.180	0.180	0.200	0.200	0.080	0.158	0.495	0.230	0.388	1.688								
Max. Dh (mm)					3.46	25.87	31.91	43.20	43.20	25.30	36.37	45.79	42.24	37.53	41.76	36.52	36.50	38.83	41.56	43.51	38.40	9.80	52.37	40.26	137.66	135.63	36.32	51.44	37.96	28.03	32.65	11.73						
Total Hole Area (cm <sup>2</sup> )					0.1	5.4	4.1	36.3	36.3	13.3	24.5	59.7	69.4	61.3	55.8	44.2	43.1	66.2	36.1	49.3	58.7	4.0	34.4	27.9	252.1	532.1	16.3	40.9	13.6	11.1	11.5	2.1						
EJECTA (Up-Range)																																						
Mass Recovered (absolute; g)					0.0074	0.0098	0.00001	0.0150	0.0150	0.0045	0.0030	0.0104	0.0046	0.0036	0.0049	0.0038	0.0046	0.1596	0.0020	0.0053	0.0112	0.0008	0.0001	0.0078	0.0032	0.0063	0.0113	0.0104	0.0030	0.0140	0.0187							
SPALL (Down-Range)																																						
Mass Recovered (absolute; g)					0.00	0.03	0.04	0.14	0.14	0.02	0.04	0.08	0.08	0.07	0.10	0.07	0.14	0.14	0.48	0.22	0.25	0.12	0.08	0.11	0.03	0.12	0.11	0.15	0.16	0.10	0.09	0.09						
WITNESS PLATE																																						
Standoff from Mesh 1 (mm)					304.8	304.8	304.8	314.4	314.4	314.4	314.4	314.4	314.4	314.4	301.6	568.3	568.3	568.3	568.3	568.3	568.3	568.3	568.3	568.3	568.3	568.3	568.3	311.2	311.2	311.2	311.2	311.2	311.2	311.2	311.2	311.2	311.2	
Standoff from 1st Mesh (mm)					304.8	279.4	254.0	187.3	187.3	187.3	187.3	85.7	85.7	85.7	171.5	111.1	111.1	111.1	111.1	111.1	111.1	111.1	111.1	111.1	111.1	111.1	111.1	260.4	235.0	209.6	209.6	209.6	209.6	209.6	209.6	209.6	209.6	

Table 1b. Powder-Propellant Gun Experiments.

GROUP	E	H	H	I	I	G <sub>a</sub>	G <sub>a</sub>	G <sub>a</sub>	F <sub>a</sub>	F <sub>a</sub>	F <sub>a</sub>		
EXPERIMENT NUMBER	3422	3423	3424	3425	3426	3427	3428	3429	3431	3432	3433	3434	3435
PROJECTILE													
Diameter (mm)	3.175	3.175	3.175	3.175	3.175	3.175	3.175	3.175	3.175	3.175	3.175	3.175	3.175
Mass (g)	0.037	0.037	0.046	0.046	0.037	0.046	0.037	0.046	0.037	0.037	0.037	0.037	0.037
Material <sup>1</sup>	SL	SL	AI	AI	SL	AI	SL	AI	SL	SL	SL	SL	SL
Velocity (km/s)	1.02	1.95	0.99	1.95	2.00	1.97	1.94	1.99	1.95	2.00	1.98	2.00	1.91
TARGET													
Areal Mass (g/cm <sup>2</sup> )	0.467	0.467	0.581	0.581	0.467	0.581	0.467	0.581	0.467	0.467	0.467	0.470	0.472
MESH 1													
Mesh Opening (mm)	1.59	1.59	1.59	1.59			3.175		3.175	3.175	3.175	3.175	3.175
Wire Diameter (mm)	0.254	0.254	0.254	0.254	0.076	0.076	0.584	0.076	0.762	1.590	0.584	0.762	1.590
Mass (loss; g)	0.0020	0.0027	0.0033	0.0015	0.0015	0.0012	0.0311	0.0005	0.0020	0.0402	0.1846	0.0039	0.0360
Hole Diameter (mm)	5.25	7.88	6.74	4.66	4.7	3.81	7.35	3.29	10.61	6.1	7.06	7.52	6.76
Shield Mass (g/cm <sup>2</sup> )	0.018	0.018	0.018	0.018	0.020	0.020	0.046	0.020	0.078	0.338	0.046	0.078	0.338
MESH 2													
Mesh Opening (mm)	1.59	1.59	1.59	1.59			3.175		3.175	3.175	3.175	3.175	3.175
Wire Diameter (mm)	0.254	0.254	0.254	0.254	0.076	0.076	0.305	0.076	0.584	0.762	0.584	0.762	1.590
Mass (loss; g)	0.0091	0.0171	0.0049	0.0059	0.0116		0.0121	0.0037					0.2694
Hole Diameter (mm)	8.07	15.47	6.47	4.4	21.76	3.06	19.29	3.78	16.85	10.07	16.68	11.22	
Shield Mass (g/cm <sup>2</sup> )	0.018	0.018	0.018	0.018	0.02	0.02	0.016	0.02	0.0459	0.0776	0.0459	0.0776	0.3376
Separation (M1 to M2),mm	50.8	50.8	50.8	50.8	50.8	50.8	25.4	50.8	25.4	25.4	25.4	25.4	25.4
MESH 3													
Mesh Opening (mm)	1.59	1.59	1.59	1.59			1.59		3.175	3.175	3.175	3.175	3.175
Wire Diameter (mm)	0.254	0.254	0.254	0.254	0.076	0.076	0.254	0.076	0.305	0.584	0.584	0.762	1.590
Mass (loss; g)	0.0130	0.0220	0.0081	0.0072	0.0074	0.0006	0.0254	0.0007	0.0099			0.0529	1.1108
Hole Diameter (mm)	16.56	18.95	6.45	6.34	62.7	3.68	21.12	3.49	20.69	9.62	15.15	5.96	
Shield Mass (g/cm <sup>2</sup> )	0.018	0.018	0.018	0.018	0.02	0.02	0.018	0.02	0.016	0.0459	0.0459	0.0776	0.3376
Separation (M2 to M3), mm	50.8	50.8	50.8	50.8	50.8	50.8	25.4	50.8	25.4	25.4	25.4	25.4	25.4
MESH 4													
Mesh Opening (mm)	1.59	1.59	1.59	1.59					1.59	3.175	3.175	3.175	3.175
Wire Diameter (mm)	0.254	0.254	0.254	0.254	0.076	0.076		0.076	0.254	0.305	0.584	0.762	1.590
Mass (loss; g)	0.0150	0.0297	0.0051	0.0056	0.0090	0.0008			0.0265	0.0031	0.0011	0.0410	
Hole Diameter (mm)	16.95	22.58	6.41	8.59	40.72	3.52		3.96	14.2	5.97	12.28		
Shield Mass (g/cm <sup>2</sup> )	0.018	0.018	0.018	0.018	0.02	0.02		0.02	0.018	0.016	0.0459	0.0776	0.3376
Separation (M3 to M4),mm	50.8	50.8	50.8	50.8	50.8	50.8		50.8	25.4	25.4	25.4	25.4	25.4

GROUP	E	H	I	G <sub>a</sub>	F <sub>a</sub>	F <sub>a</sub>	F <sub>a</sub>	F <sub>a</sub>	F <sub>a</sub>				
EXPERIMENT NUMBER	3422	3423	3424	3425	3426	3427	3428	3429	3431	3432	3433	3434	3435
<b>MESH 5</b>													
Mesh Opening (mm)	1.59	1.59	1.59	1.59						1.59	3.175	3.175	3.175
Wire Diameter (mm)	0.254	0.254	0.254	0.254	0.076	0.076		0.076		0.254	0.584	0.762	1.590
Mass (loss; g)	0.0088	0.0269	0.0056	0.0078		0.0003				0.0142	0.2315	0.2283	1.1010
Hole Diameter (mm)	12.11	23.85	8.95	6.76	38.66	3.44		3.72		6.37	6.43		
Shield Mass (g/cm <sup>2</sup> )	0.018	0.018	0.018	0.018	0.020	0.020		0.020		0.018	0.046	0.078	0.338
Separation (M4 to M5), mm	50.8	50.8	50.8	50.8	50.8	50.8		50.8		25.4	25.4	25.4	25.4
<b>MESHES 6 - 10</b>													
Mesh Opening (mm)	1.590	1.590	1.590	1.590									
Wire Diameter (mm)	0.254	0.254	0.254	0.254	0.076	0.076		0.076					
<b>MESH 6</b>													
Mass (loss; g)	0.0054		0.0087	0.0102		0.0005		0.0007					
Hole Diameter (mm)		3.17	5.93	6.81	10.66	3.64		4.51					
<b>MESH 7</b>													
Mass (loss; g)	0.0006	0.0088	0.0060	0.0117		0.0015		0.0001					
Hole Diameter (mm)		3.98	5.28	7.88	8.71	3.64		4.01					
<b>MESH 8</b>													
Mass (loss; g)	0.0018	0.0071	0.0078	0.0091		0.0127		0.0001					
Hole Diameter (mm)		2.43	4.23	6.99	5.48	3.93		4.59					
<b>MESH 9</b>													
Mass (loss; g)	0.0016	0.0031	0.0058	0.0074		0.0010							
Hole Diameter (mm)			5.97	6.68	4.15	3.77		3.91					
<b>MESH 10</b>													
Mass (loss; g)	0.0024	0.0029	0.0094	0.0068		0.0007		0.0005					
Hole Diameter (mm)			5.84	6.84	2.07	3.78		3.91					
<b>TOTAL TARGET</b>													
Mass Loss (absolute; g)	0.0596		0.0648	0.0732	0.0078		0.0687				0.0532	0.5955	1.8341
Total Shield Mass (g/cm <sup>2</sup> )	0.180	0.180	0.180	0.180	0.200	0.200	0.080	0.200	0.158	0.495	0.230	0.388	1.688
Total Hole Area (cm <sup>2</sup> )	6.3	13.9	3.1	3.5	61.4	1.0	6.9	1.2	8.1	2.4	5.9	1.7	0.4
<b>EJECTA (Up-Range)</b>													
Mass Recovered (absolute; g)	0.0017	0.0019	0.0016	0.0002	0.0007	0.0001	0.0202	0.0029	0.0024	0.0012	0.0005	0.0005	0.0376
<b>SPALL (Down-Range)</b>													
Mass Recovered (absolute; g)	0.0417	0.1582	0.0632	0.0872	0.0303	0.0064	0.0545	0.0089	0.0394	0.0309	0.0156	0.0365	0.0480
<b>WITNESS PLATE</b>													
Separation from Mesh 1 (mm)	568.3	568.3	568.3	568.3	568.3	568.3	311.2	568.3	311.2	311.2	311.2	311.2	311.2
Separation from last Mesh (mm)	111.1	111.1	111.1	111.1	111.1	111.1	260.4	111.1	235.0	209.6	209.6	209.6	209.6

1SL - soda-lime glass, Al - aluminum 2024, SS - stainless steel 304.

## REFERENCES

- Anderson, C.E, ed. (1987) *Hypervelocity Impact, Proceedings of the 1986 Symposium, Int. J. Impact Engn.*, 5, 759 p.
- Anderson, C.E. ed. (1990) *Hypervelocity Impact, Proceedings of the 1989 Symposium, Int. J. Impact Engn.*, 10, 639 p.
- Christiansen, E.L. (1990) Advanced Meteoroid and Debris Bumpering Concepts, AIAA/NASA/DOD Orbital Debris Conference, *AIAA 90-1336*, 14 p.
- Christiansen, E.L., Horn, J.R. and Crews, J.L. (1990) Augmentation of Orbital Debris Bumpering for Space Station Freedom, *AIAA Space Programs and Technologies Conference, AIAA 90, 3665*, 11 p.
- Christiansen, E.L. (1992) Performance Equations for Advanced Orbital Debris Bumpers, *AIAA Space Programs and Technologies Conference, AIAA 92 1462*, 8 p.
- Christiansen, E.L. and Kerr, J.H. (1993) Mesh Double-Bumper Shield: A Low-Weight Alternative for Spcecraft Meteoroid and Orbital Debris Protection, submitted to the *Int. J. Impact Engn.*, November, 1992.
- Cour-Palais, B.G. (1987) Hypervelocity Impact in Metals, Glass and Composites, *Int. J. Impact Engn.* 5, p. 221-237.
- Cour-Palais, B.G. and Crews, J.L. (1990) A Multi-shock Concept for Space Craft Bumpering, *Int. J. Impact Engn.*, 10, p. 135-146.
- Dickinson, D.L., Yatteau, J.D. and Recht, R.F. (1987) Fragment Breakup, *Int. J. Impact Engn.*, 5, p. 249-260.
- Gehring, J. (1970) Theory of Impact on Thin Targets and Bumpers and Correlation with Experiment, In *High Velocity Impact Phenomena*, Kinslow, R. ed., Academic Press, p. 105-156.
- Herrmann, W. and Wilbeck, J.S. (1987) Review of Hypervelocity Penetration Theories, *Int. J. Impact Engn.* 5, p. 307-322.
- Hohler, V. and Stilp, A.J. (1977) Penetration of Steel and High Density Rods in Semi-Infinite Targets., *Proc. Third Intl. Sym. on Ballistics*, Karlsruhe, FRG.
- Hörz, F., Cintala, M.J., See T.H., Bernhard, R.P., Cardenas, F., Davidson, W. and Haynes, G. (1992a) Comparisons of Continuous and Discontinuous Bumpers. Dimensionally Scaled Impact Experiments into Single Wire Meshes, *NASA TM 104749*, 83 p.
- Hörz, F., Cintala, M.J., Bernhard, R.P. and See, T.H. (1992b) Dimensionally Scaled Penetration Experiments. Aluminum Targets and Glass Projectiles 50  $\mu\text{m}$  to 3.2 mm in Diameter, submitted to *Int. J. Impact Engn.*, April 1992.
- Piekutowsky, A.J. (1987) Debris Clouds Generated by Hypervelocity Impact of Cylindrical Projectiles with Thin Aluminum Plates, *Int. J. Impact Engn.*, 5, p. 509-518.
- Piekutowsky, A.J. (1990) A simple Dynamic Model for the Formation of Debris Clouds, *Int. J. Impact Engn.*, 10, p. 453-471.
- Richardson, A.J. (1970) Theoretical penetration Mechanics of Multi-Sheet Structures Based on Discrete Particle Modeling, *J. Spacecraft and Rockets*, 7, p. 486-489.
- Schonberg, W.P. and Taylor, R.A. (1989) Penetration and Ricochet Phenomena in Oblique Hypervelocity Impacts, *AIAA Journal*, 27, p. 639-646.

- Stilp, A.J., Hohler, V, Schneider, E. and Weber, K. (1990) Debris Cloud Expansion Studies, *Int. J. Impact Engn.*, 10, p. 543-554.
- Whipple, F.L. (1958) The Meteoritic Risk to Space Vehicles, *Proc. Intl. Astronautical Congress*, Springer Verlag, Wien, p. 418-428.



## APPENDIX

This Appendix contains photodocumentation of each individual experiment described in this document. Two illustrations are offered per experiment: (1) impact damage suffered by successive grids or foils and (2) damage suffered by the witness plate at the rear of each stack.

The legend defines the following parameters:

<b>PROJECTILE:</b>	SL	=	SODA-LIME GLASS
	Al	=	ALUMINUM (2024)
	SS	=	STAINLESS STEEL (304)
	$D_p$	=	PROJECTILE DIAMETER
	V	=	IMPACT VELOCITY
<b>TARGET:</b>	M	=	MESH OPENING (center-to-center distance)
	T	=	WIRE (FOIL) THICKNESS
	N	=	NUMBER OF MESHES (FOILS) USED
	S	=	SEPARATION DISTANCE
	SM	=	TOTAL SPECIFIC BUMPER MASS

### SCALES:

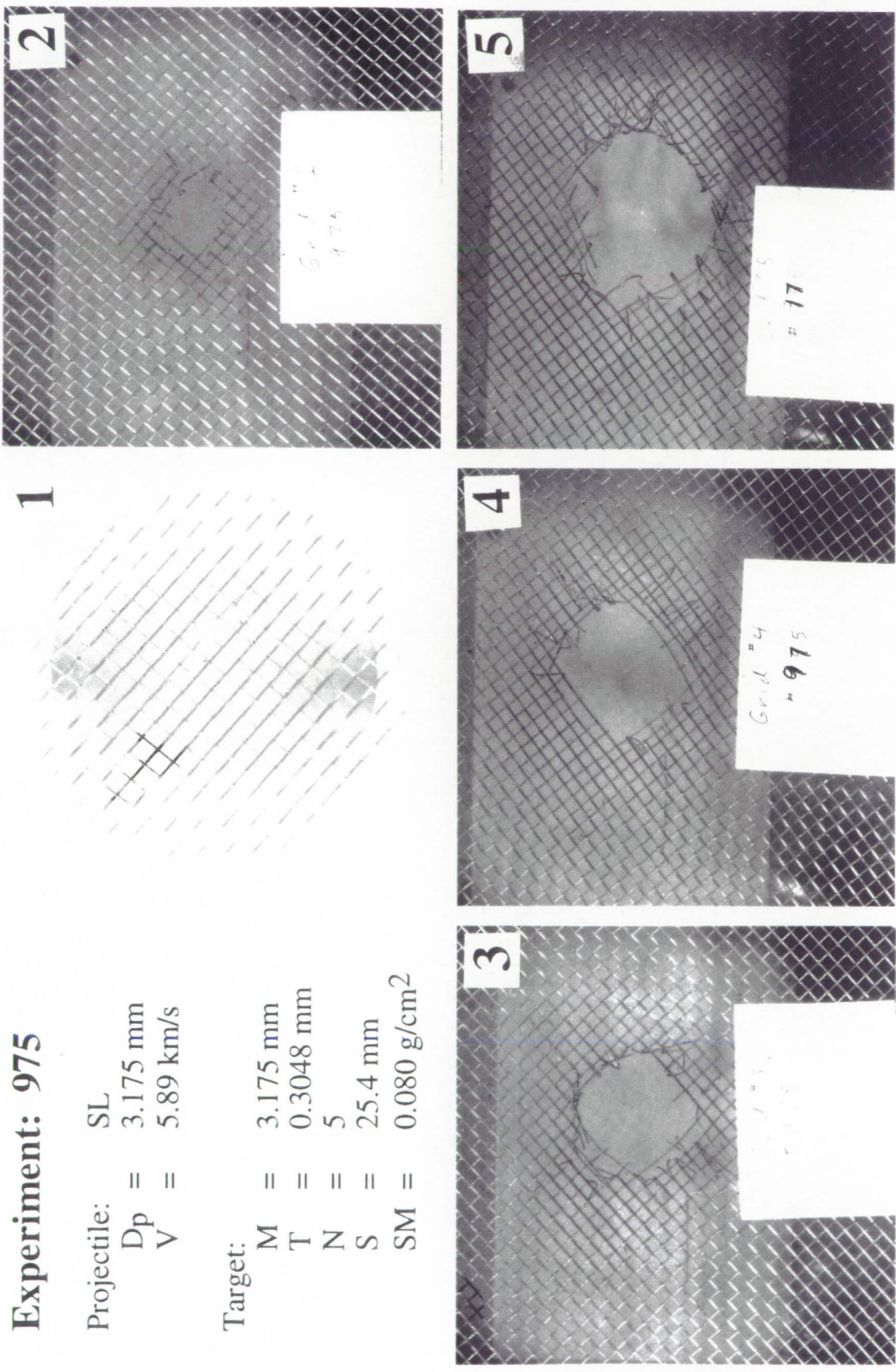
Mesh opening (M) provides internal scales for all mesh photos.  
Scale bars are given for the foil experiments.  
Each witness plate is a consistent 30 cm on the side.

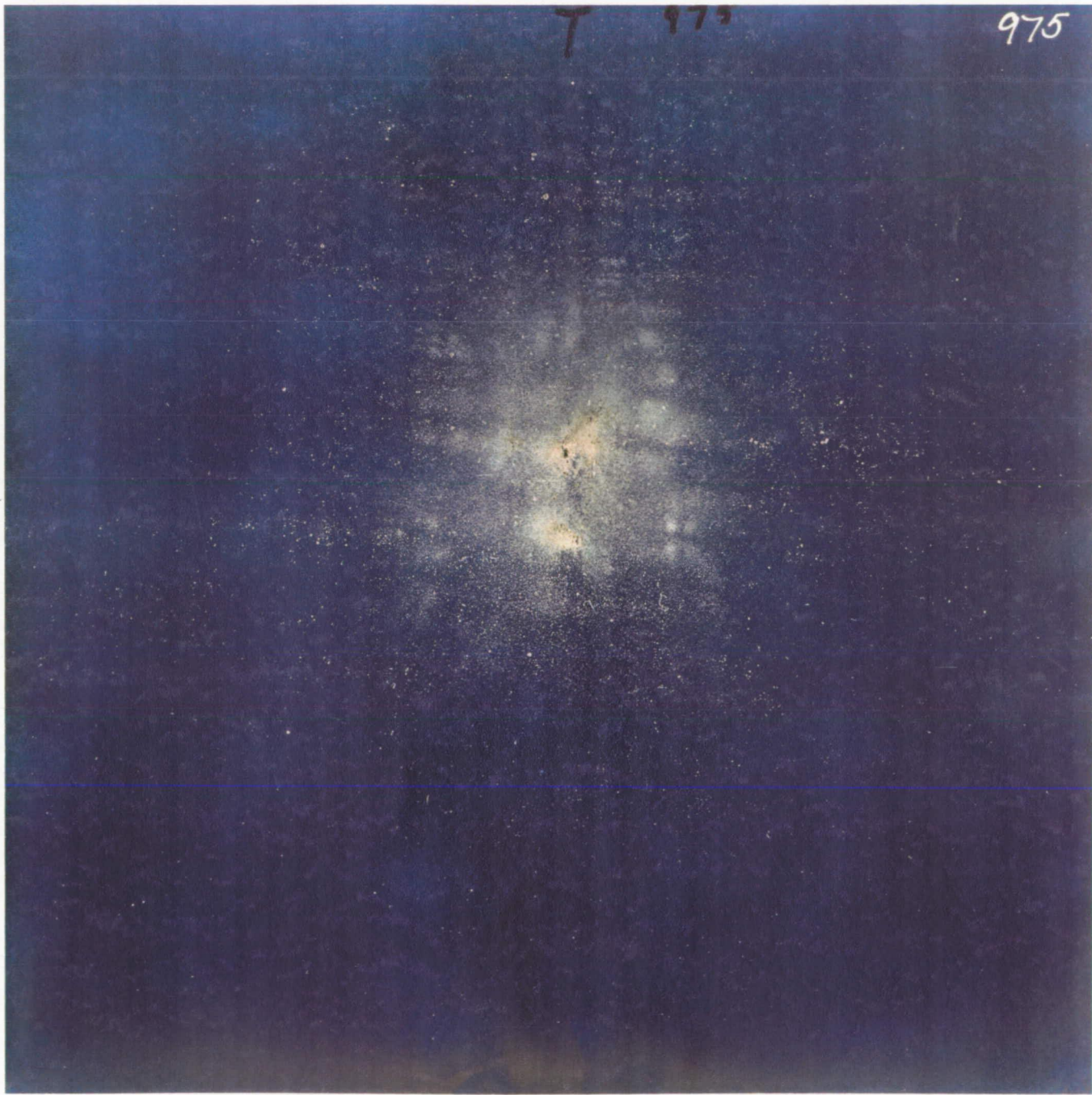
All experiments are arranged in **numerical** sequence, consistent with Table 1, so that the reader may easily refer to the following plates and Table 1 for specific initial conditions and results. This sequence also reflects a chronological sequence for each of the two gun facilities employed in this study; powder-propellant gun experiments at low velocities were conducted in parallel with the light-gas gun experiments.

# Experiment: 975

Projectile: SL  
Dp = 3.175 mm  
V = 5.89 km/s

Target: M = 3.175 mm  
T = 0.3048 mm  
N = 5  
S = 25.4 mm  
SM = 0.080 g/cm<sup>2</sup>

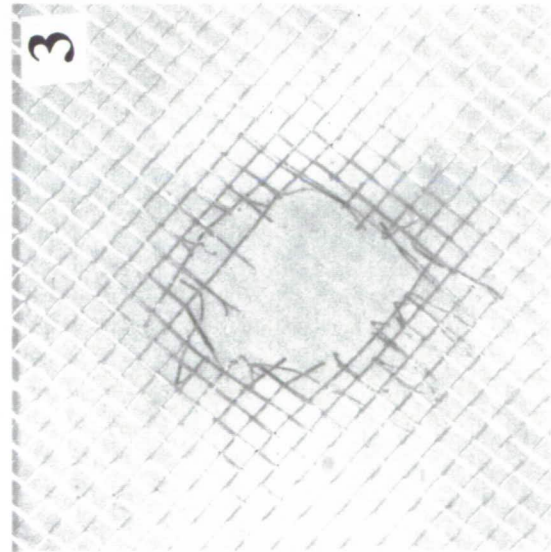
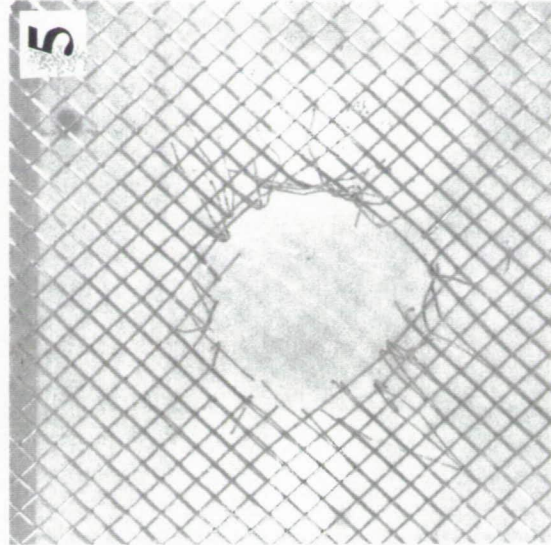
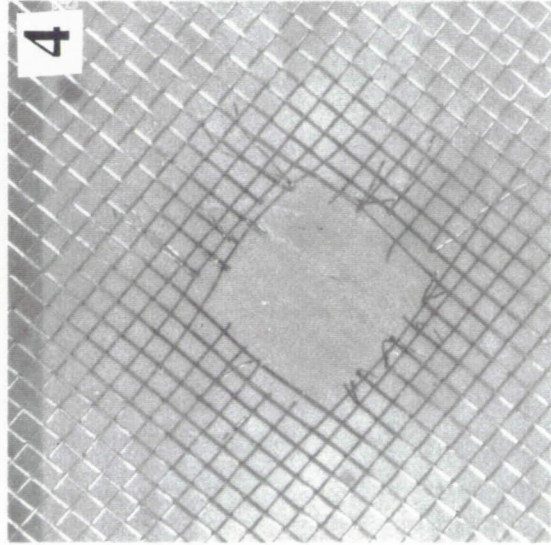
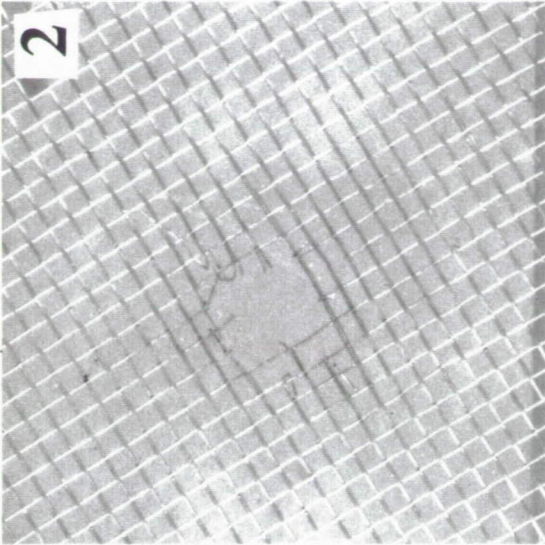
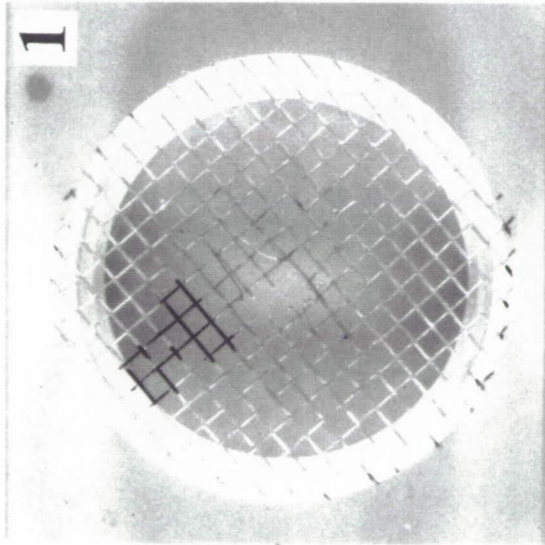




# Experiment: 976

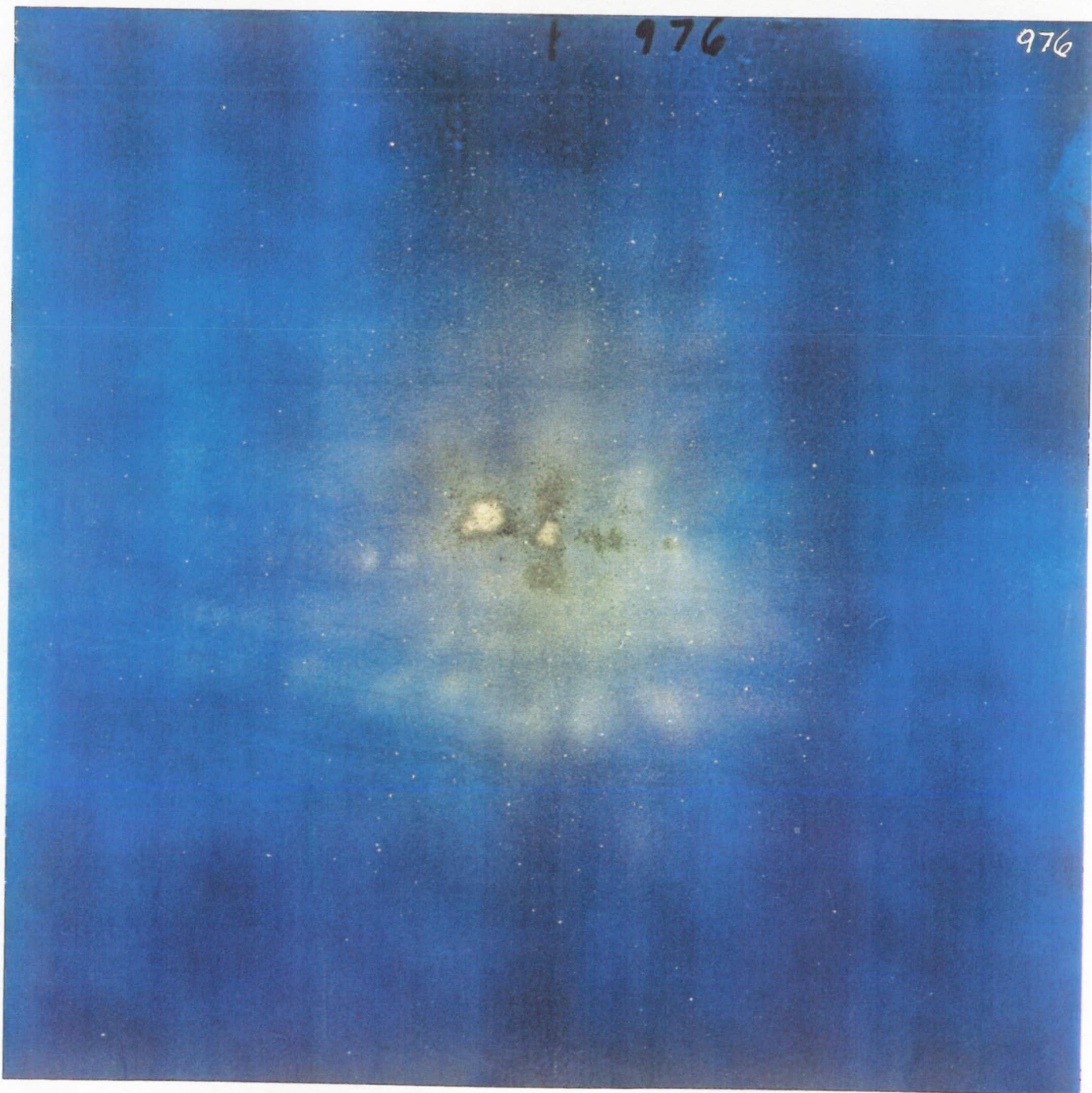
Projectile: SL  
Dp = 3.175 mm  
V = 4.28 km/s

Target: M = 3.175 mm  
T = 0.3048 mm  
N = 5  
S = 25.4 mm  
SM = 0.080 g/cm<sup>2</sup>



PRECEDING PAGE BLANK NOT FILMED

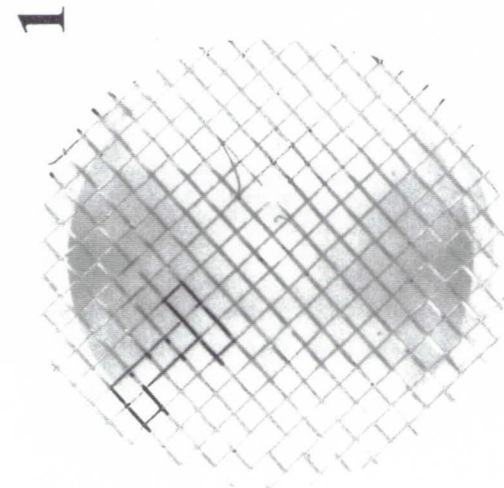
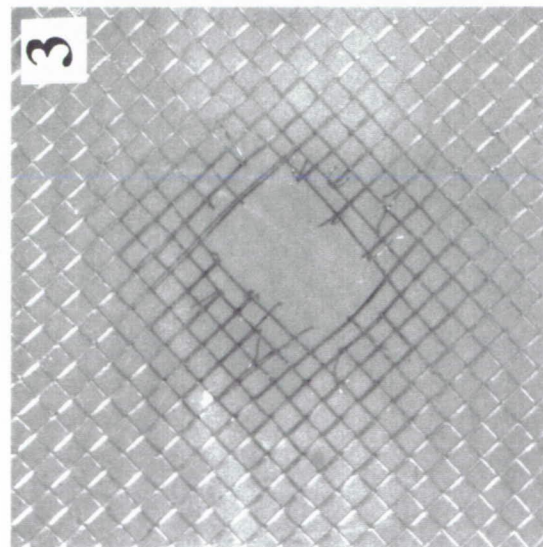
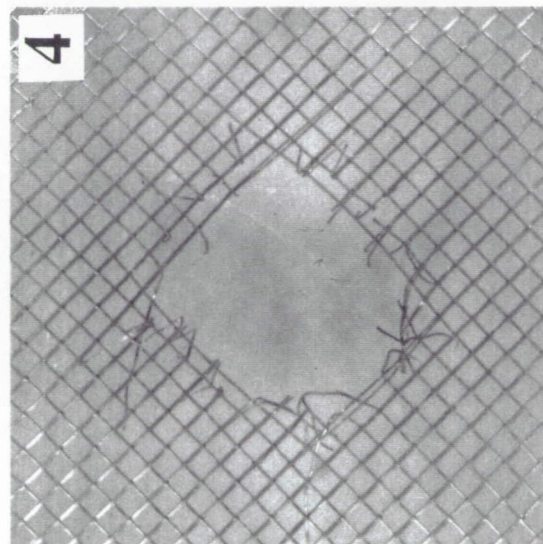
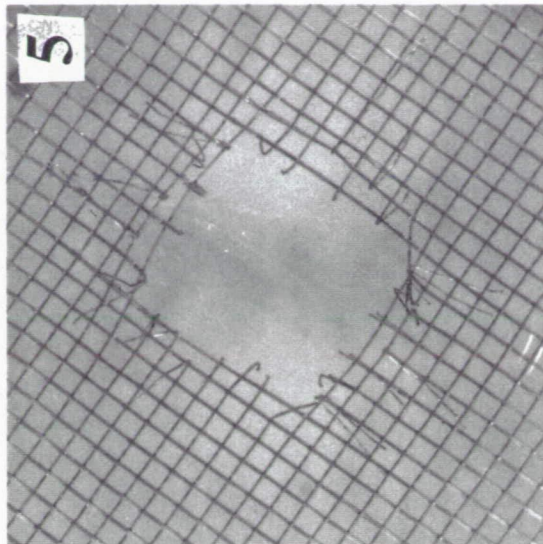
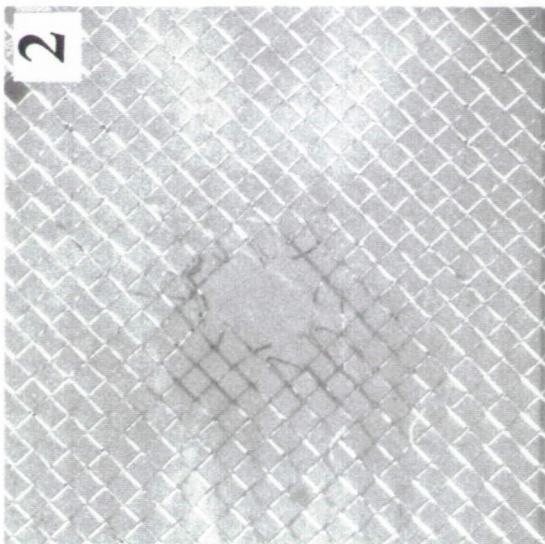
ORIGINAL PAGE  
BLACK AND WHITE PHOTOGRAPH



# Experiment: 977

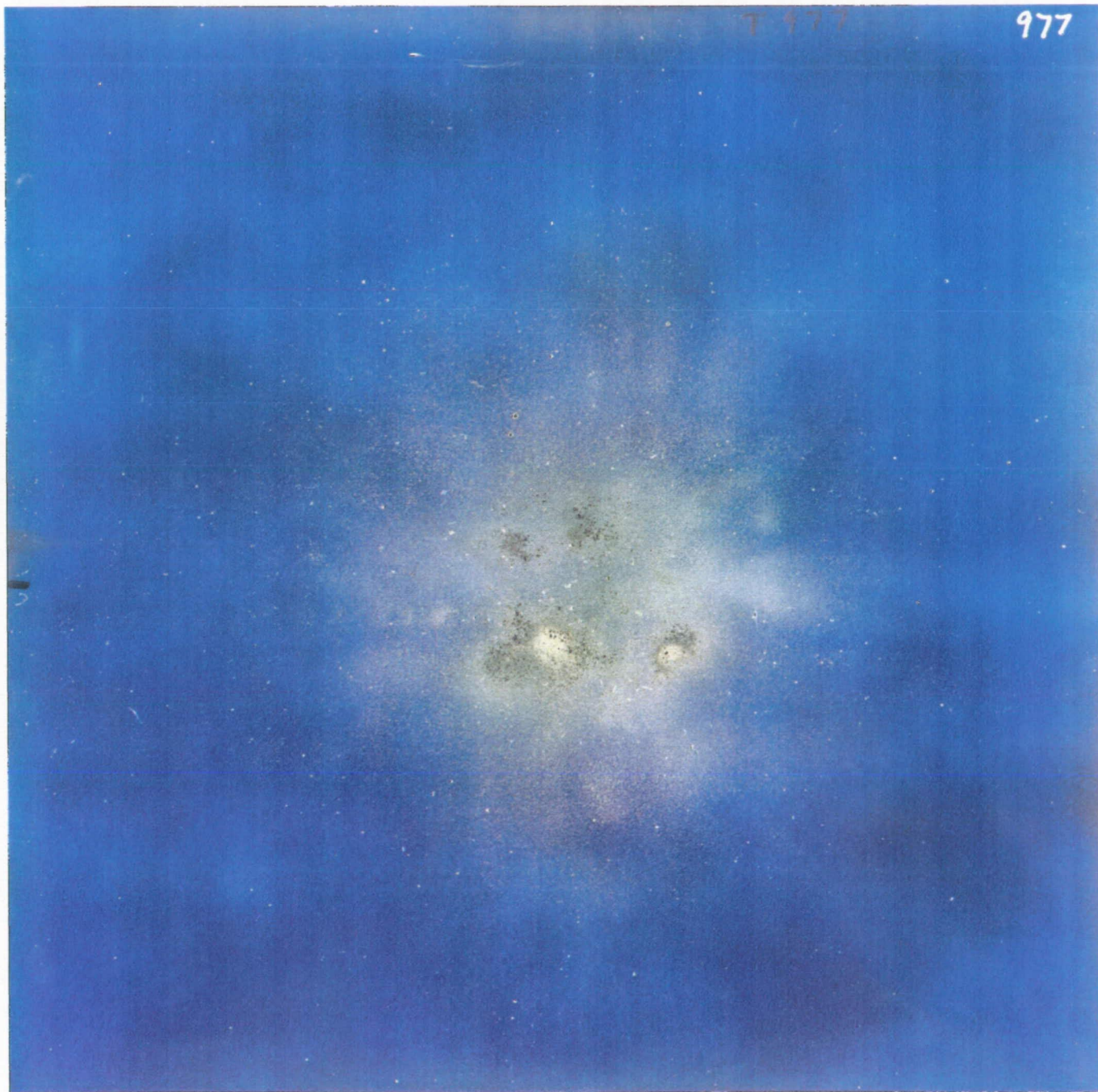
Projectile: SL  
Dp = 3.175 mm  
V = 5.25 km/s

Target: M = 3.175 mm  
T = 0.3048 mm  
N = 5  
S = 25.4 mm  
SM = 0.080 g/cm<sup>2</sup>



T 977

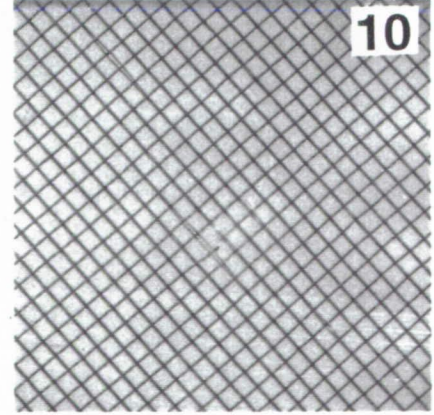
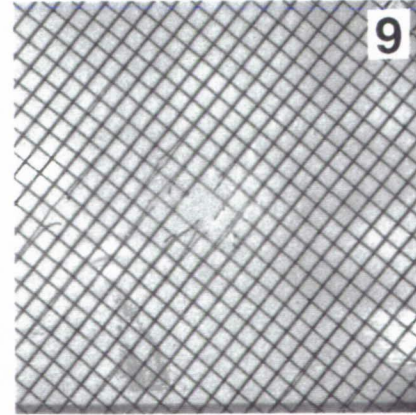
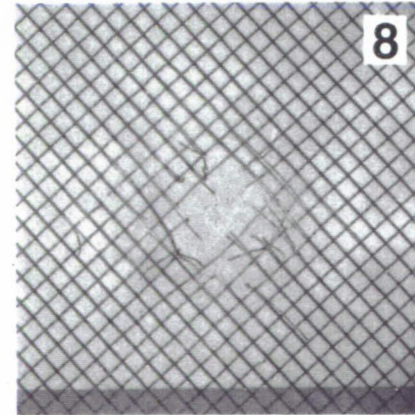
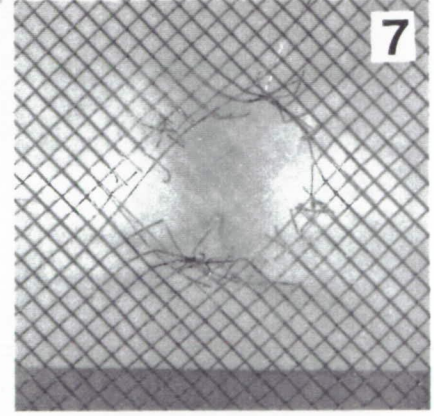
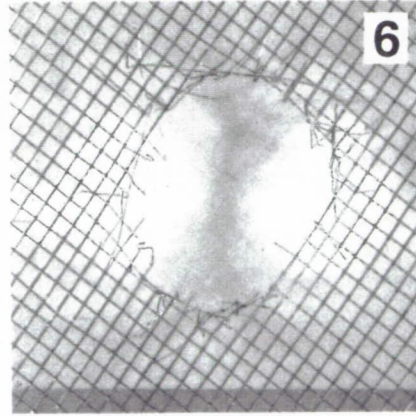
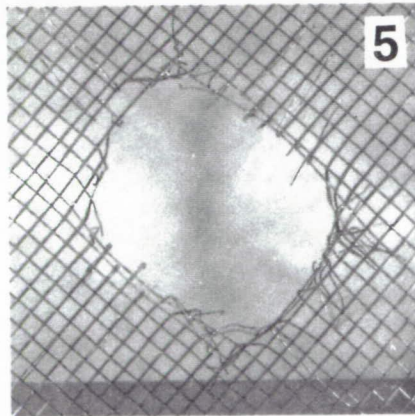
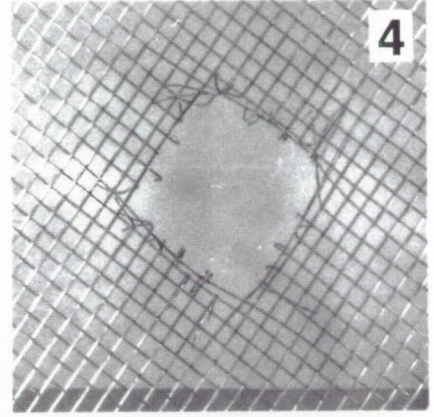
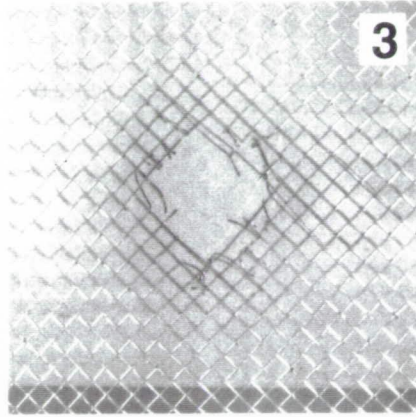
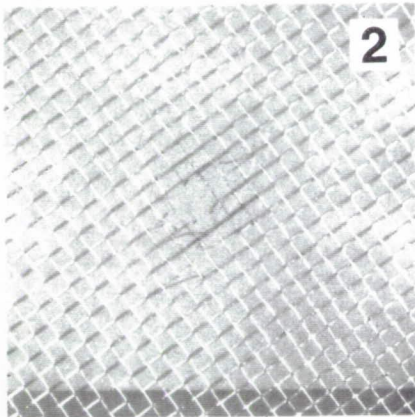
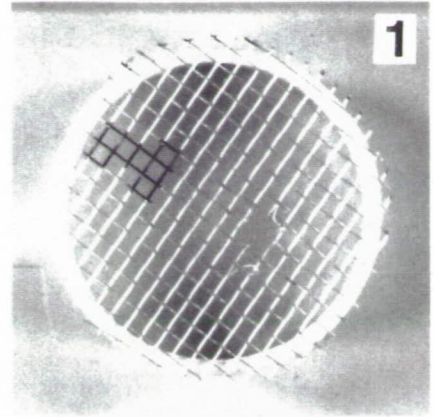
977



# Experiment: 979

Projectile: SL  
D<sub>p</sub> = 3.175 mm  
V = 5.86 km/s

Target:  
M = 3.175 mm  
T = 0.3048 mm  
N = 10  
S = 25.4 mm  
SM = 0.160 g/cm<sup>2</sup>





979

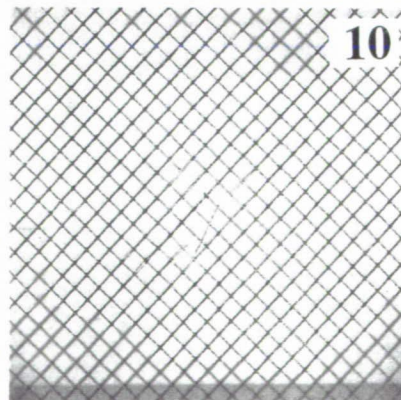
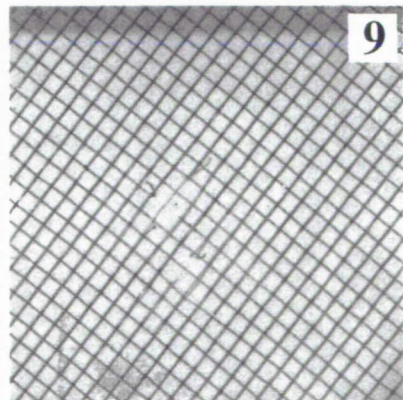
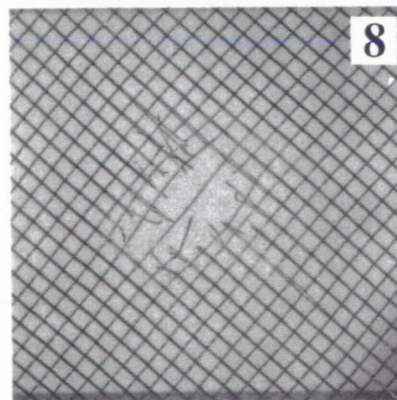
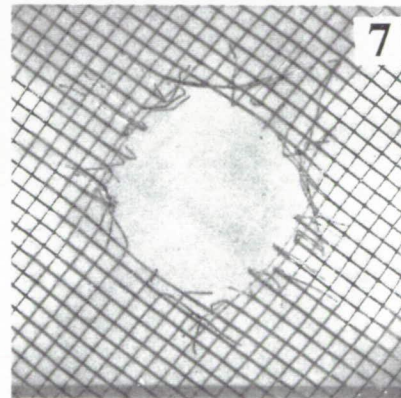
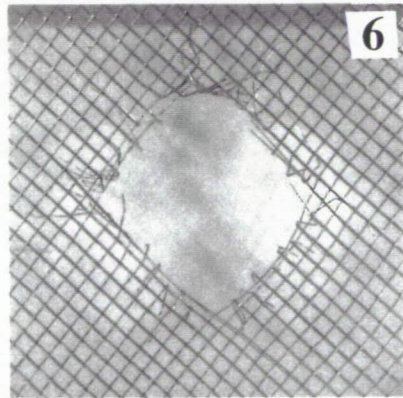
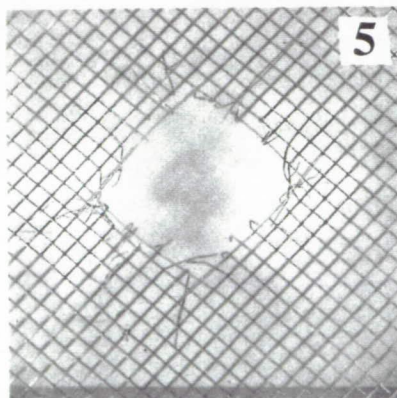
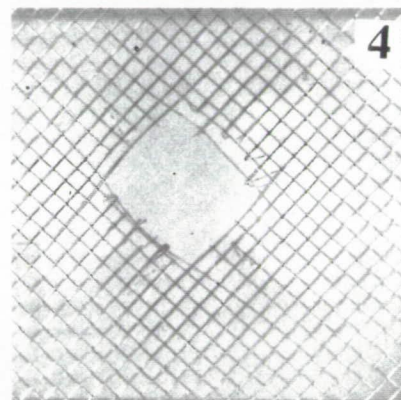
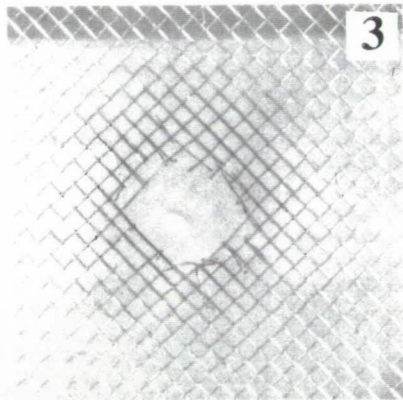
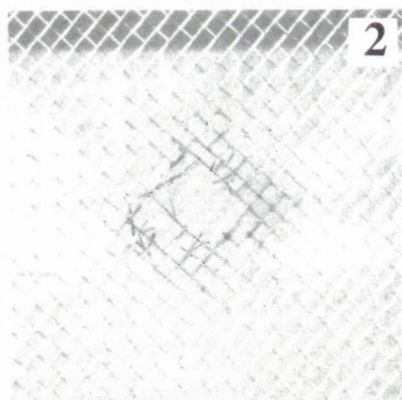
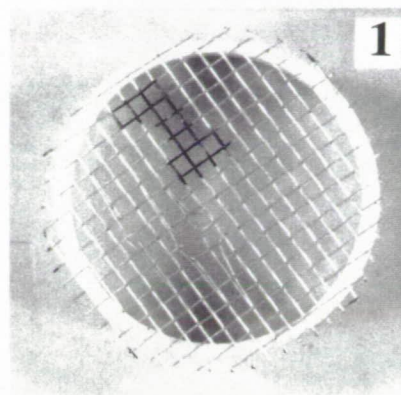
T 979



# Experiment: 980

Projectile: SL  
D<sub>p</sub> = 3.175 mm  
V = 5.12 km/s

Target:  
M = 3.175 mm  
T = 0.3048 mm  
N = 10  
S = 25.4 mm  
SM = 0.160 g/cm<sup>2</sup>



ORIGINAL PAGE  
BLACK AND WHITE PHOTOGRAPH

PRECEDING PAGE BLANK NOT FILMED

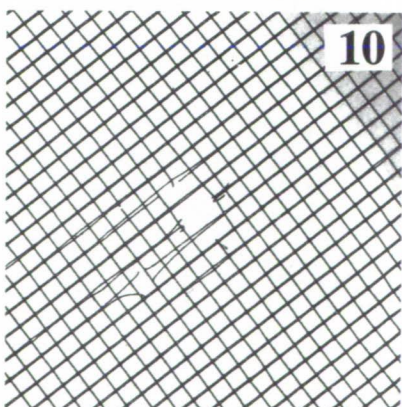
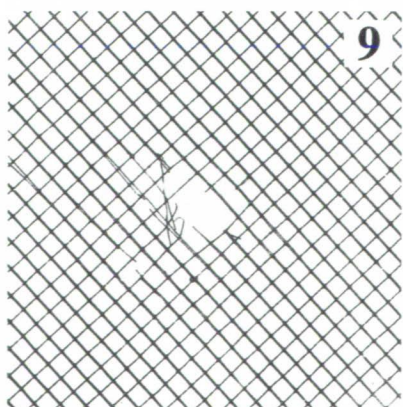
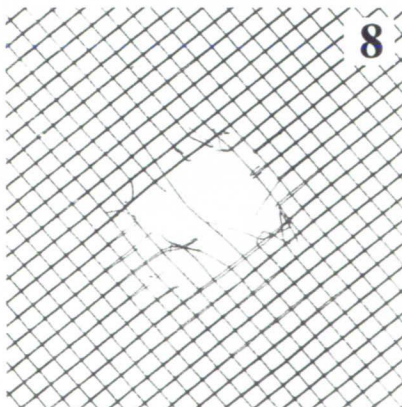
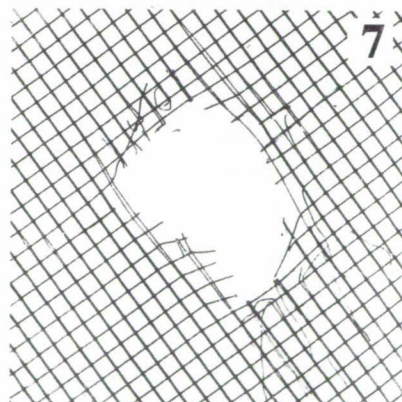
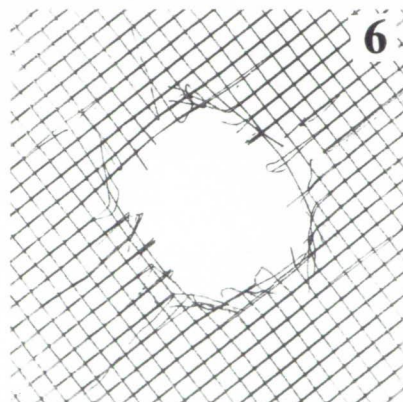
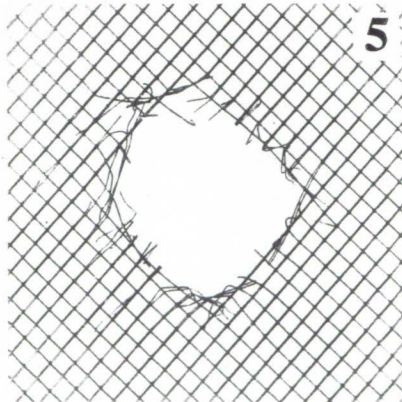
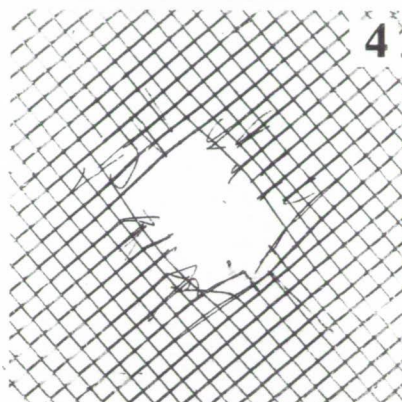
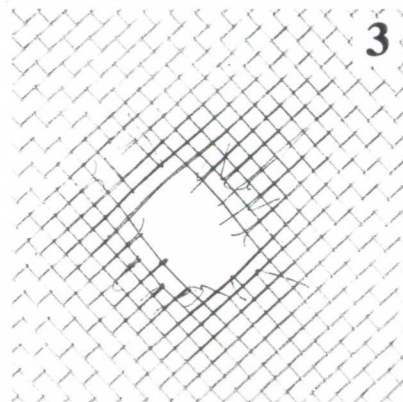
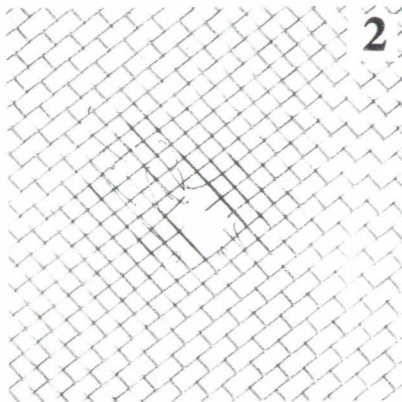
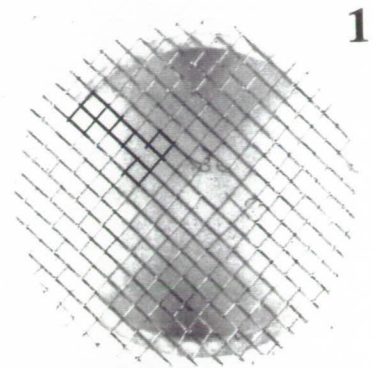
T 980



# Experiment: 981

Projectile: SL  
D<sub>p</sub> = 3.175 mm  
V = 4.41 km/s

Target:  
M = 3.175 mm  
T = 0.3048 mm  
N = 10  
S = 25.4 mm  
SM = 0.160 g/cm<sup>2</sup>

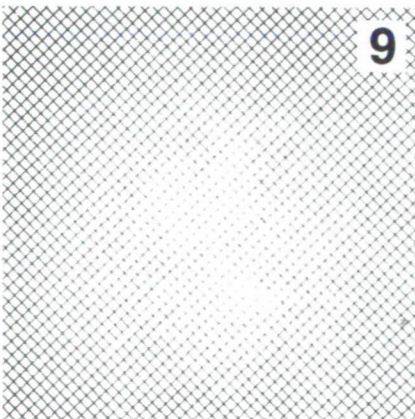
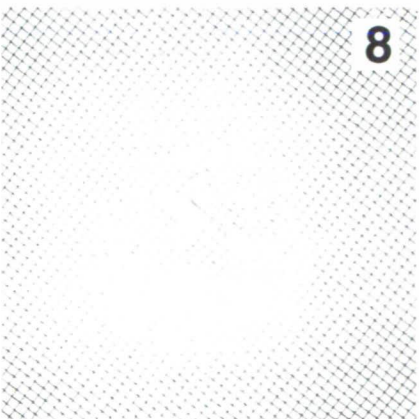
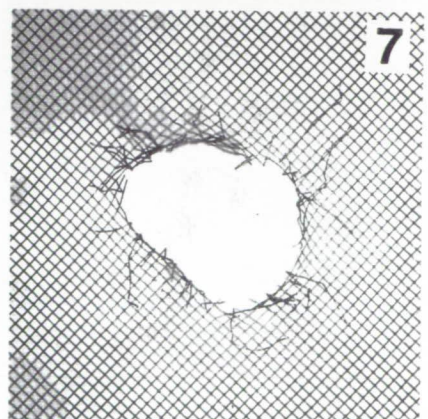
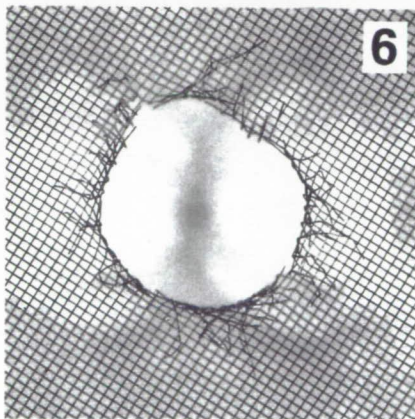
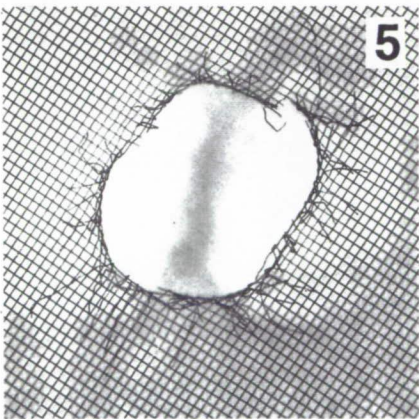
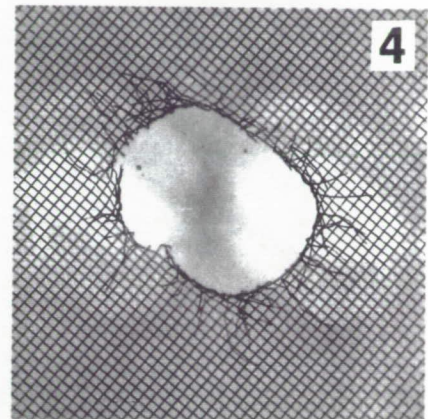
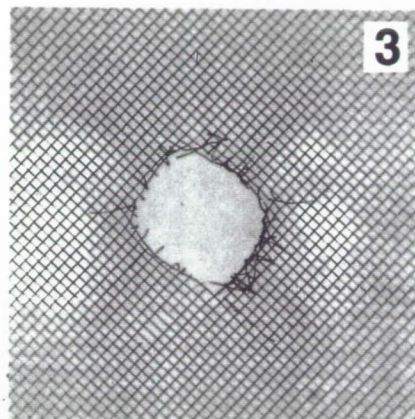
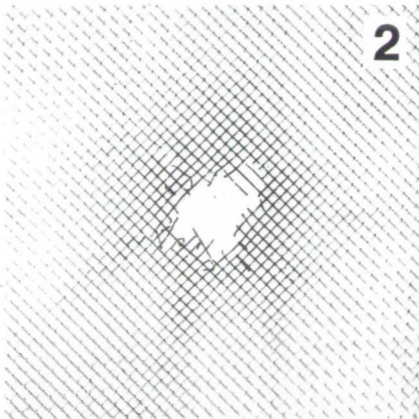
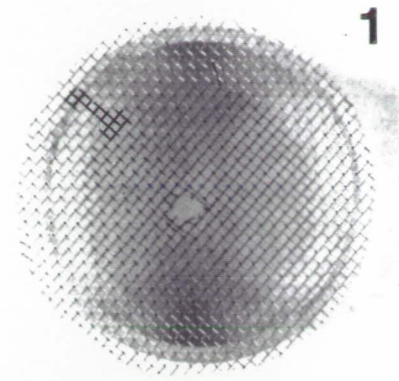




# Experiment: 982

Projectile: SL  
 $D_p = 3.175 \text{ mm}$   
 $V = 5.74 \text{ km/s}$

Target:  
 $M = 1.590 \text{ mm}$   
 $T = 0.2540 \text{ mm}$   
 $N = 10$   
 $S = 25.4 \text{ mm}$   
 $SM = 0.180 \text{ g/cm}^2$



T 982

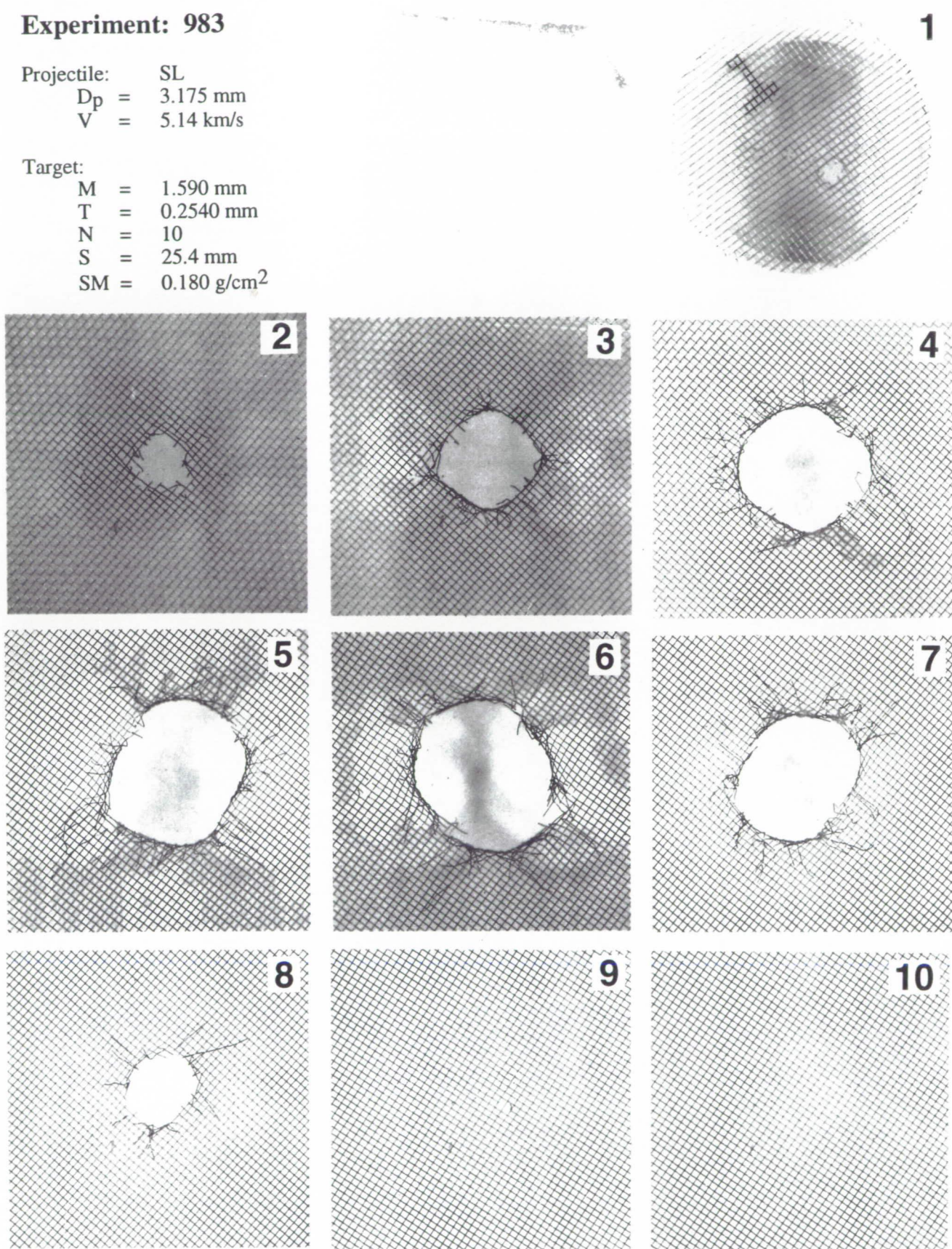
982



# Experiment: 983

Projectile: SL  
 $D_p = 3.175 \text{ mm}$   
 $V = 5.14 \text{ km/s}$

Target:  
 $M = 1.590 \text{ mm}$   
 $T = 0.2540 \text{ mm}$   
 $N = 10$   
 $S = 25.4 \text{ mm}$   
 $SM = 0.180 \text{ g/cm}^2$



PRECEDING PAGE BLANK NOT FILMED

ORIGINAL PAGE  
BLACK AND WHITE PHOTOGRAPH





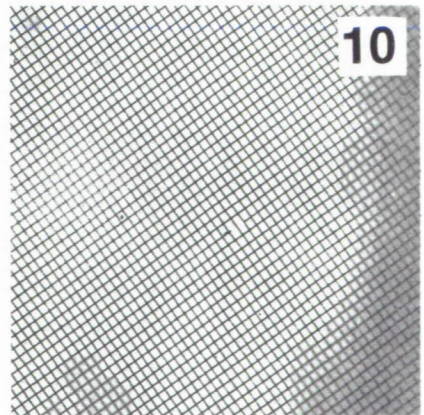
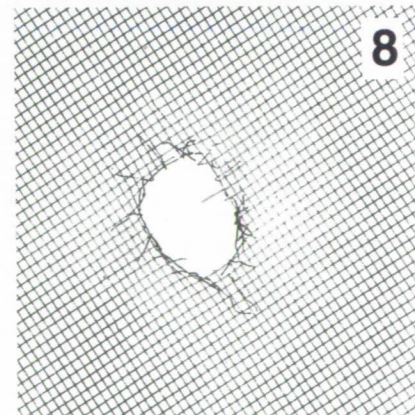
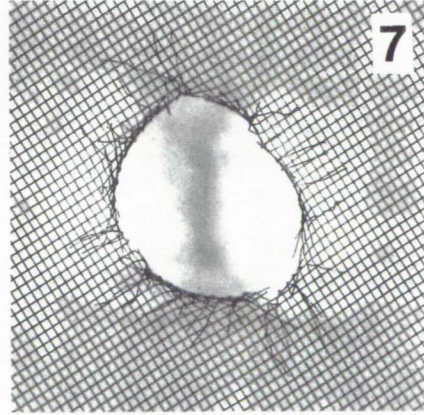
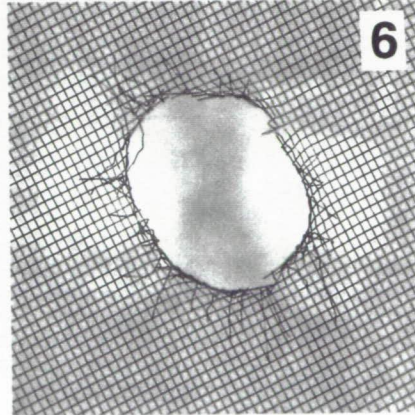
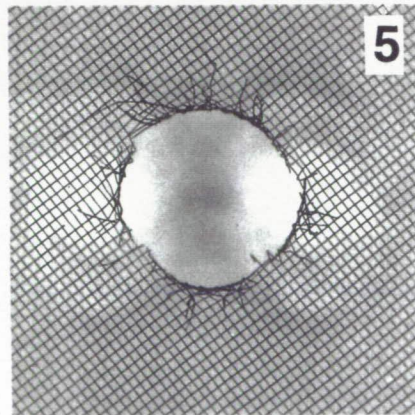
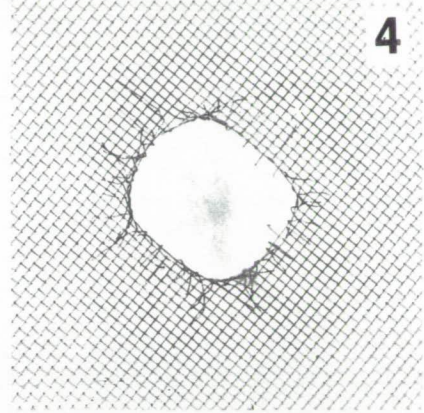
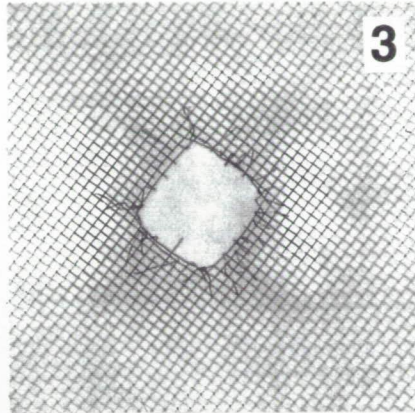
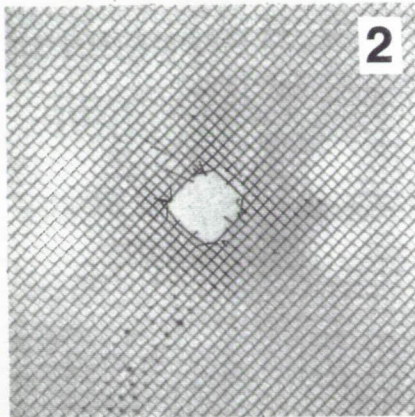
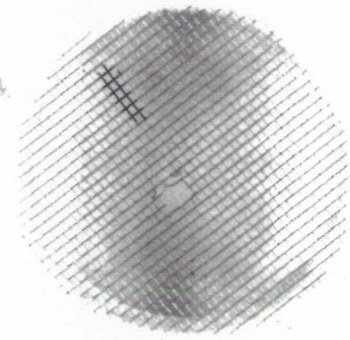
983

983

# Experiment: 988

Projectile: SL  
D<sub>p</sub> = 3.175 mm  
V = 4.16 km/s

Target:  
M = 1.590 mm  
T = 0.2540 mm  
N = 10  
S = 25.4 mm  
SM = 0.180 g/cm<sup>2</sup>



988

988

T

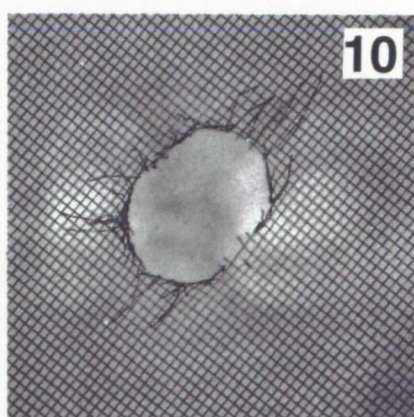
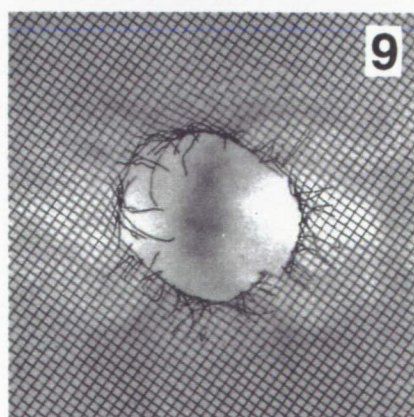
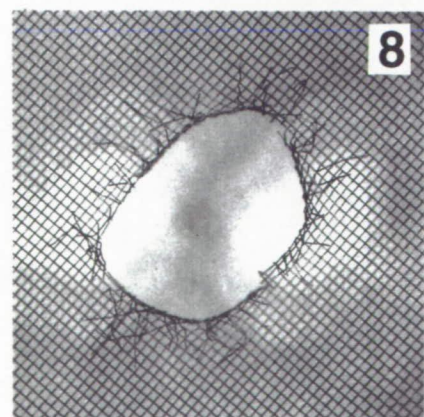
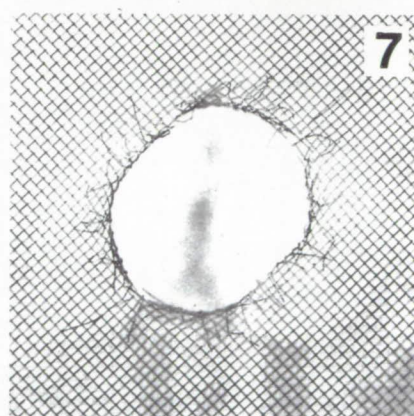
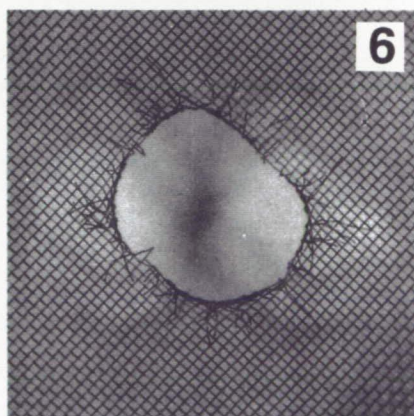
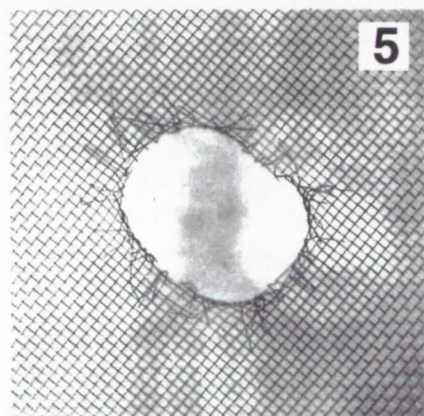
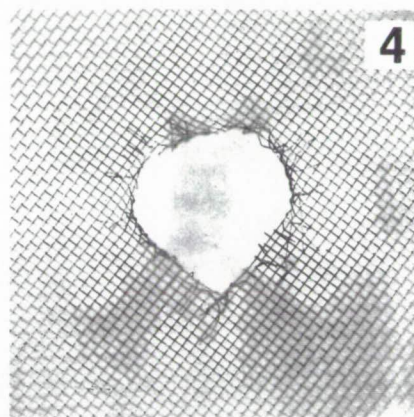
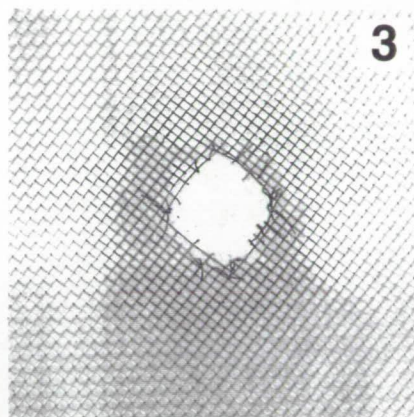
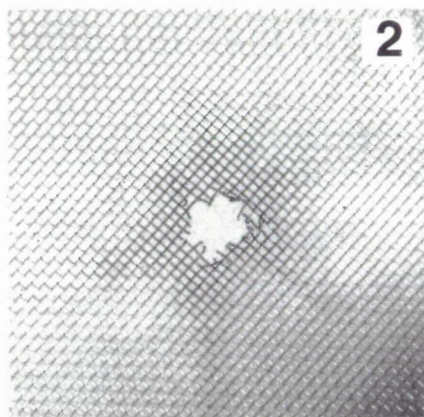
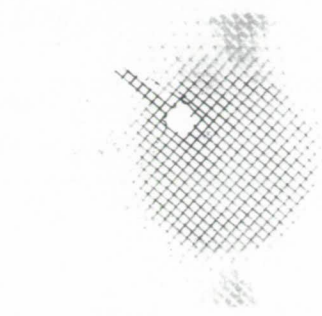


# Experiment: 989

Projectile: SL  
D<sub>p</sub> = 3.175 mm  
V = 5.81 km/s

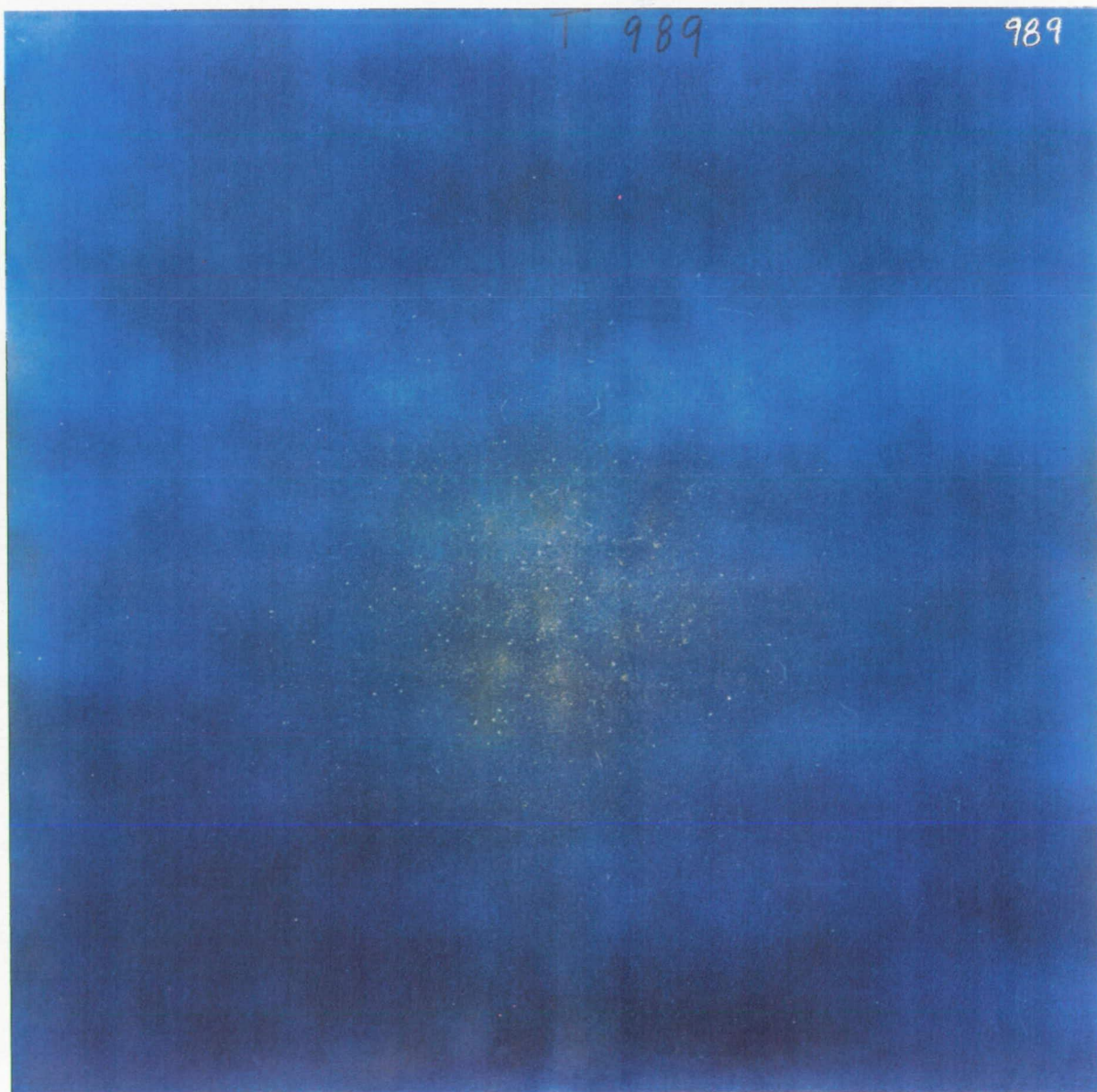
Target:  
M = 1.590 mm  
T = 0.2540 mm  
N = 10  
S = 12.7 mm  
SM = 0.180 g/cm<sup>2</sup>

1



PRECEDING PAGE BLANK NOT FILMED

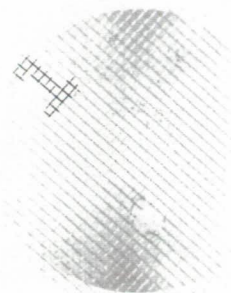
ORIGINAL PAGE  
BLACK AND WHITE PHOTOGRAPH



# Experiment: 990

Projectile: SL  
D<sub>p</sub> = 3.175 mm  
V = 5.97 km/s

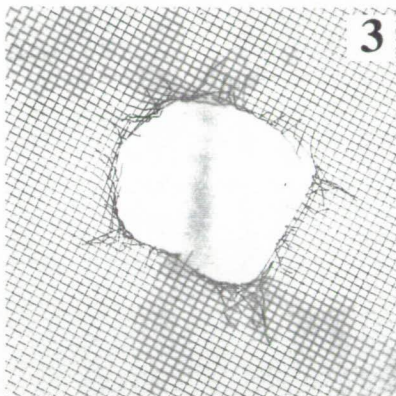
Target:  
M = 1.590 mm  
T = 0.2540 mm  
N = 10  
S = 50.8 mm  
SM = 0.180 g/cm<sup>2</sup>



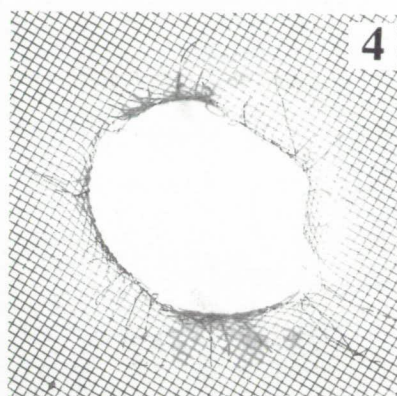
1



2



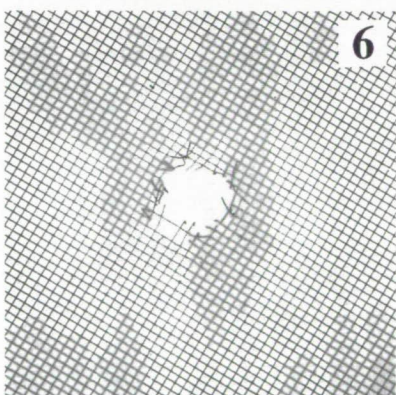
3



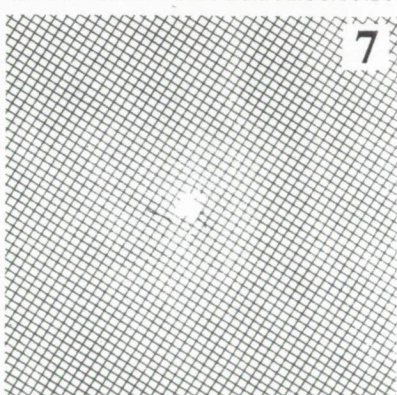
4



5



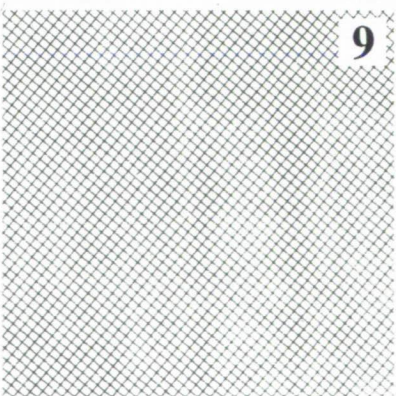
6



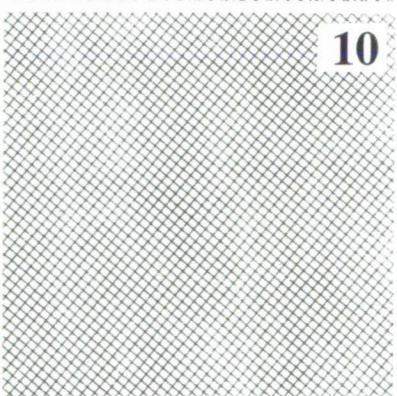
7



8



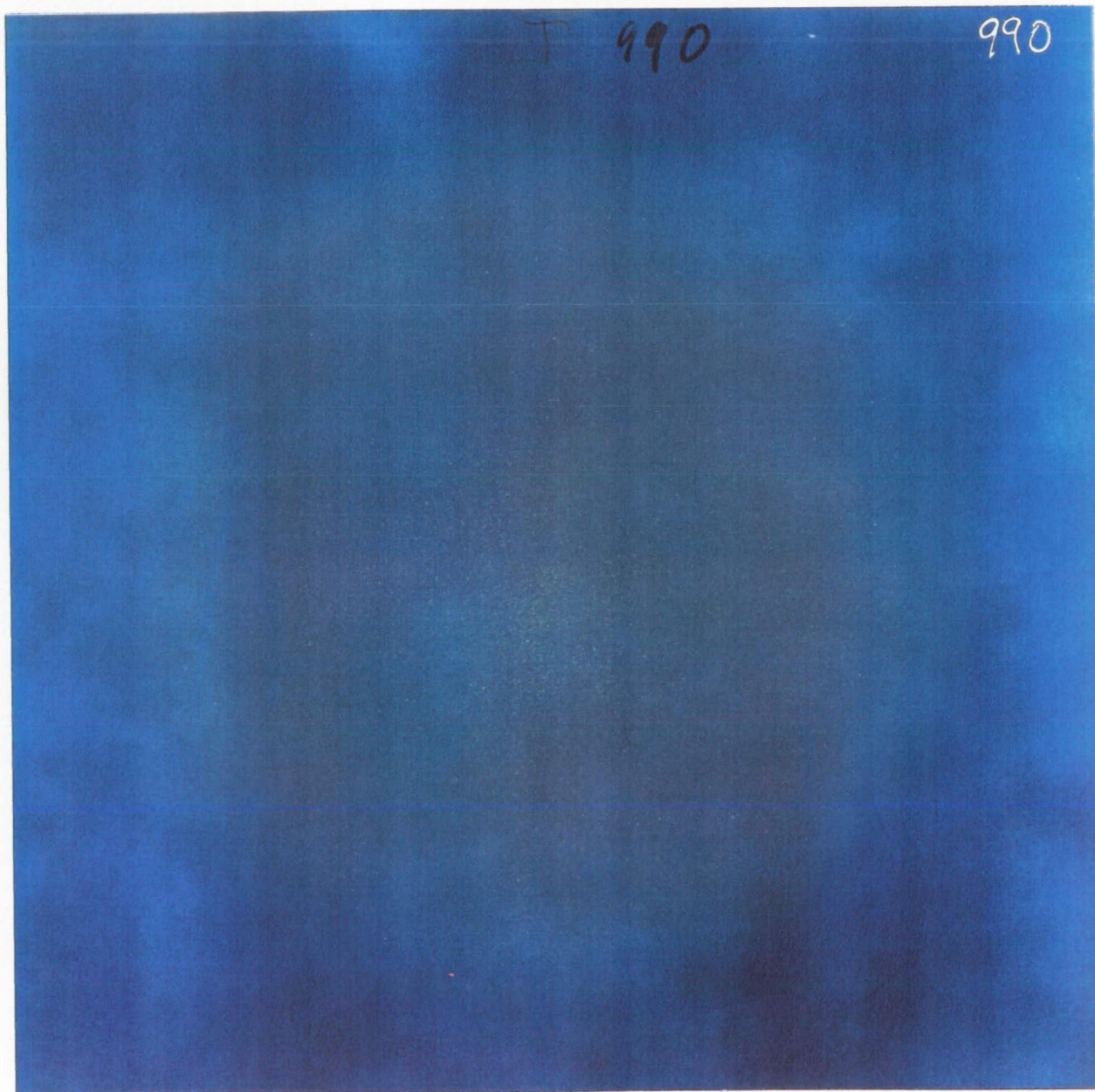
9



10

PRECEDING PAGE BLANK NOT FILMED

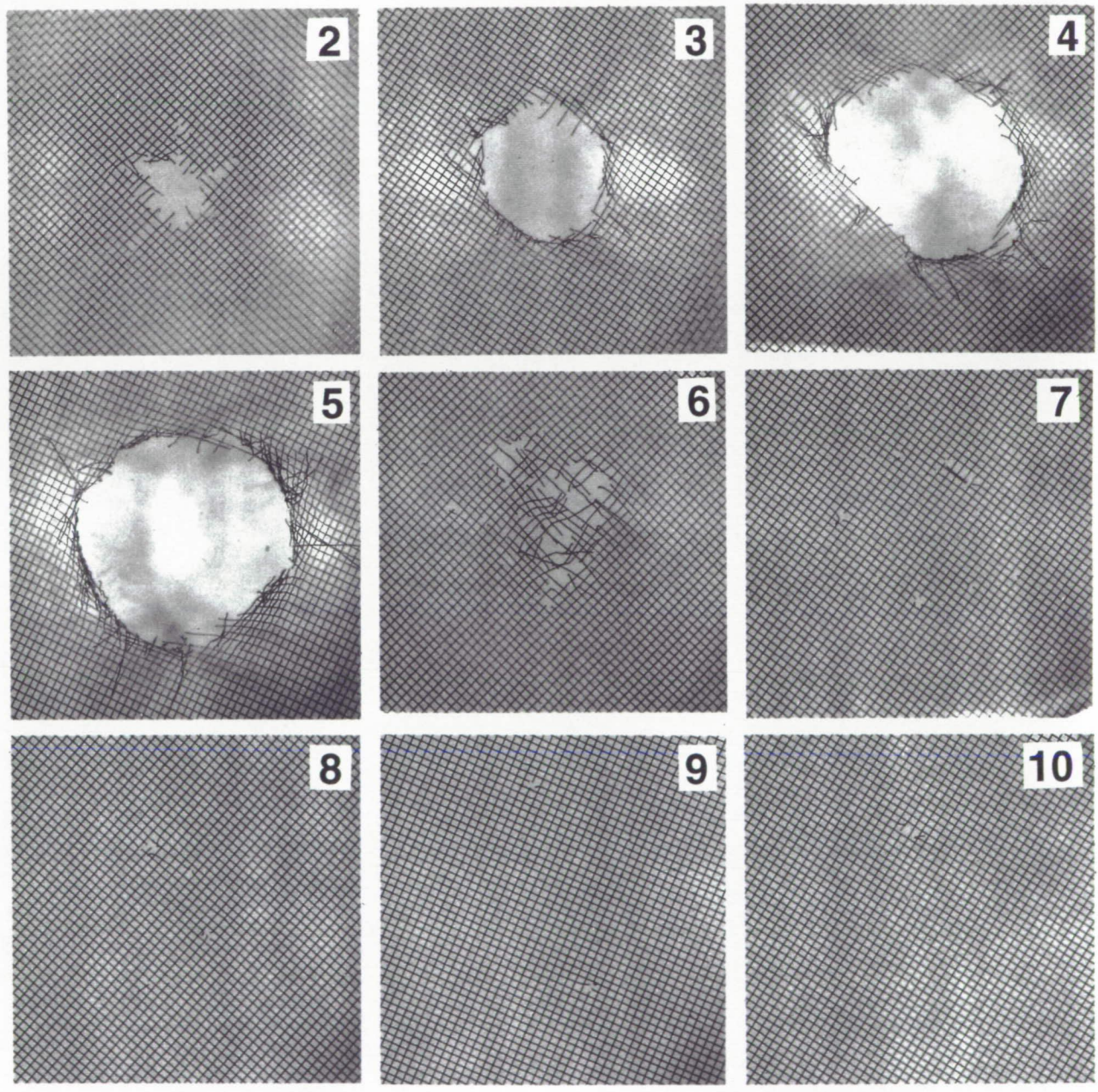
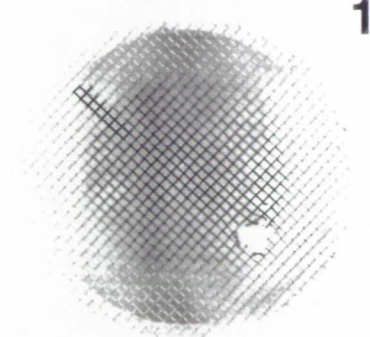
ORIGINAL PAGE  
BLACK AND WHITE PHOTOGRAPH



# Experiment: 991

Projectile: Al  
 $D_p = 3.175 \text{ mm}$   
 $V = 5.90 \text{ km/s}$

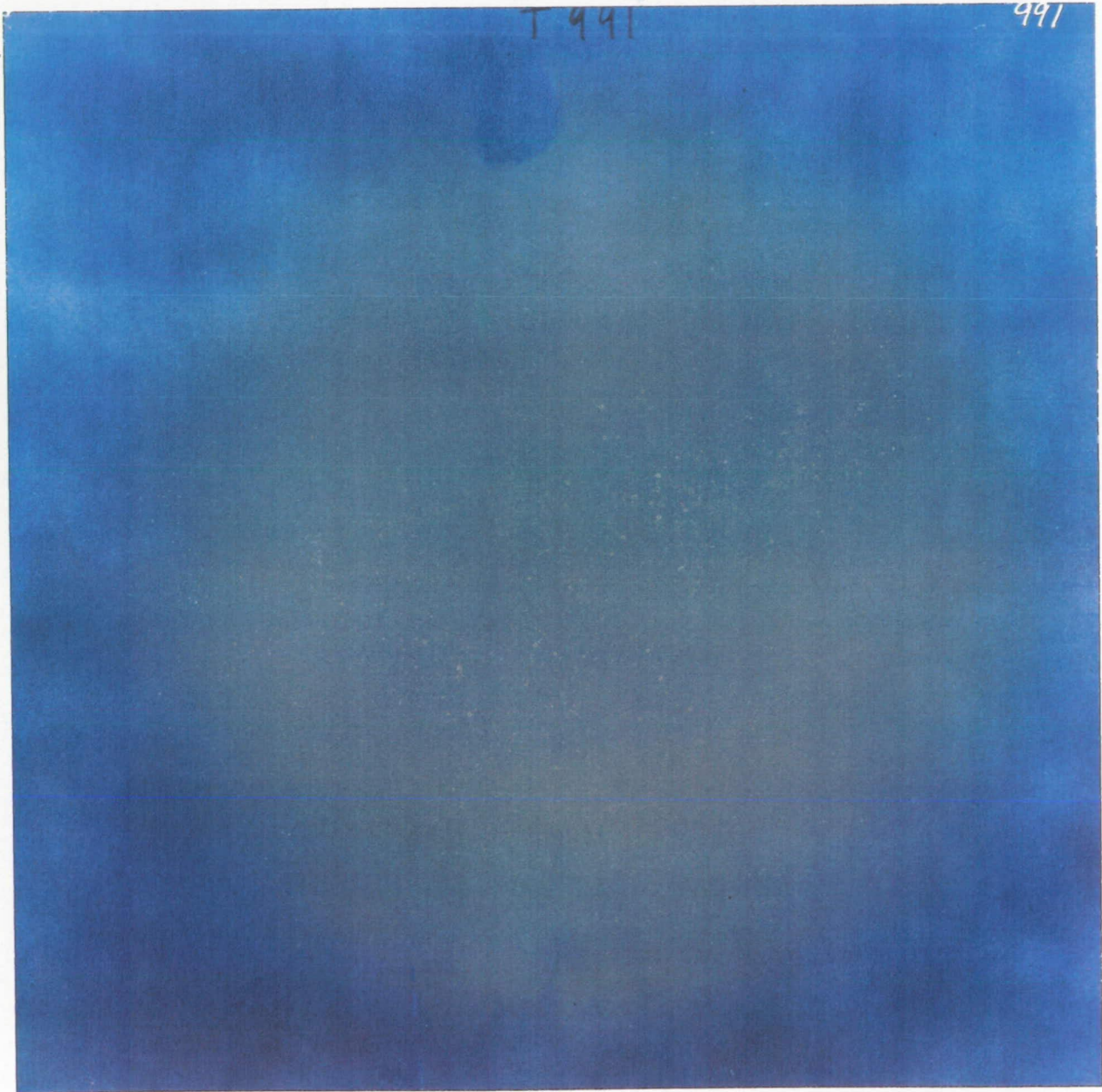
Target:  
 $M = 1.590 \text{ mm}$   
 $T = 0.2540 \text{ mm}$   
 $N = 10$   
 $S = 50.8 \text{ mm}$   
 $SM = 0.180 \text{ g/cm}^2$





T 991

991

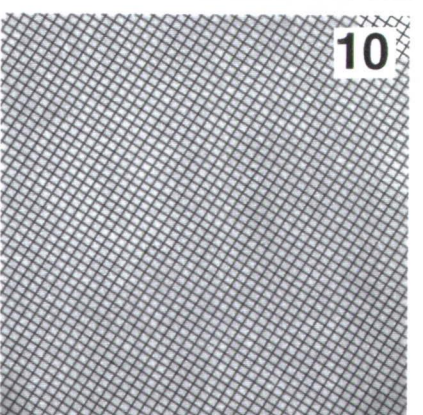
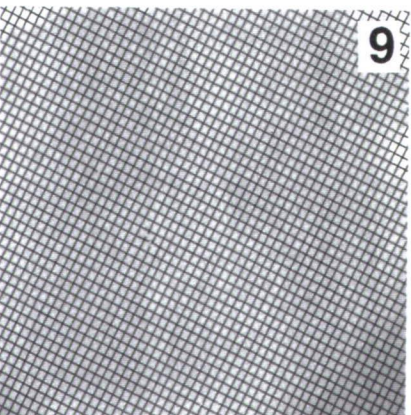
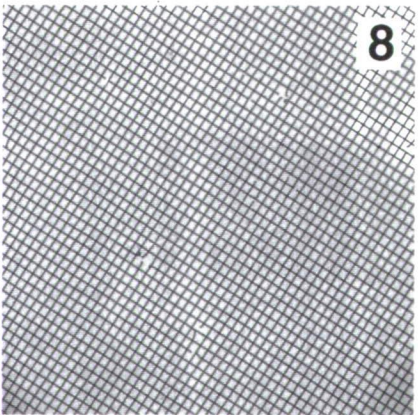
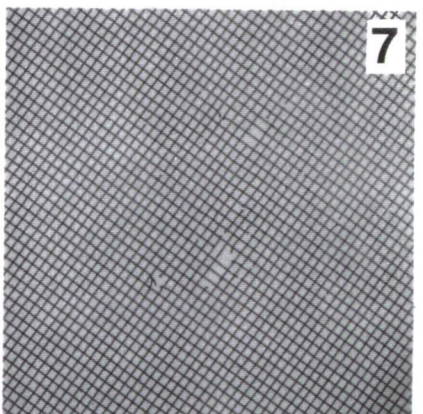
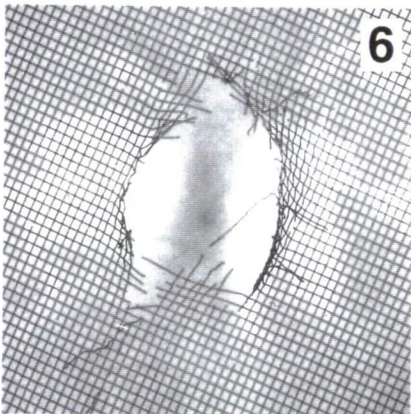
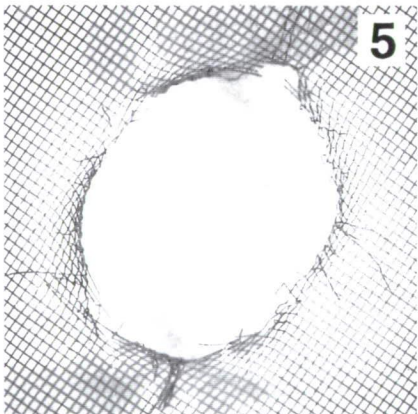
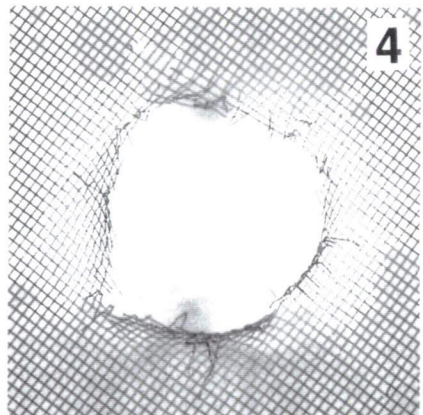
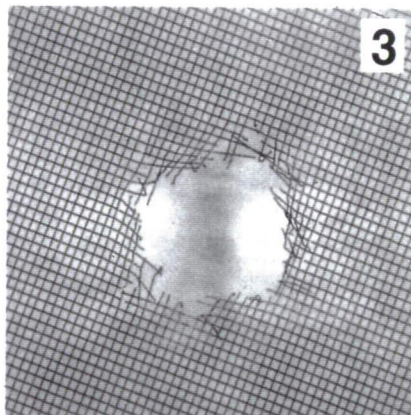
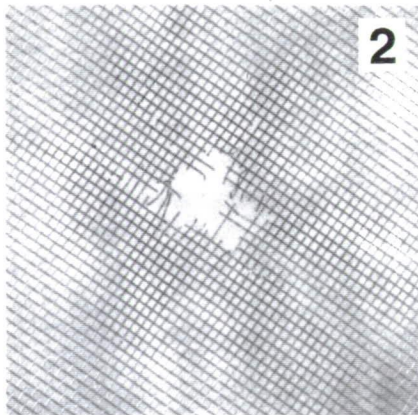
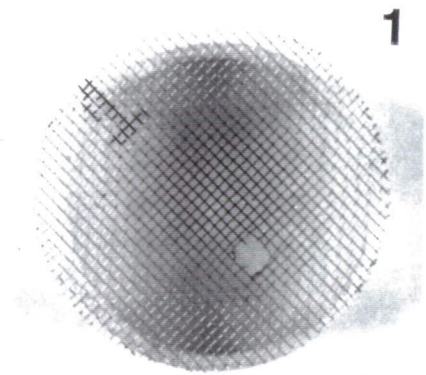




# Experiment: 993

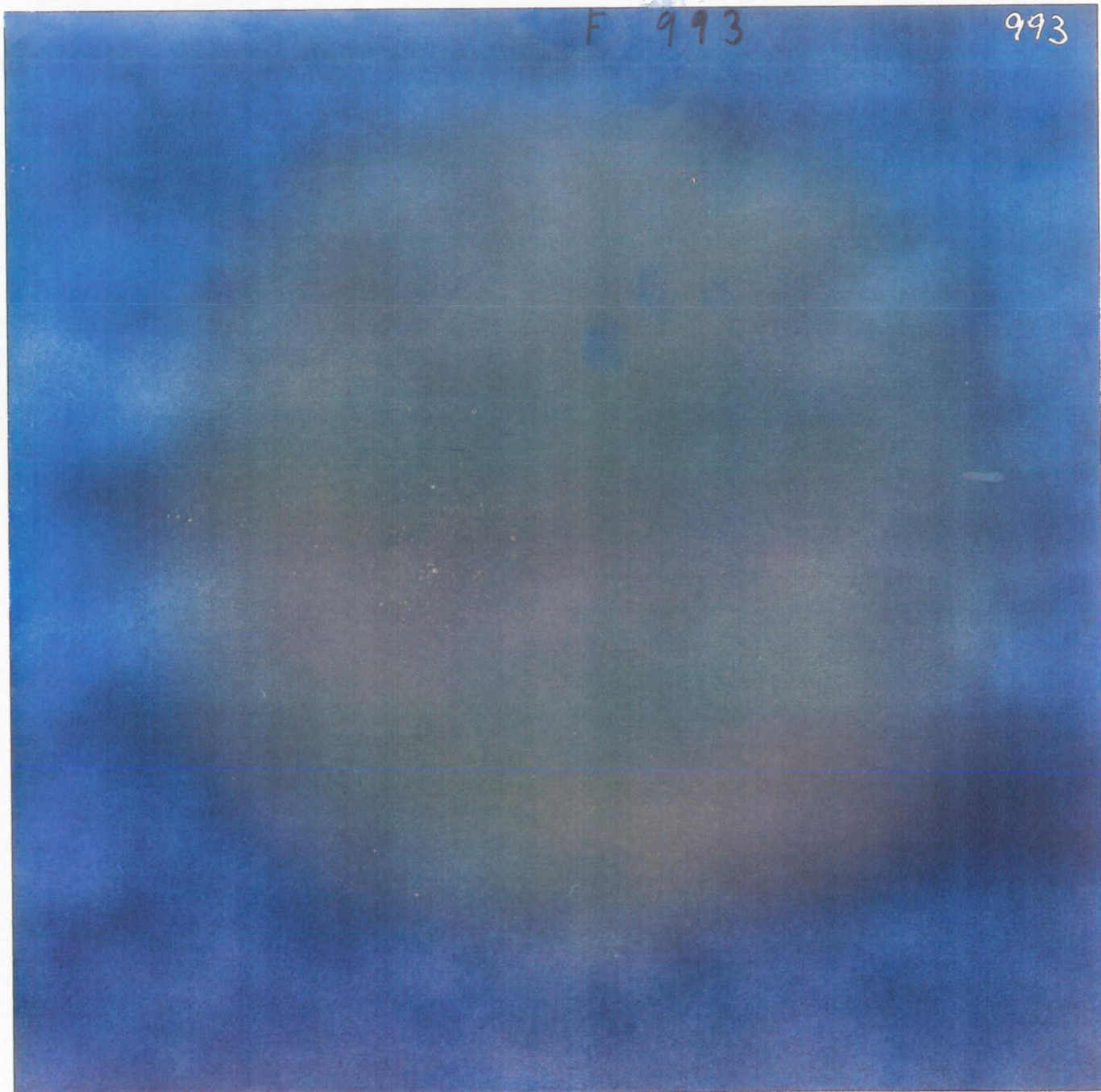
Projectile: Al  
D<sub>p</sub> = 3.175 mm  
V = 5.76 km/s

Target:  
M = 1.590 mm  
T = 0.2540 mm  
N = 10  
S = 50.8 mm  
SM = 0.180 g/cm<sup>2</sup>



F 993

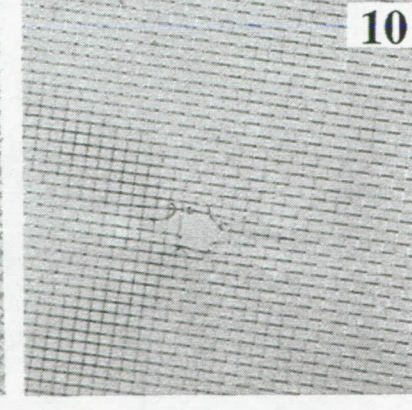
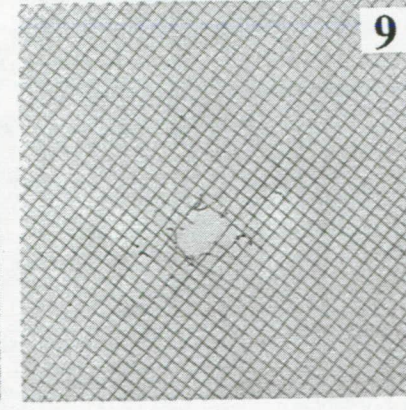
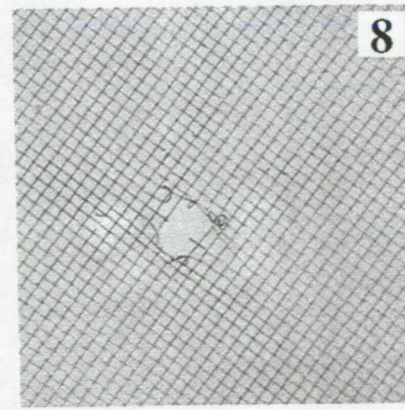
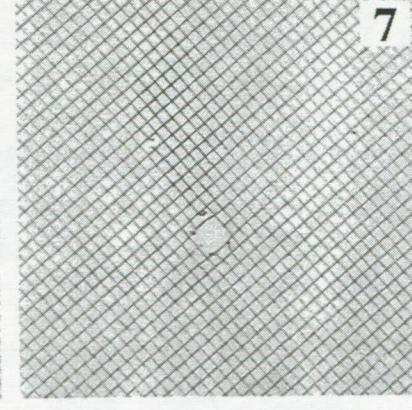
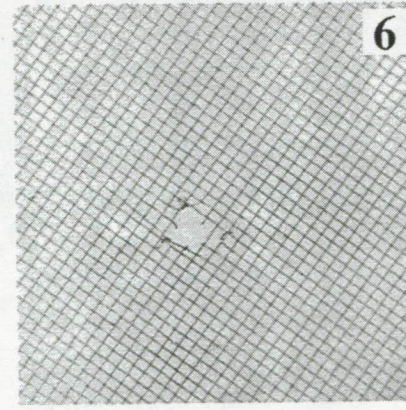
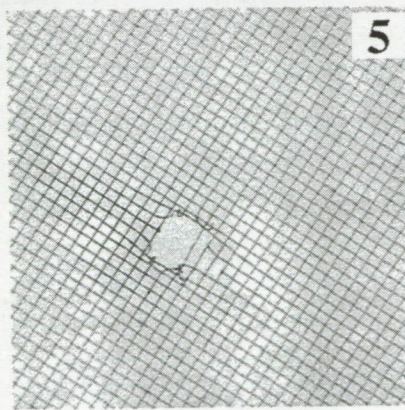
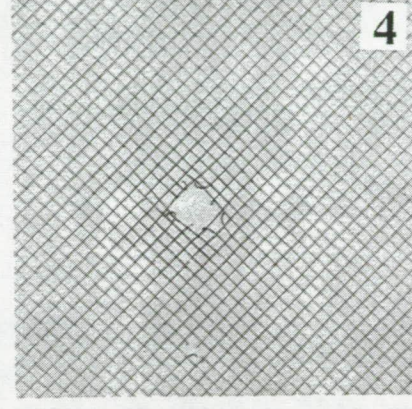
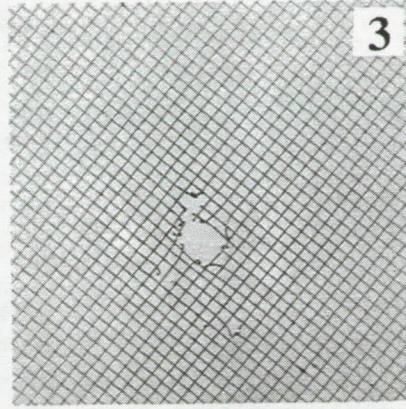
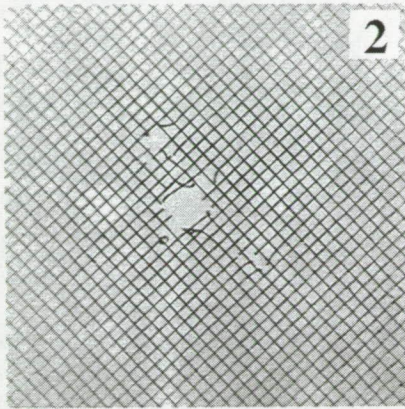
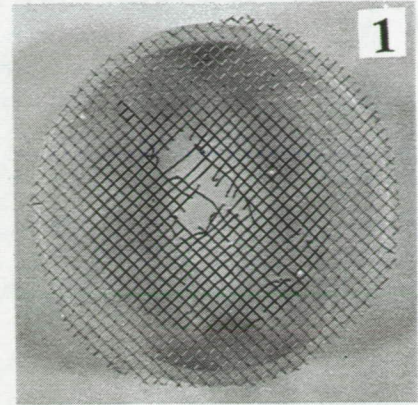
993



# Experiment: 995

Projectile: SS 440  
 $D_p = 3.175 \text{ mm}$   
 $V = 4.59 \text{ km/s}$

Target:  
 $M = 1.590 \text{ mm}$   
 $T = 0.2540 \text{ mm}$   
 $N = 10$   
 $S = 50.8 \text{ mm}$   
 $SM = 0.180 \text{ g/cm}^2$



995

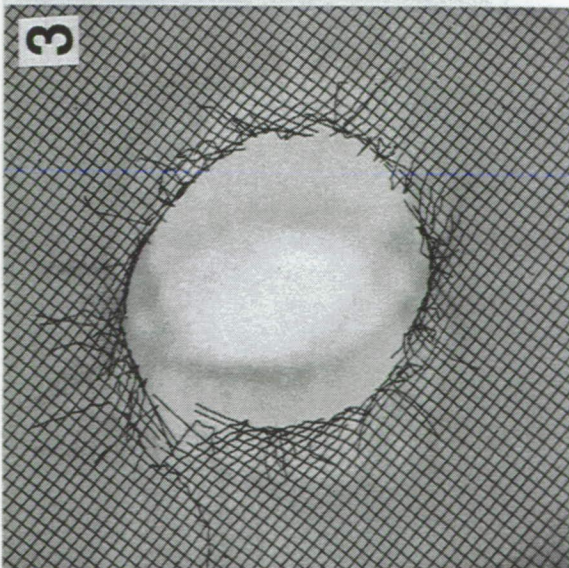
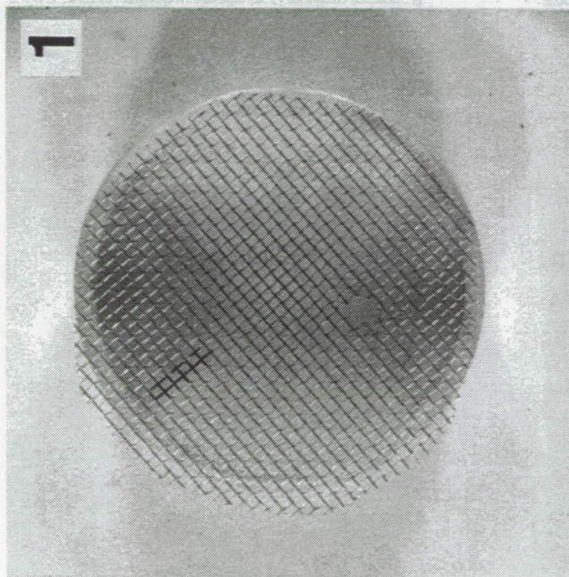
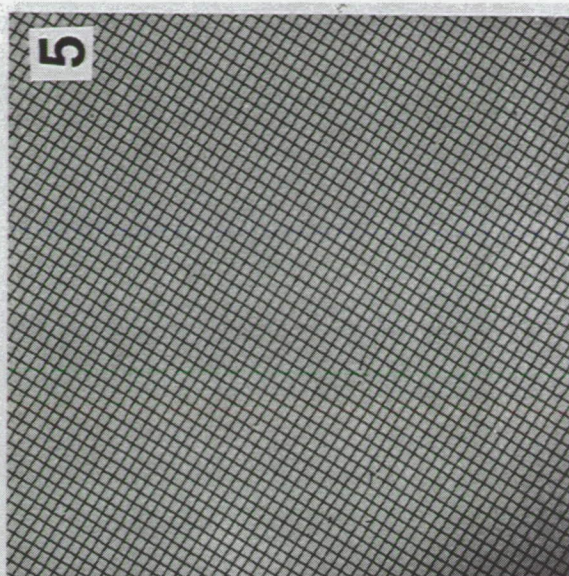
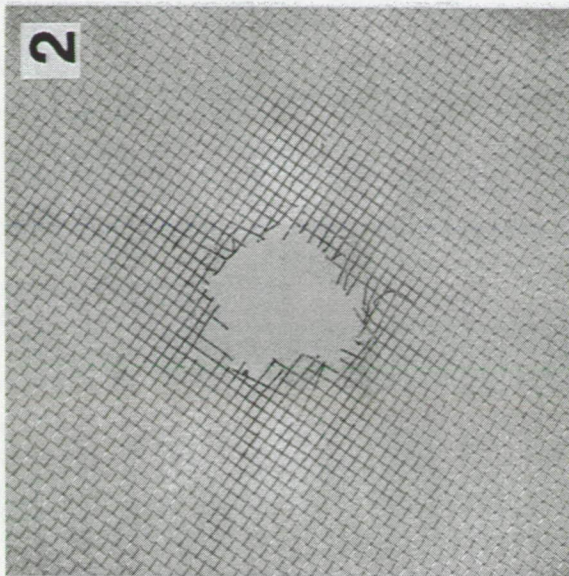
995

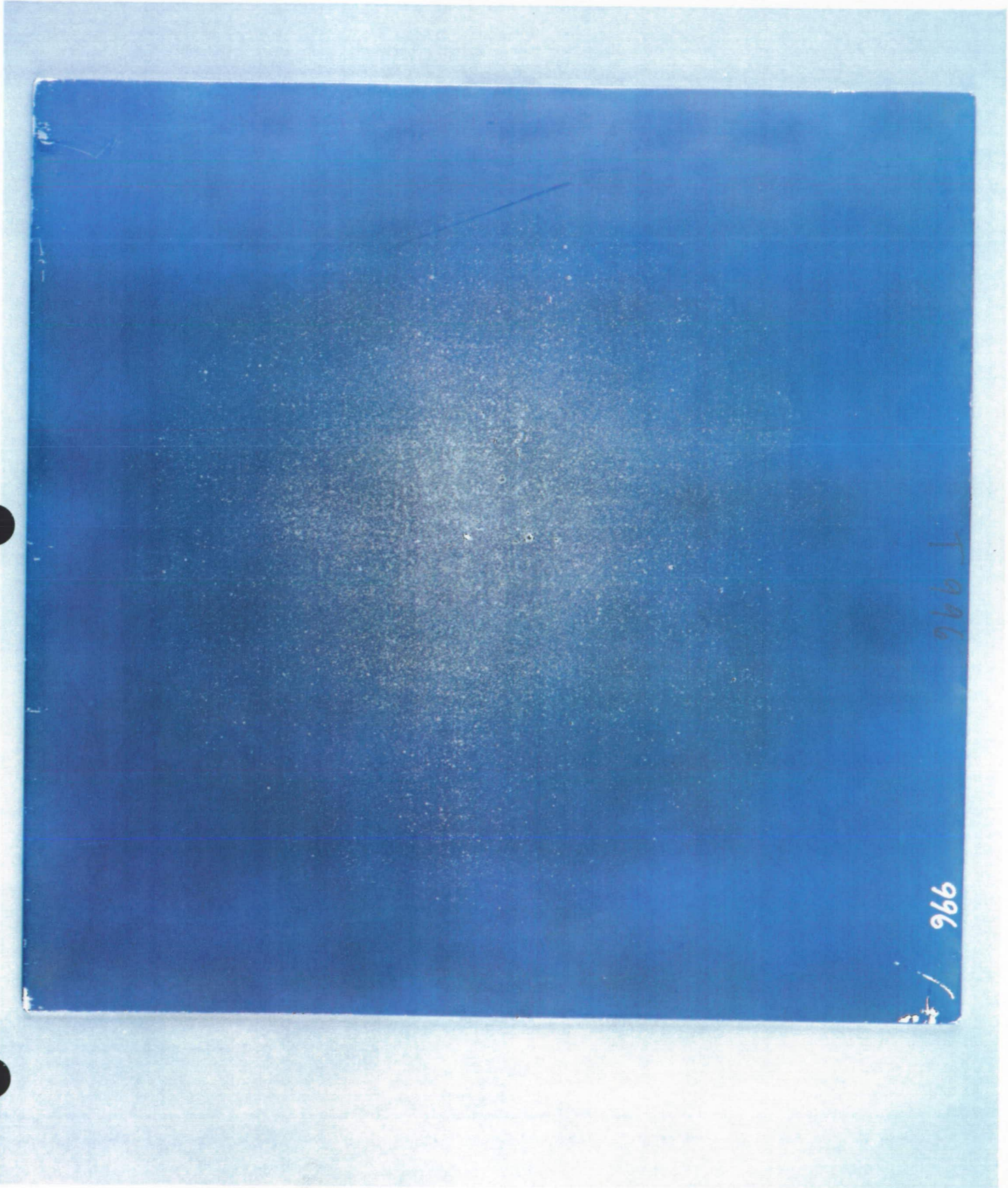


# Experiment: 996

Projectile: SL = 1.590 mm  
Dp = 3.175 mm  
V = 5.86 km/s

Target: M = 0.2540 mm  
T = 5  
S = 101.6 mm  
SM = 0.090 g/cm<sup>2</sup>



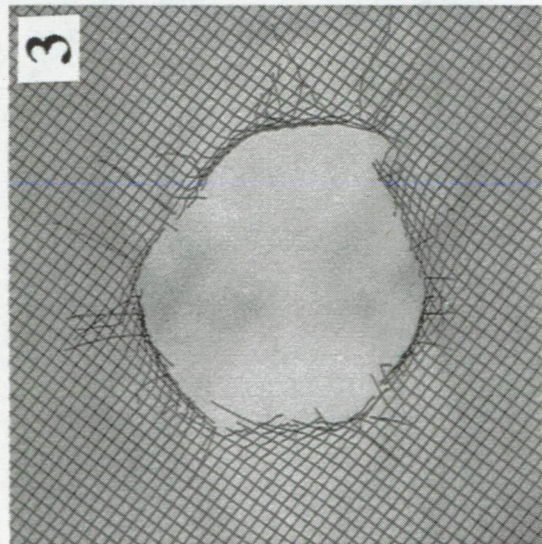
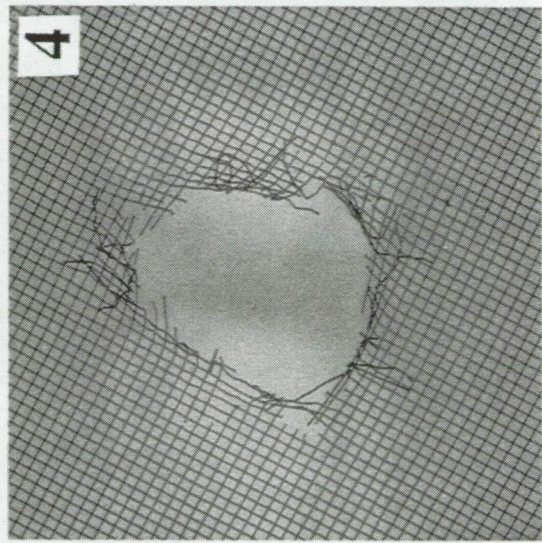
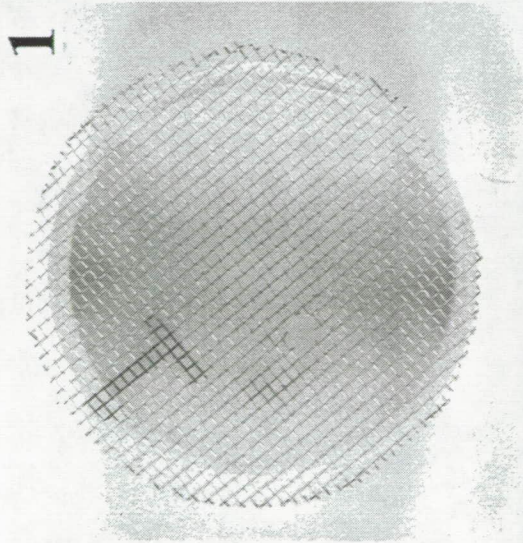
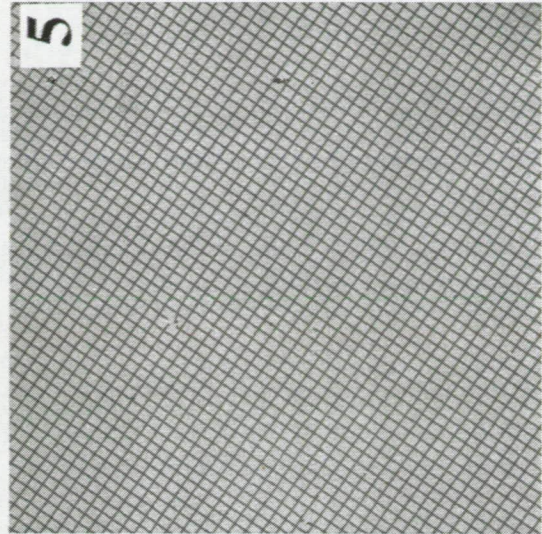
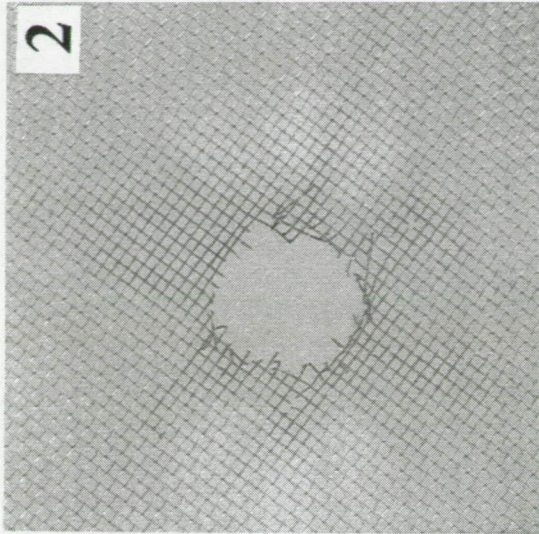




# Experiment: 997

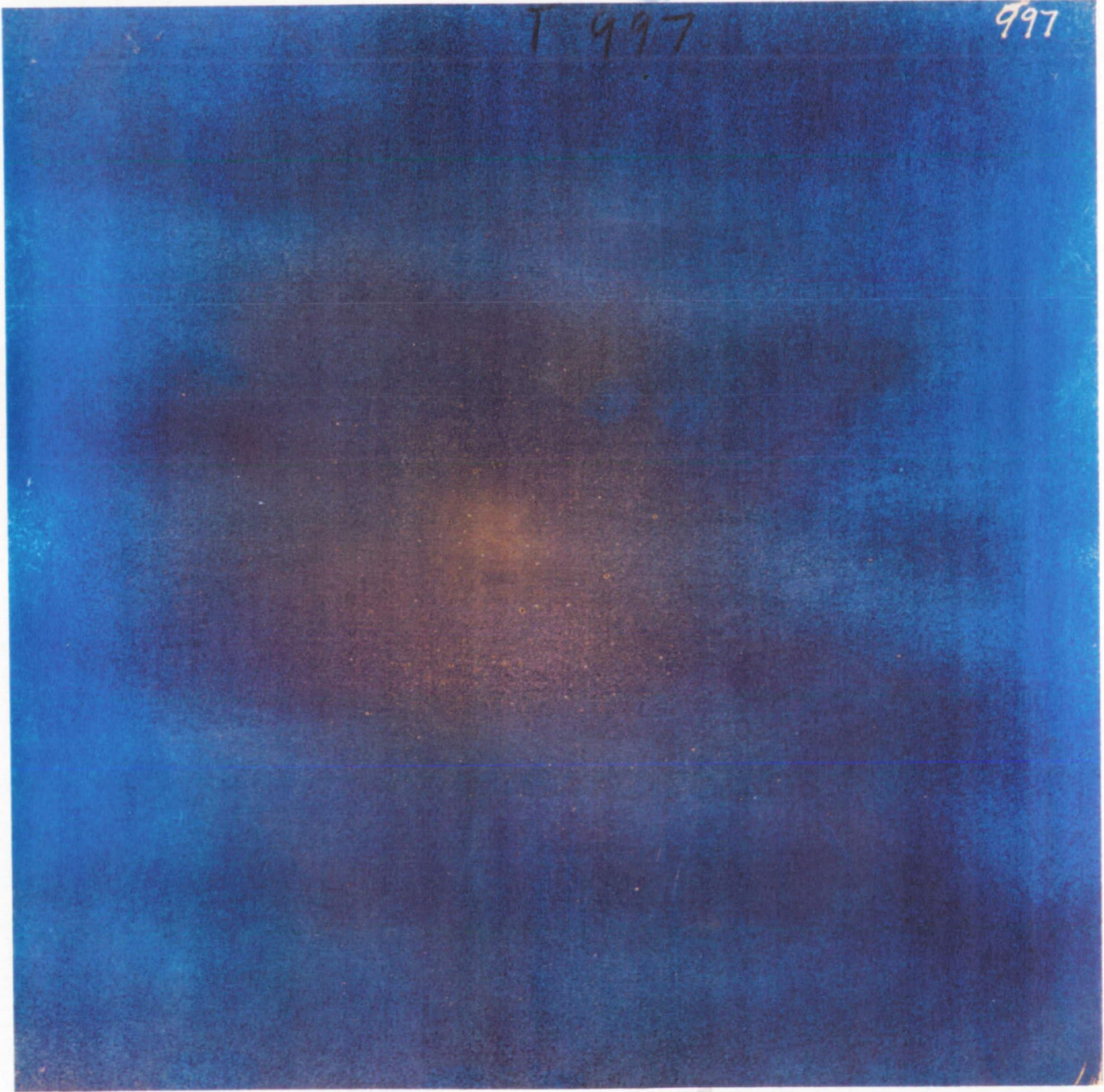
Projectile: SL  
Dp = 3.175 mm  
V = 5.93 km/s

Target: M = 1.590 mm  
T = 0.2540 mm  
N = 5  
S = 101.6 mm  
SM = 0.090 g/cm<sup>2</sup>



T 997

997

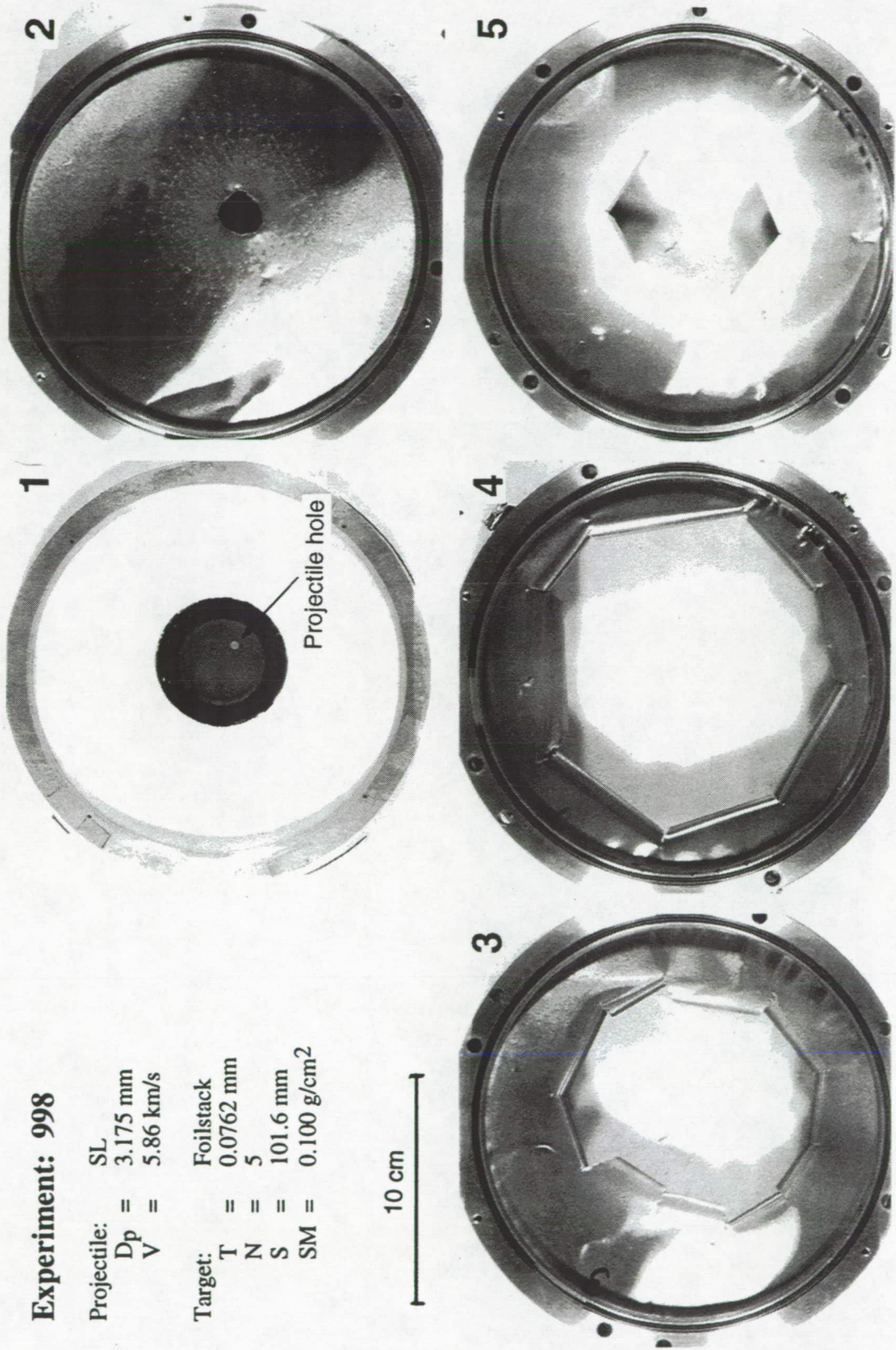


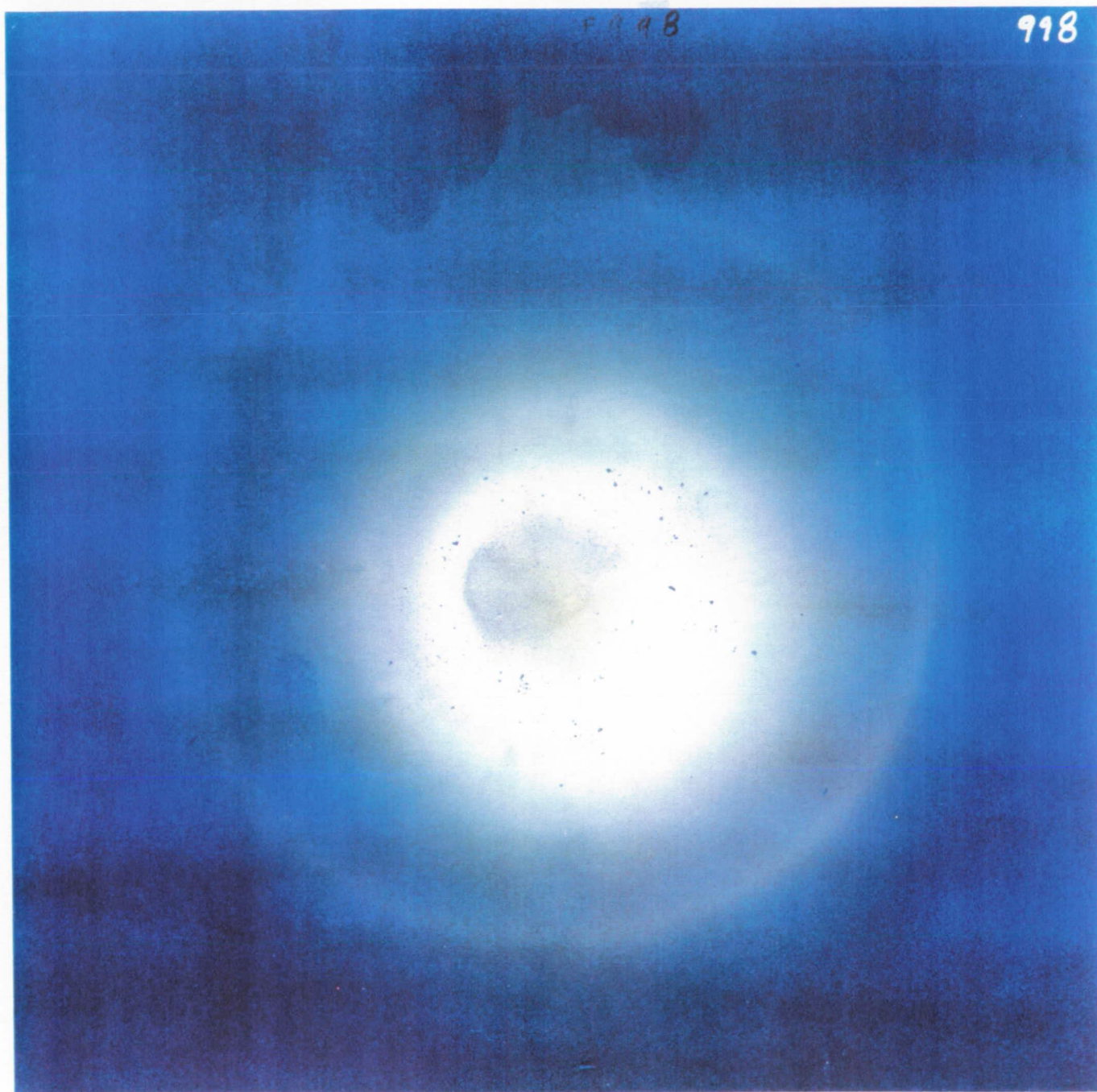
**Experiment: 998**

Projectile: SL  
Dp = 3.175 mm  
V = 5.86 km/s

Target: Foilstack  
T = 0.0762 mm  
N = 5  
S = 101.6 mm  
SM = 0.100 g/cm<sup>2</sup>

10 cm



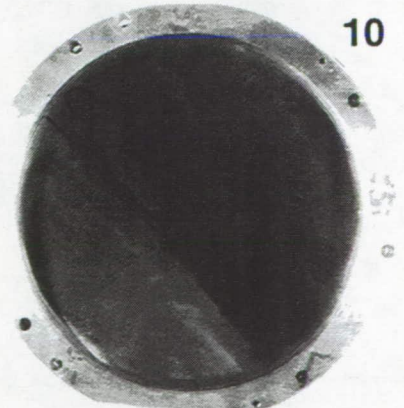
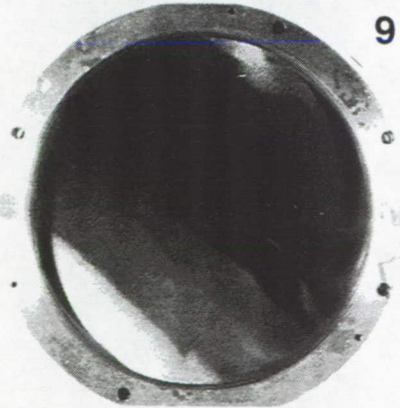
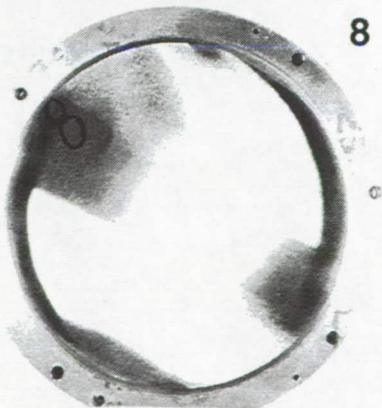
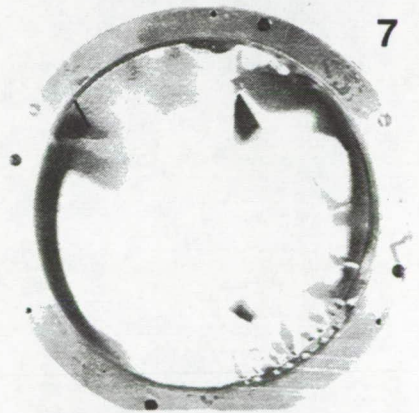
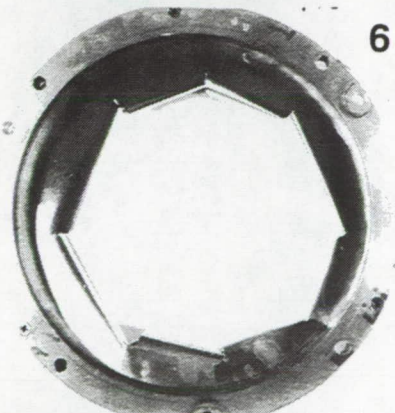
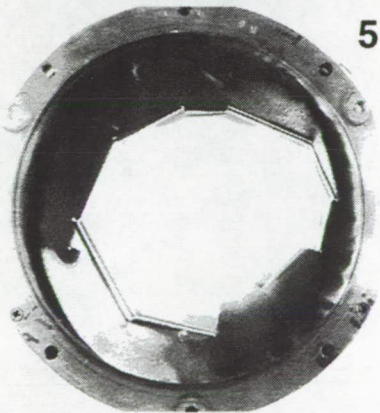
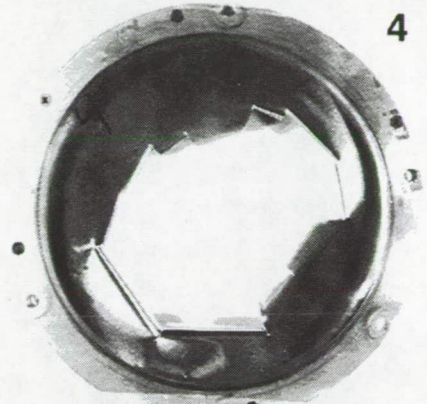
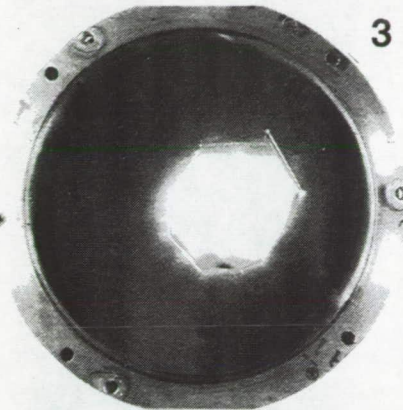
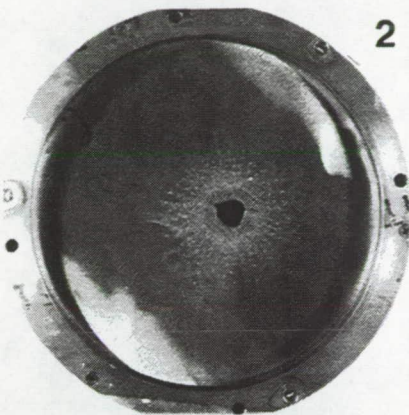
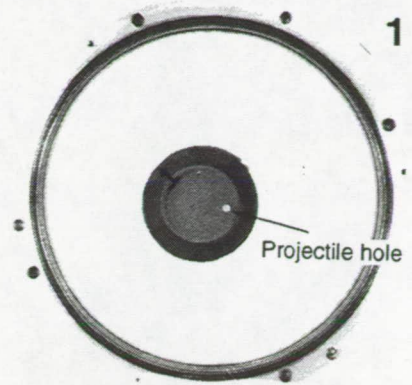


**Experiment: 999**

Projectile: SL  
 $D_p = 3.175 \text{ mm}$   
 $V = 6.03 \text{ km/s}$

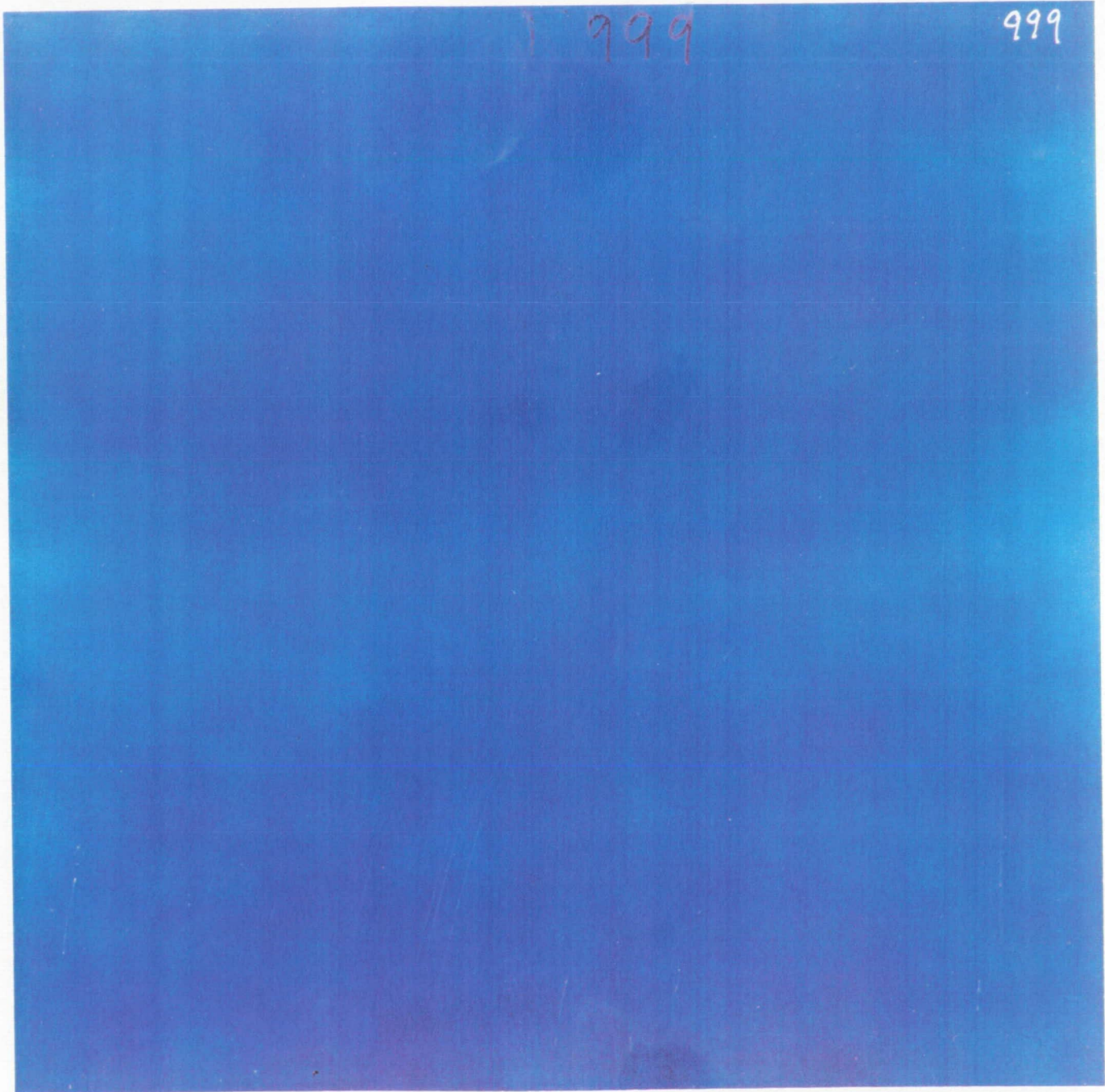
Target: Foilstack  
 $T = 0.0762 \text{ mm}$   
 $N = 10$   
 $S = 50.8 \text{ mm}$   
 $SM = 0.200 \text{ g/cm}^2$

10 cm



999

999

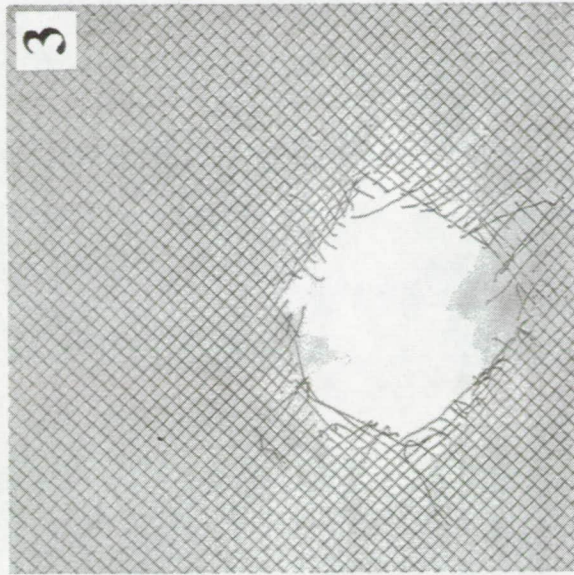
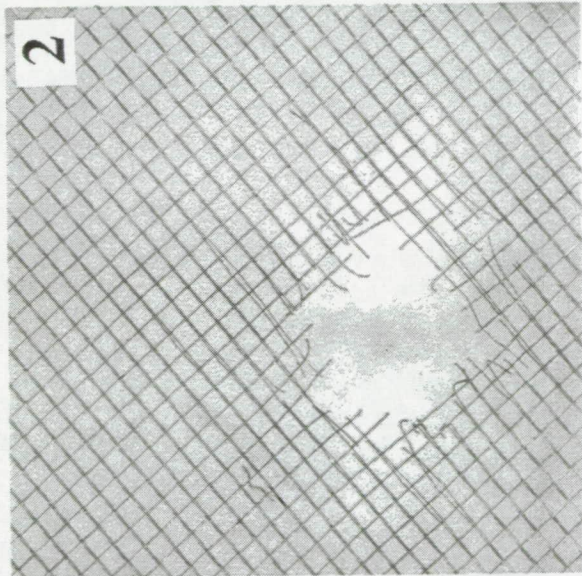
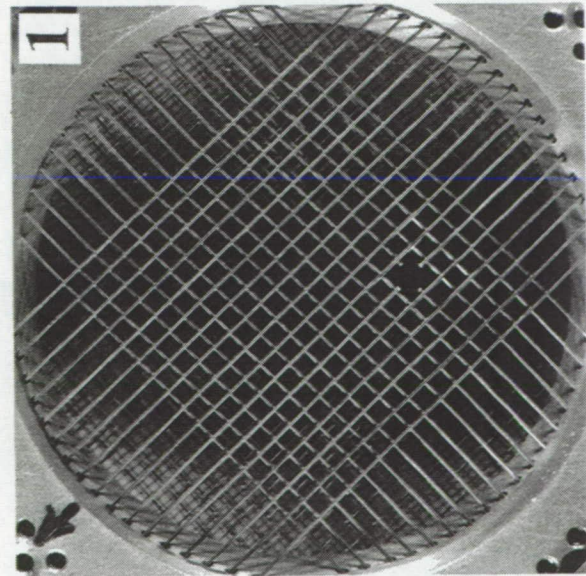


# Experiment: 1002

Projectile: SL  
Dp = 3.175 mm  
V = 5.87 km/s

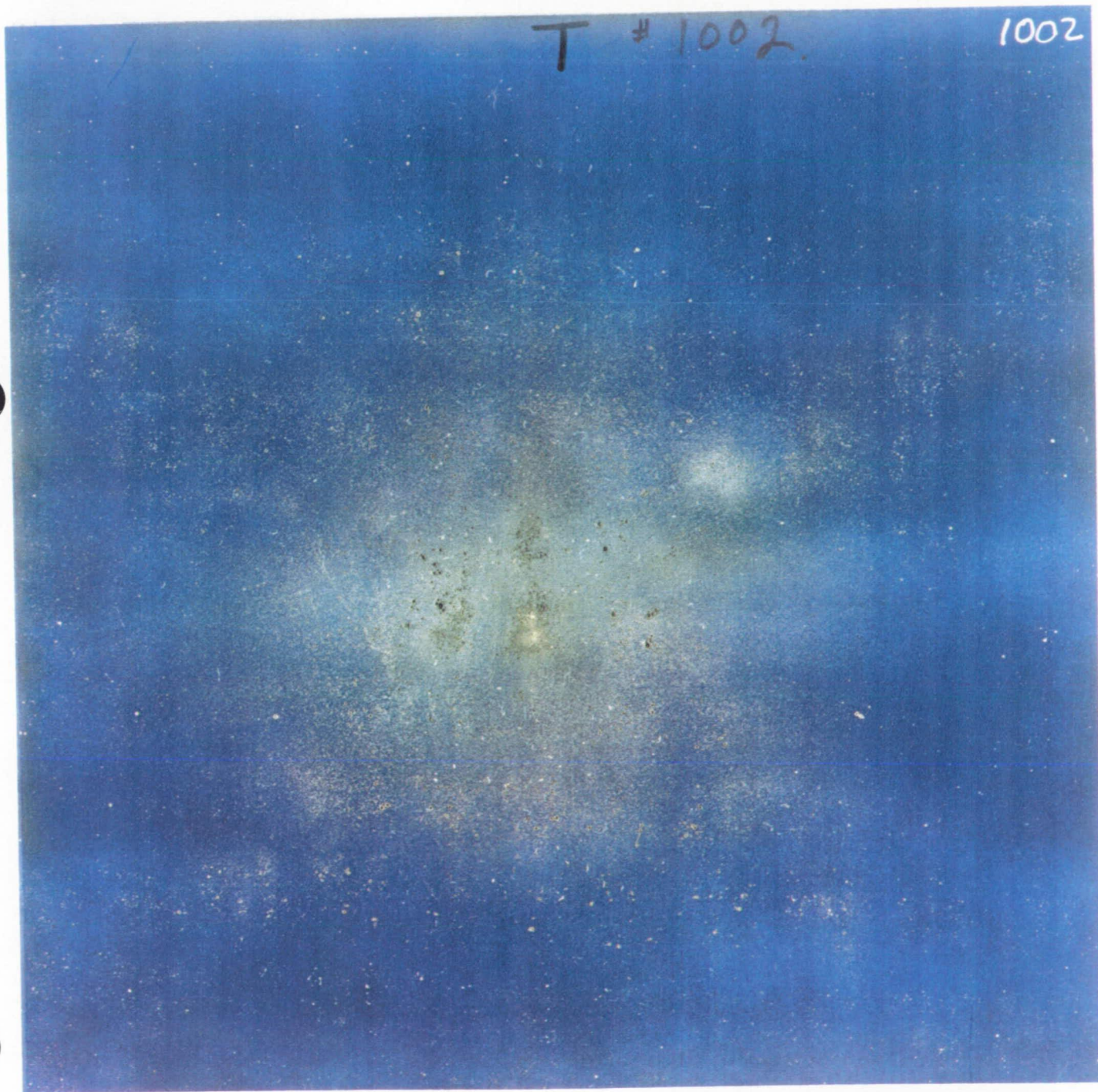
Target: Mixed Meshes  
M = Variable  
T = Variable  
N = 3  
S = 25.4 mm  
SM = 0.080 g/cm<sup>2</sup>

SM  
1 ——— 0.046  
2 ——— 0.016  
3 ——— 0.018



T # 1002

1002





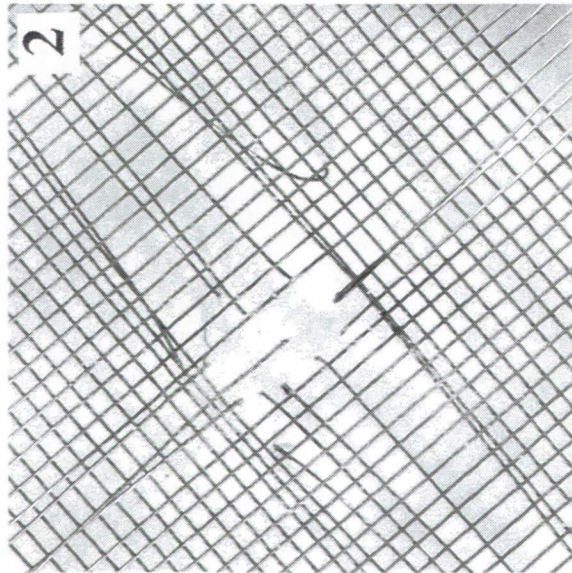
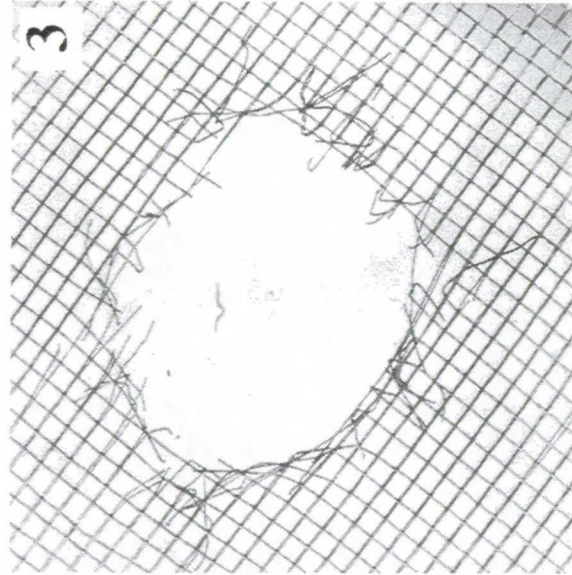
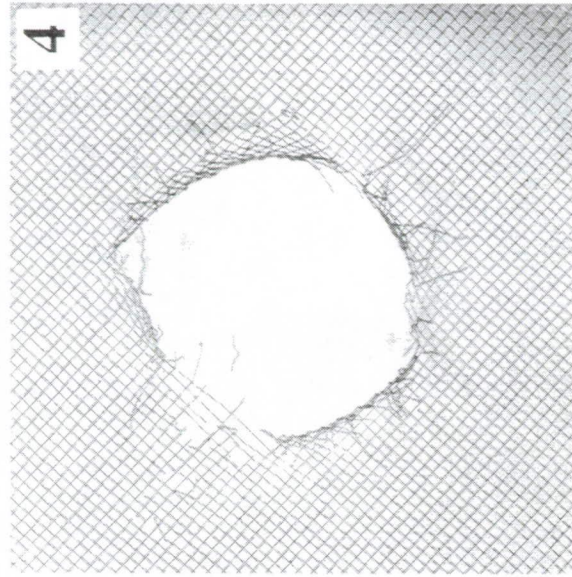
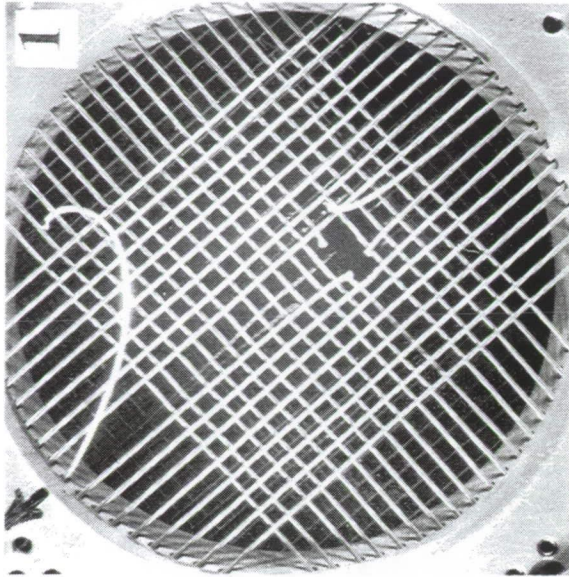
RECORDING TAPE BLANK NOT FILMED

# Experiment: 1003

Projectile: SL  
 Dp = 3.175 mm  
 V = 5.91 km/s

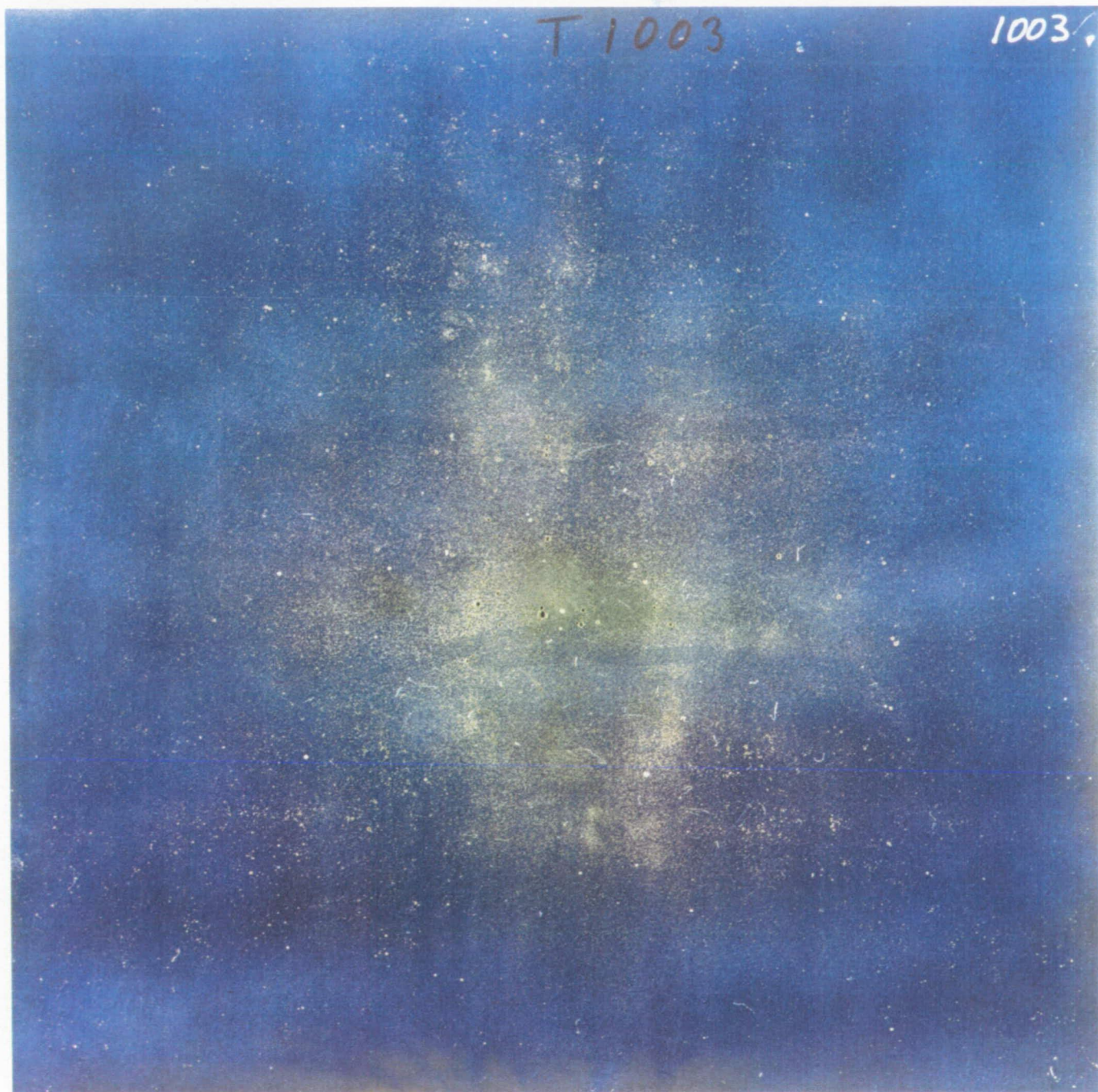
Target: Mixed Meshes  
 M = Variable  
 T = Variable  
 N = 4  
 S = 25.4 mm  
 SM = 0.158 g/cm<sup>2</sup>

	SM
1	0.078
2	0.046
3	0.016
4	0.018



T 1003

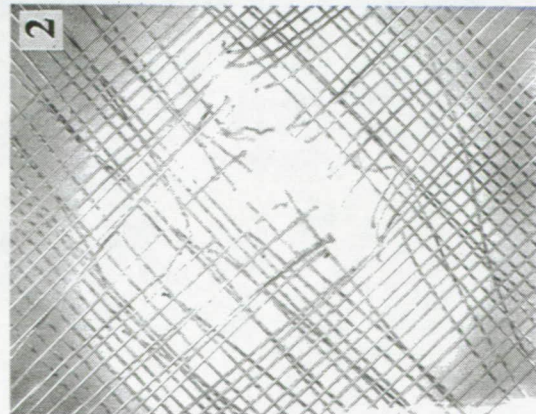
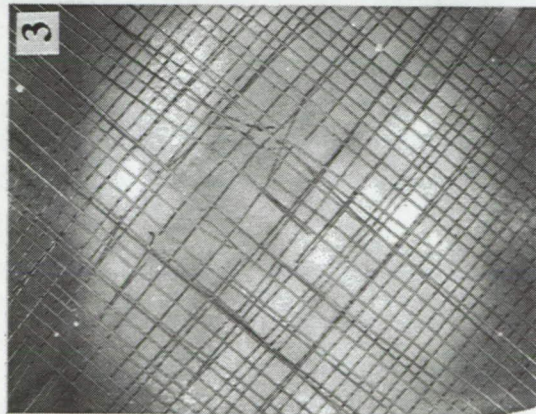
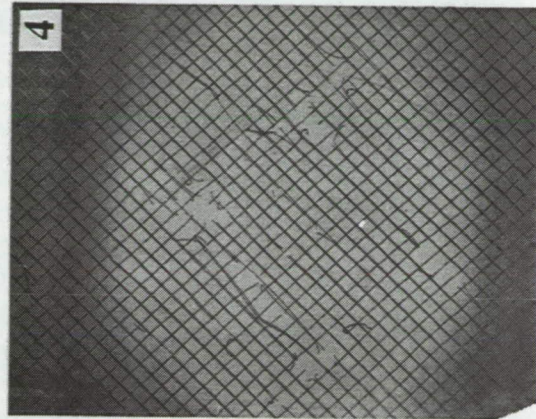
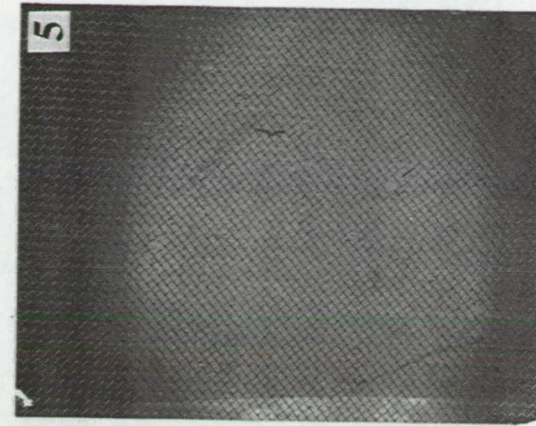
1003/



**Experiment: 1004**

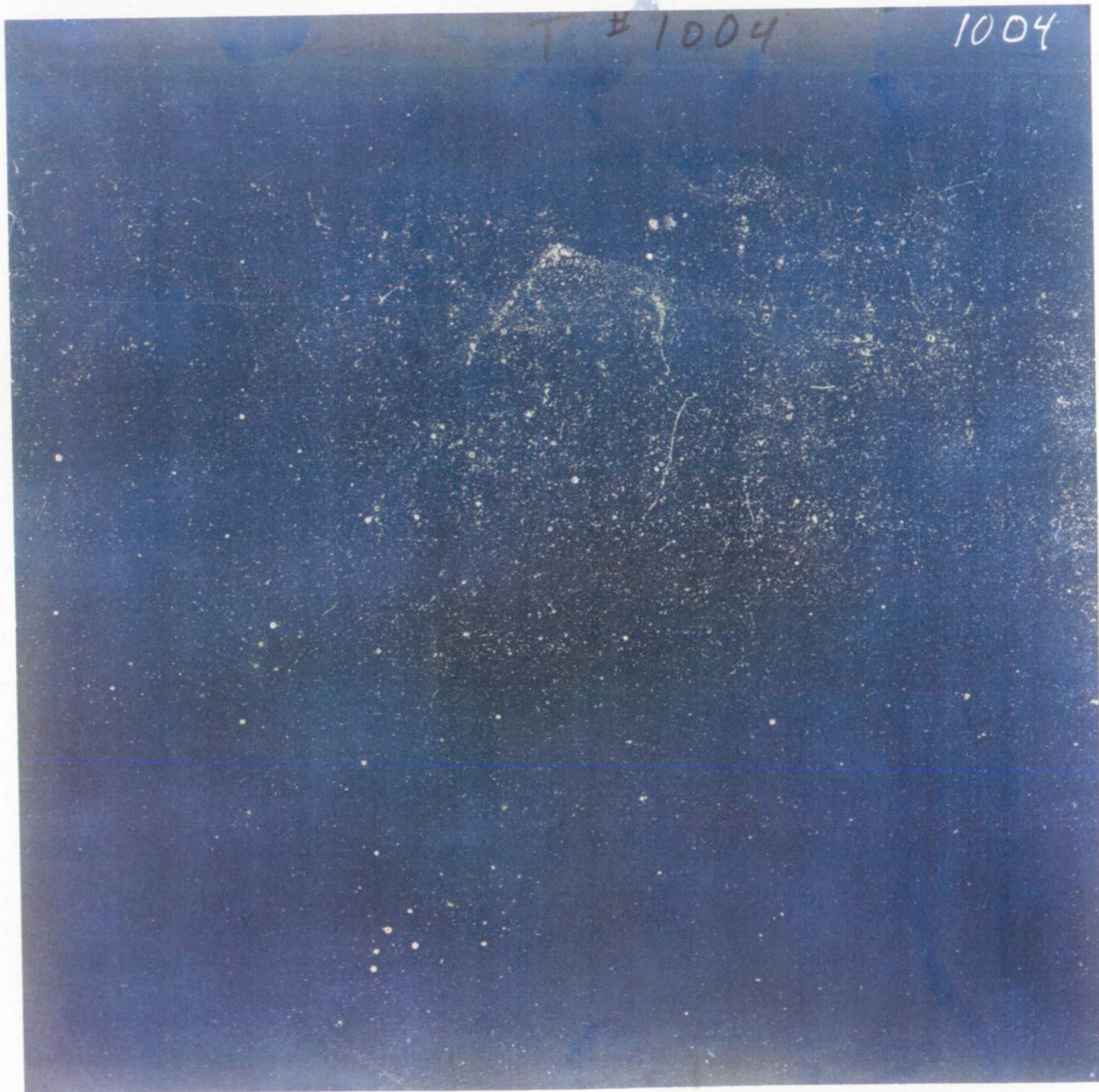
Projectile: SL = 3.175 mm  
 Dp = 5.80 km/s  
 V =  
 Target: Mixed Meshes  
 M = Variable  
 T = Variable  
 N = 5  
 S = 25.4 mm  
 SM = 0.495 g/cm<sup>2</sup>

SM  
 1 \_\_\_\_\_ 0.338  
 2 \_\_\_\_\_ 0.078  
 3 \_\_\_\_\_ 0.046  
 4 \_\_\_\_\_ 0.016  
 5 \_\_\_\_\_ 0.018



T # 1004

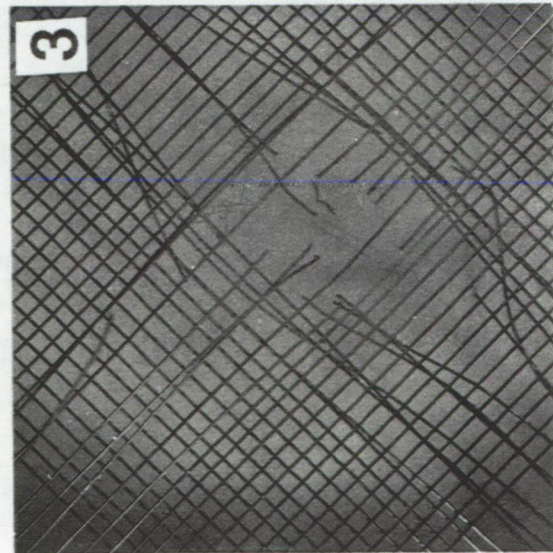
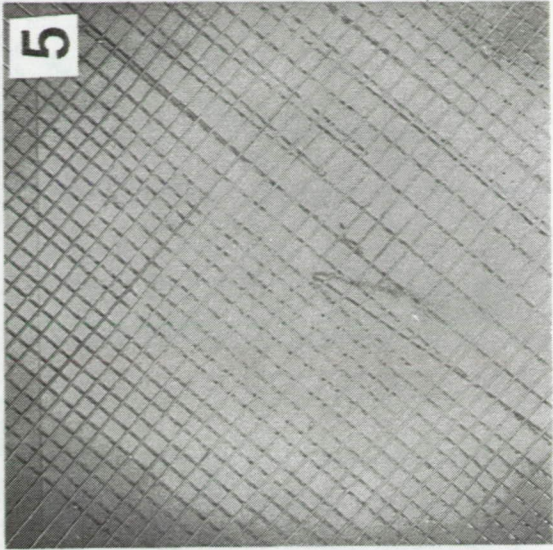
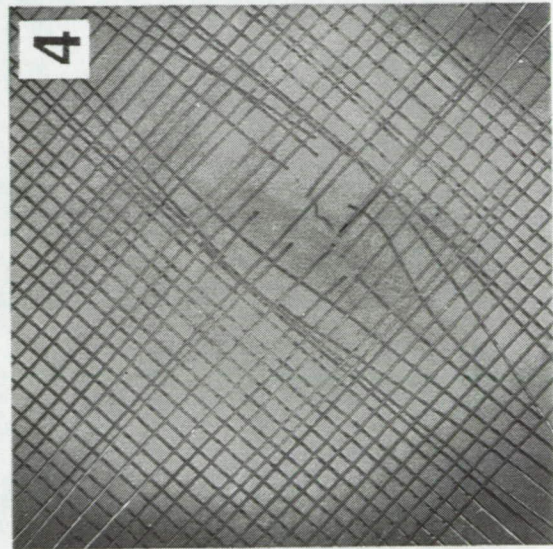
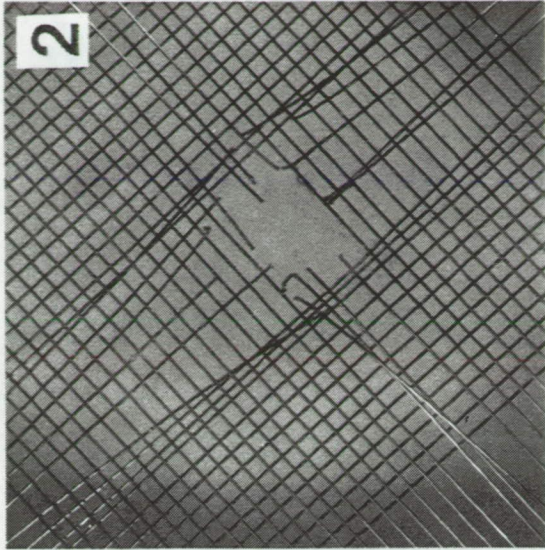
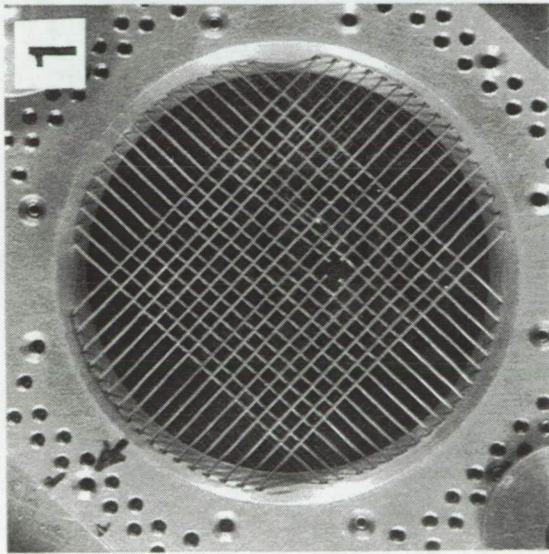
1004



# Experiment: 1006

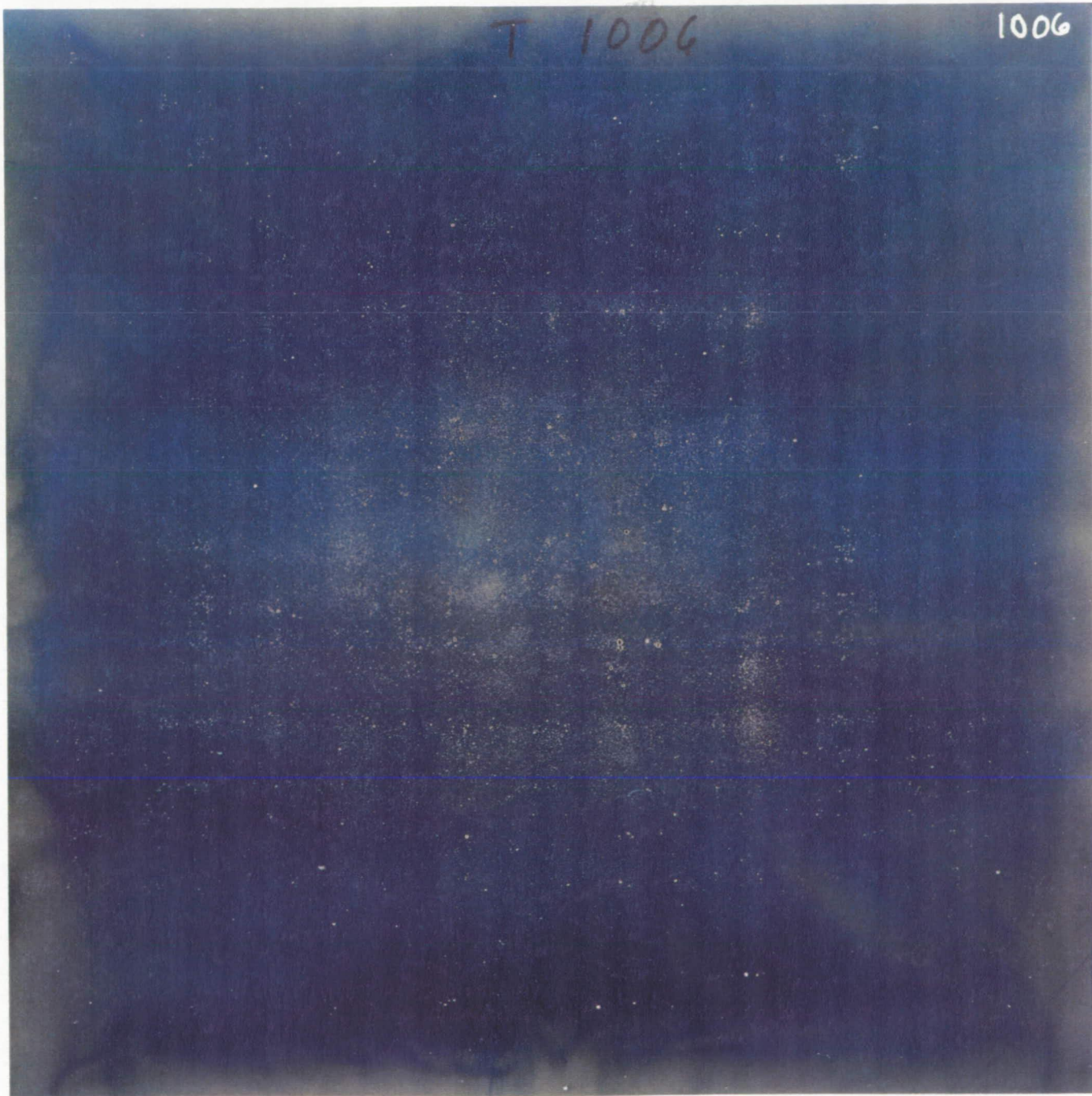
Projectile: SL  
Dp = 3.175 mm  
V = 5.80 km/s

Target: M = 3.175 mm  
T = 0.5842 mm  
N = 5  
S = 25.4 mm  
SM = 0.230 g/cm<sup>2</sup>



T 1006

1006



REPRODUCTION OF THIS DOCUMENT IS PROHIBITED  
UNLESS THE ORIGINAL SOURCE IS CITED

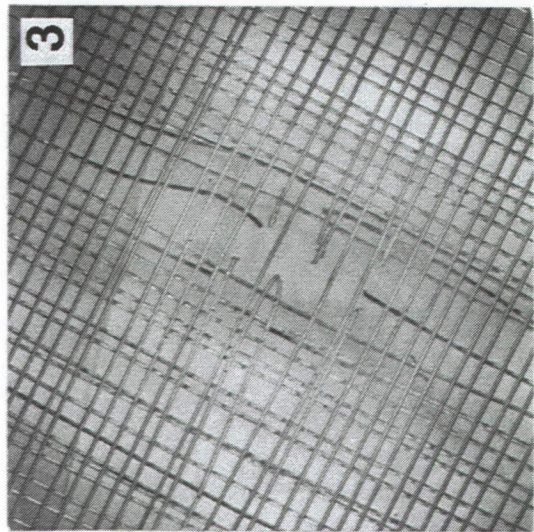
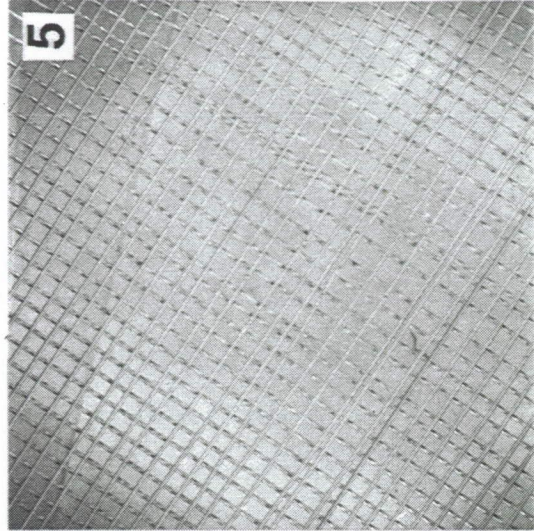
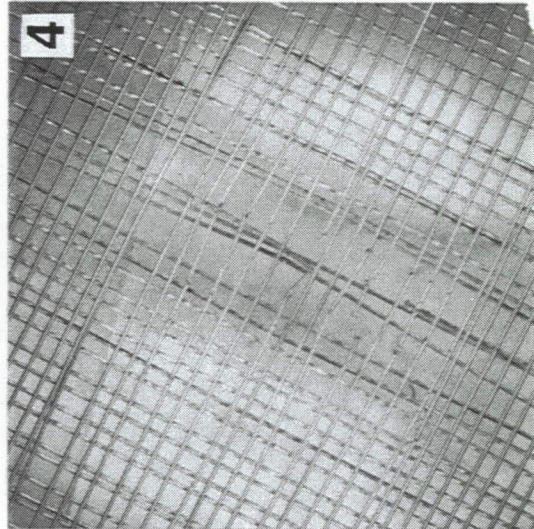
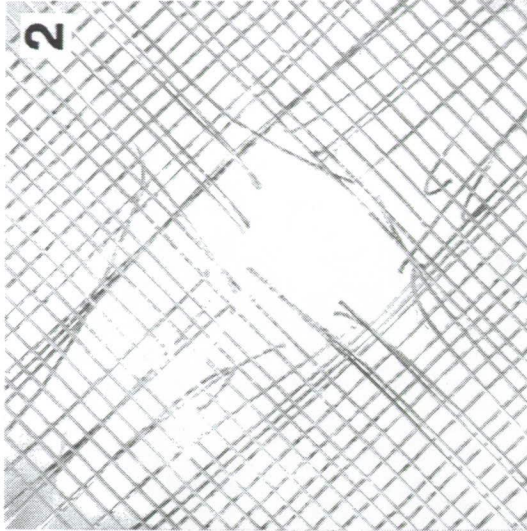
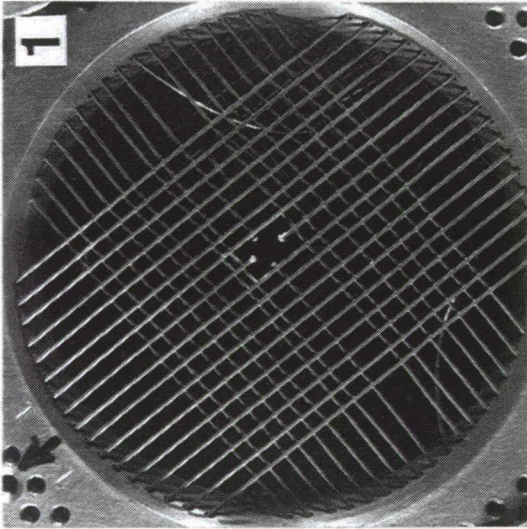
REPRODUCTION OF THIS DOCUMENT IS PROHIBITED  
UNLESS THE ORIGINAL SOURCE IS CITED



**Experiment: 1007**

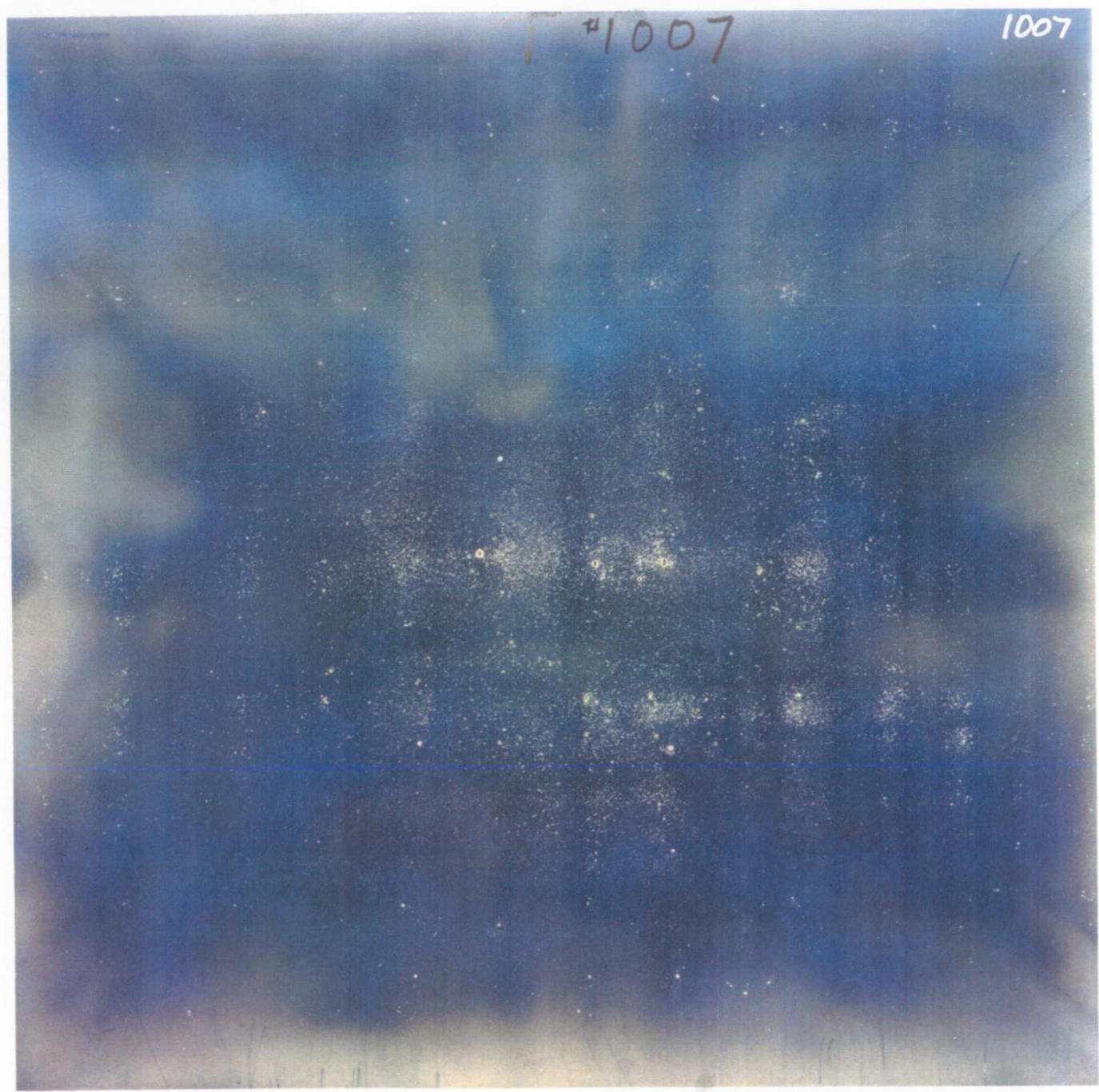
Projectile: SL  
Dp = 3.175 mm  
V = 5.83 km/s

Target: M = 3.175 mm  
T = 0.7620 mm  
N = 5  
S = 25.4 mm  
SM = 0.388 g/cm<sup>2</sup>



ORIGINAL PAGE  
BLACK AND WHITE PHOTOGRAPH

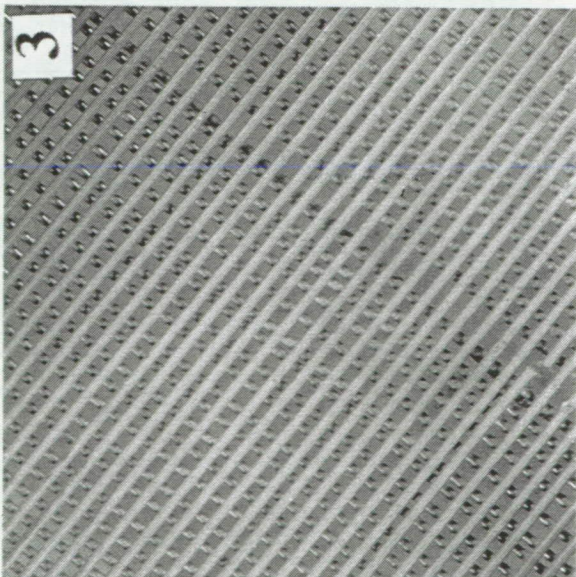
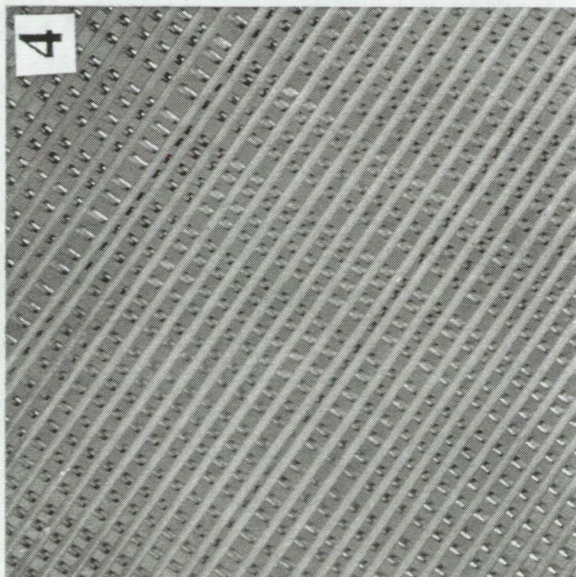
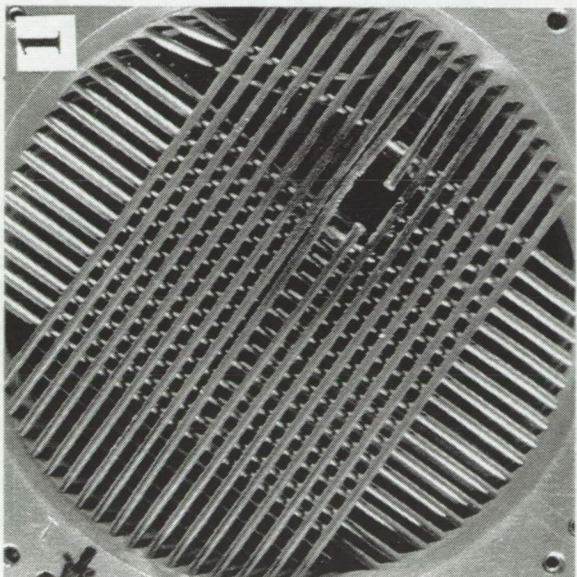
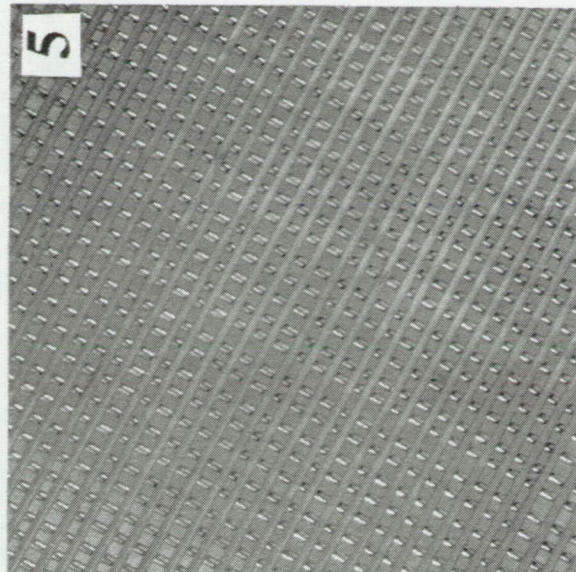
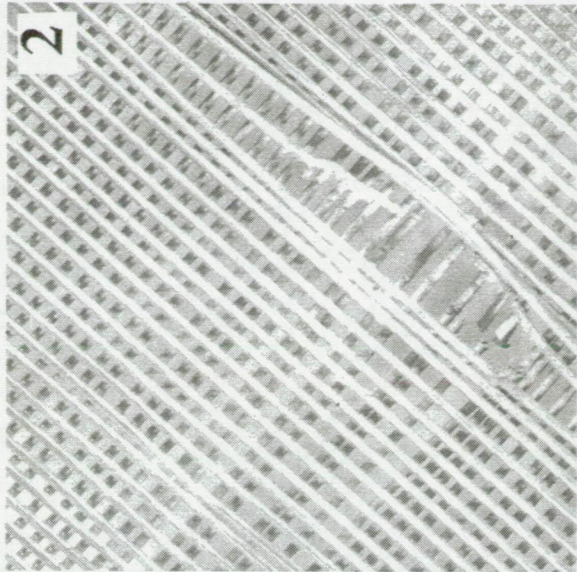
C-2



# Experiment: 1008

Projectile: SL  
Dp = 3.175 mm  
V = 5.94 km/s

Target: M = 3.175 mm  
T = 1.5900 mm  
N = 5  
S = 25.4 mm  
SM = 1.688 g/cm<sup>2</sup>



1008

1008

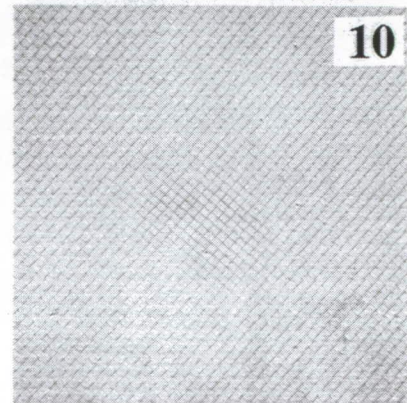
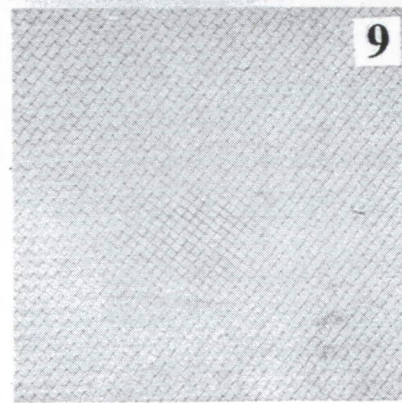
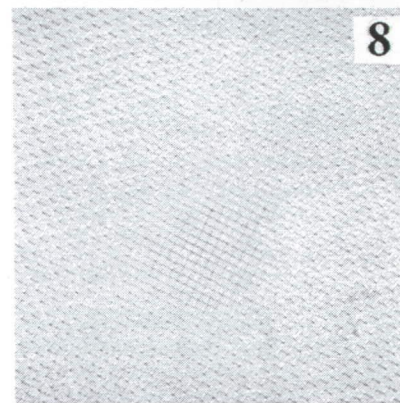
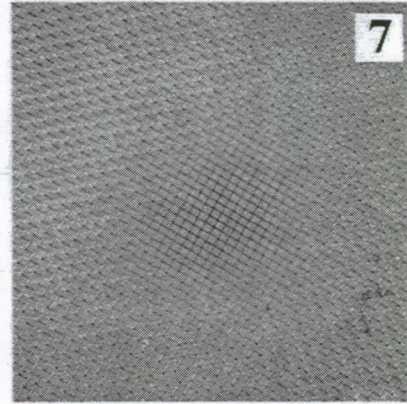
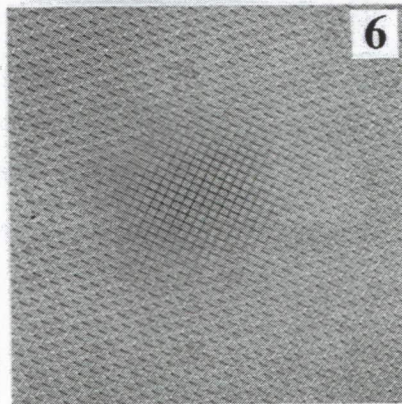
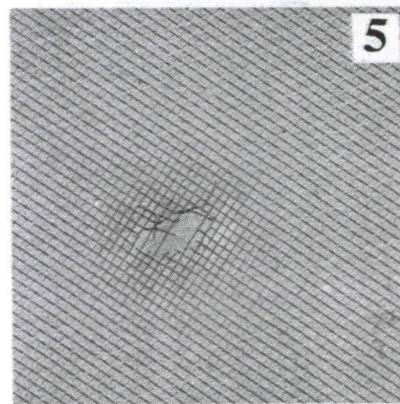
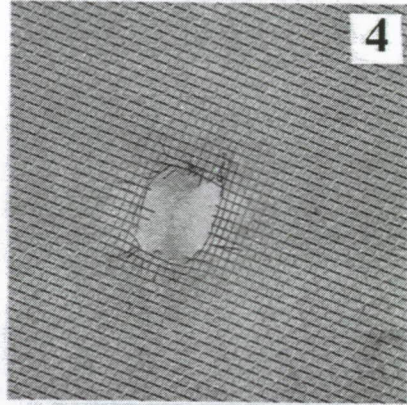
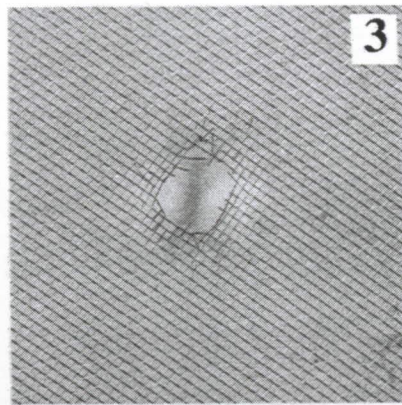
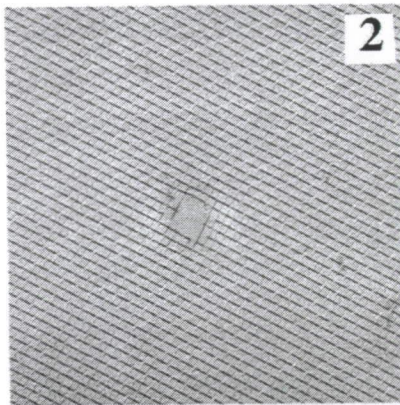
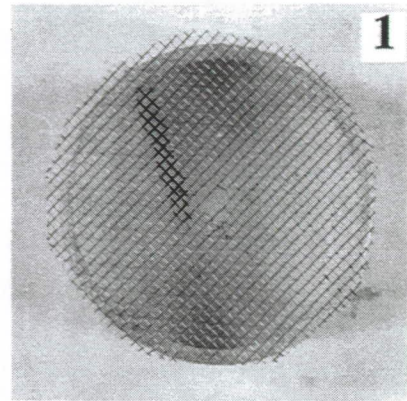




# Experiment: 3422

Projectile: SL  
D<sub>p</sub> = 3.175 mm  
V = 1.02 km/s

Target:  
M = 1.590 mm  
T = 0.254 mm  
N = 10  
S = 50.8 mm  
SM = 0.180 g/cm<sup>2</sup>



ORIGINAL PAGE  
BLACK AND WHITE PHOTOGRAPH

3422

3422

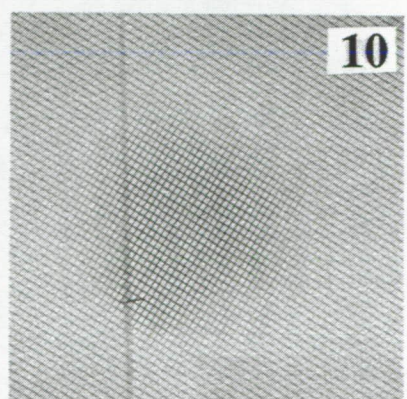
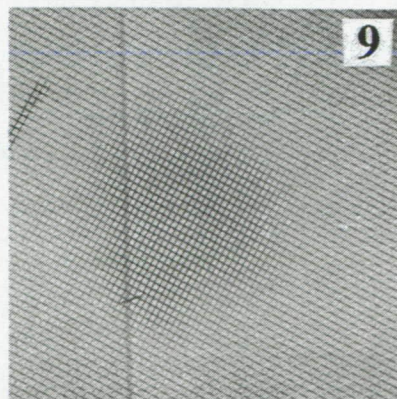
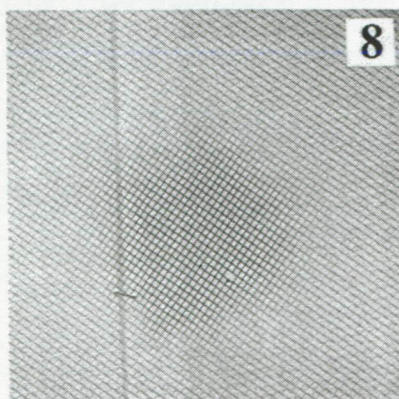
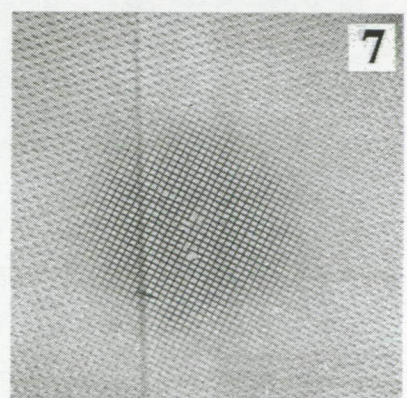
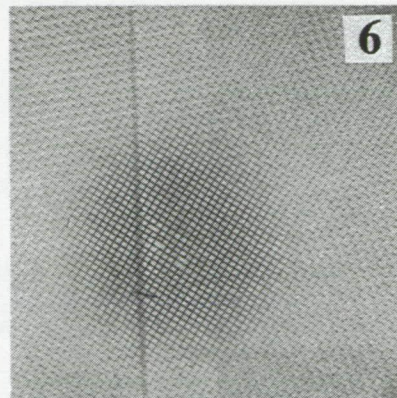
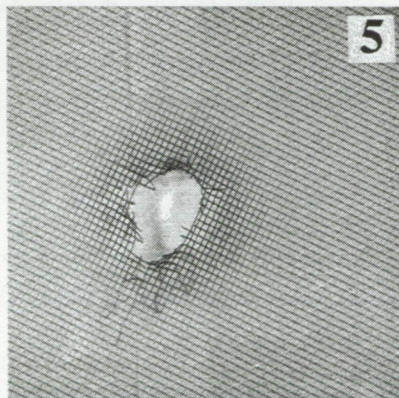
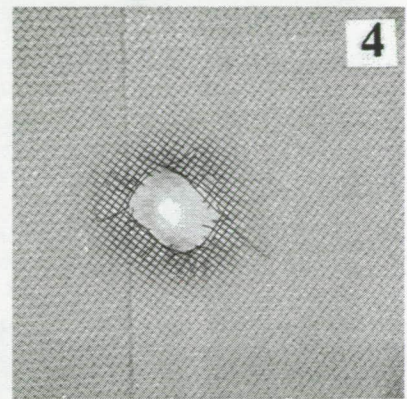
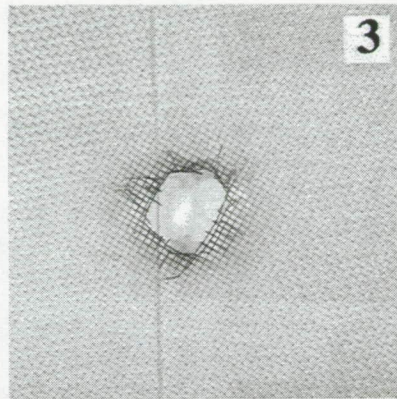
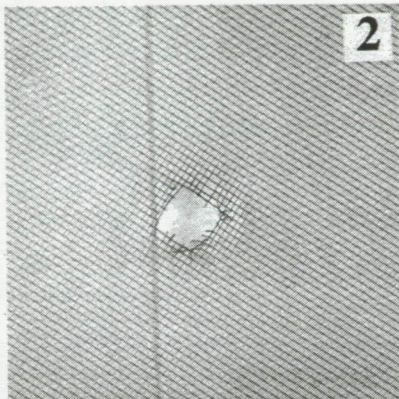
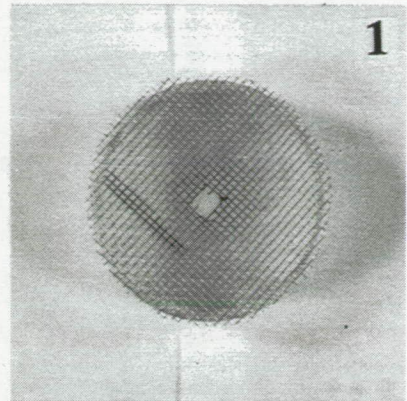


F # 3422

**Experiment: 3423**

Projectile: SL  
D<sub>p</sub> = 3.175 mm  
V = 1.95 km/s

Target:  
M = 1.590 mm  
T = 0.254 mm  
N = 10  
S = 50.8 mm  
SM = 0.180 g/cm<sup>2</sup>





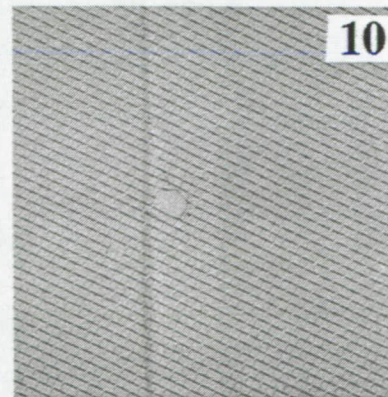
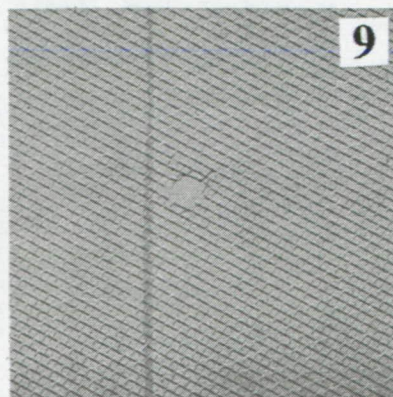
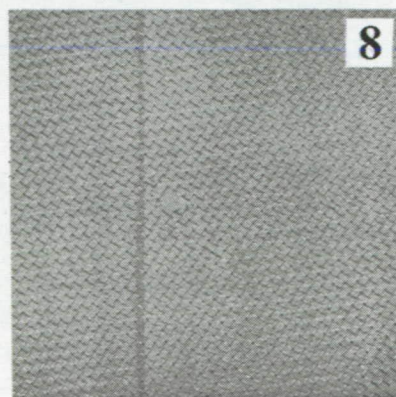
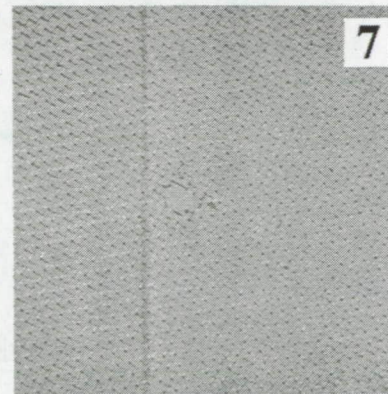
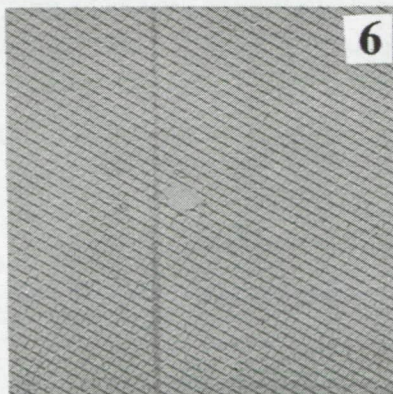
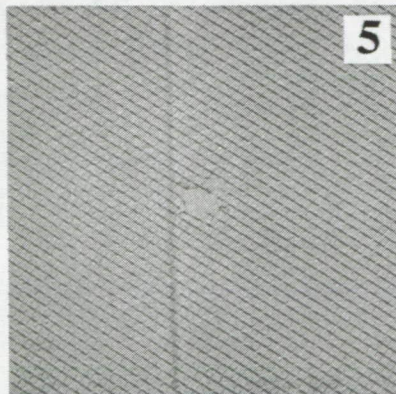
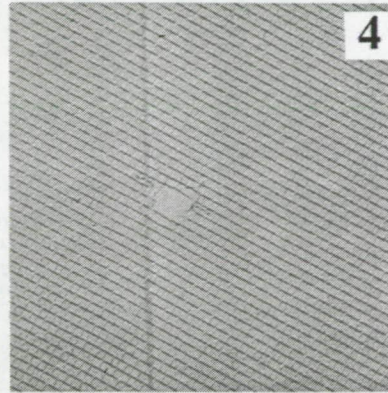
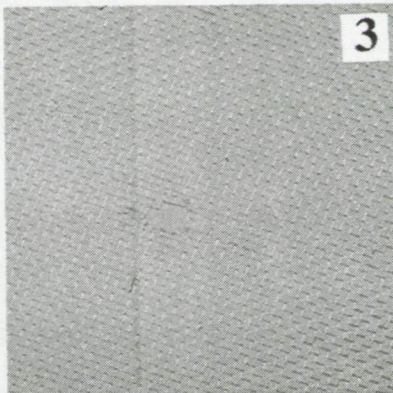
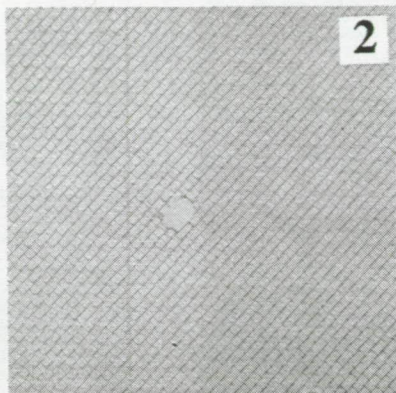
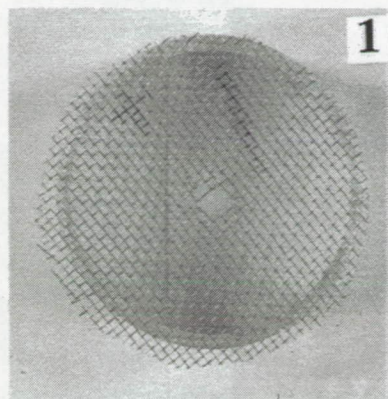
F 3423

3423

**Experiment: 3424**

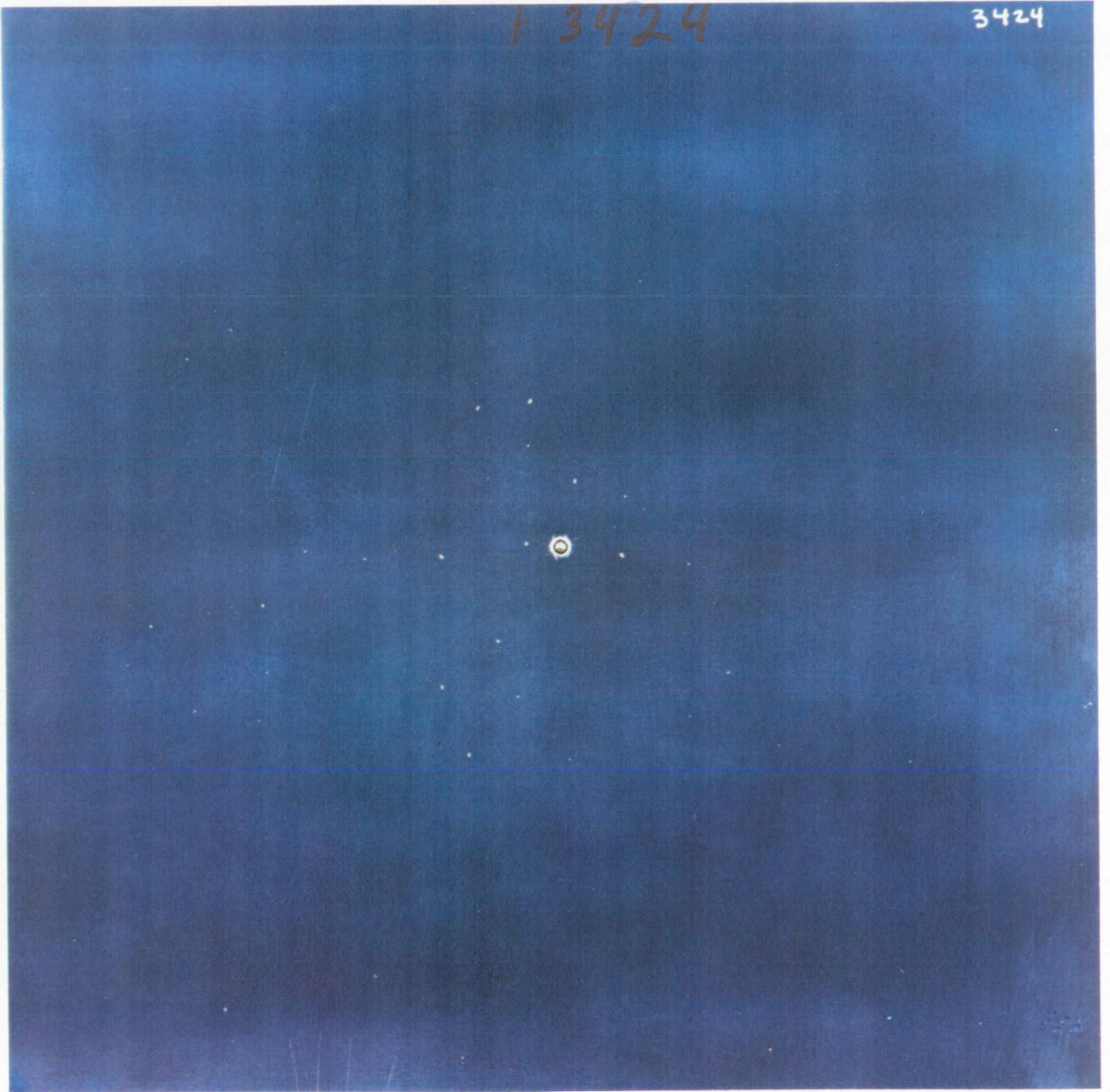
Projectile: Al  
D<sub>p</sub> = 3.175 mm  
V = 0.99 km/s

Target:  
M = 1.590 mm  
T = 0.254 mm  
N = 10  
S = 50.8 mm  
SM = 0.180 g/cm<sup>2</sup>



F 3424

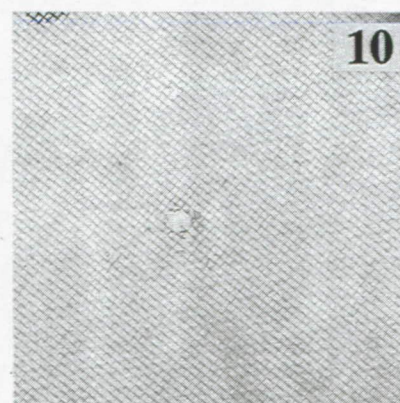
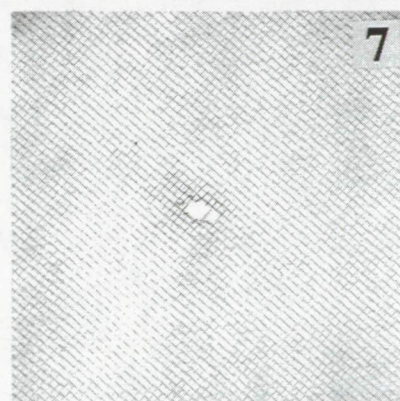
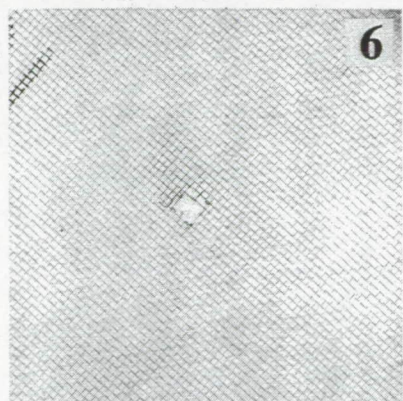
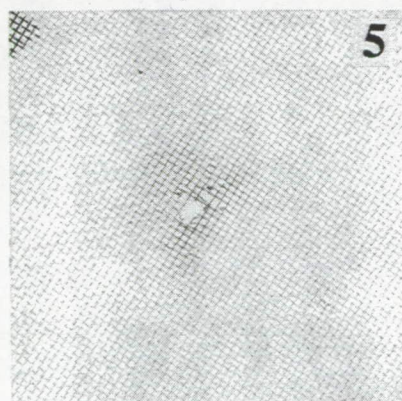
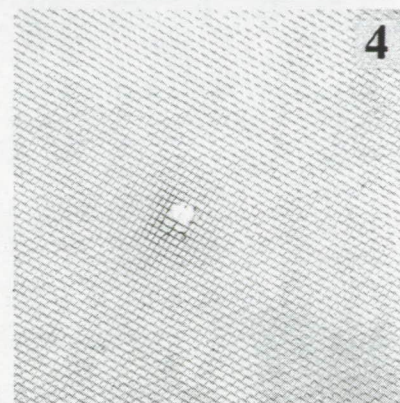
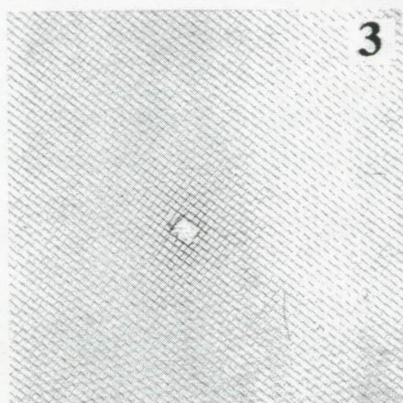
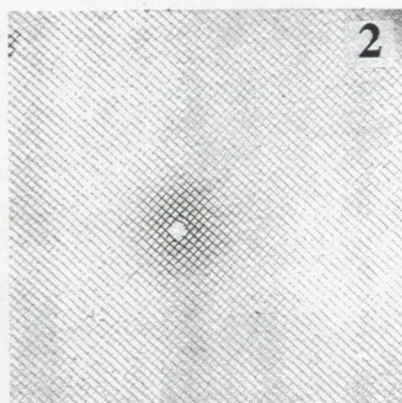
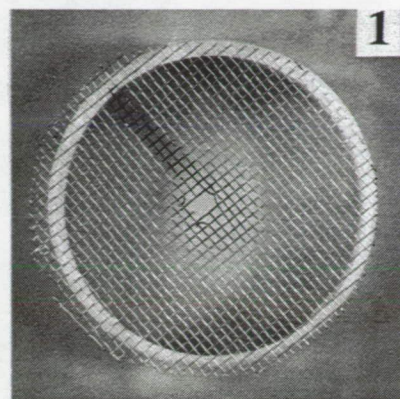
3424



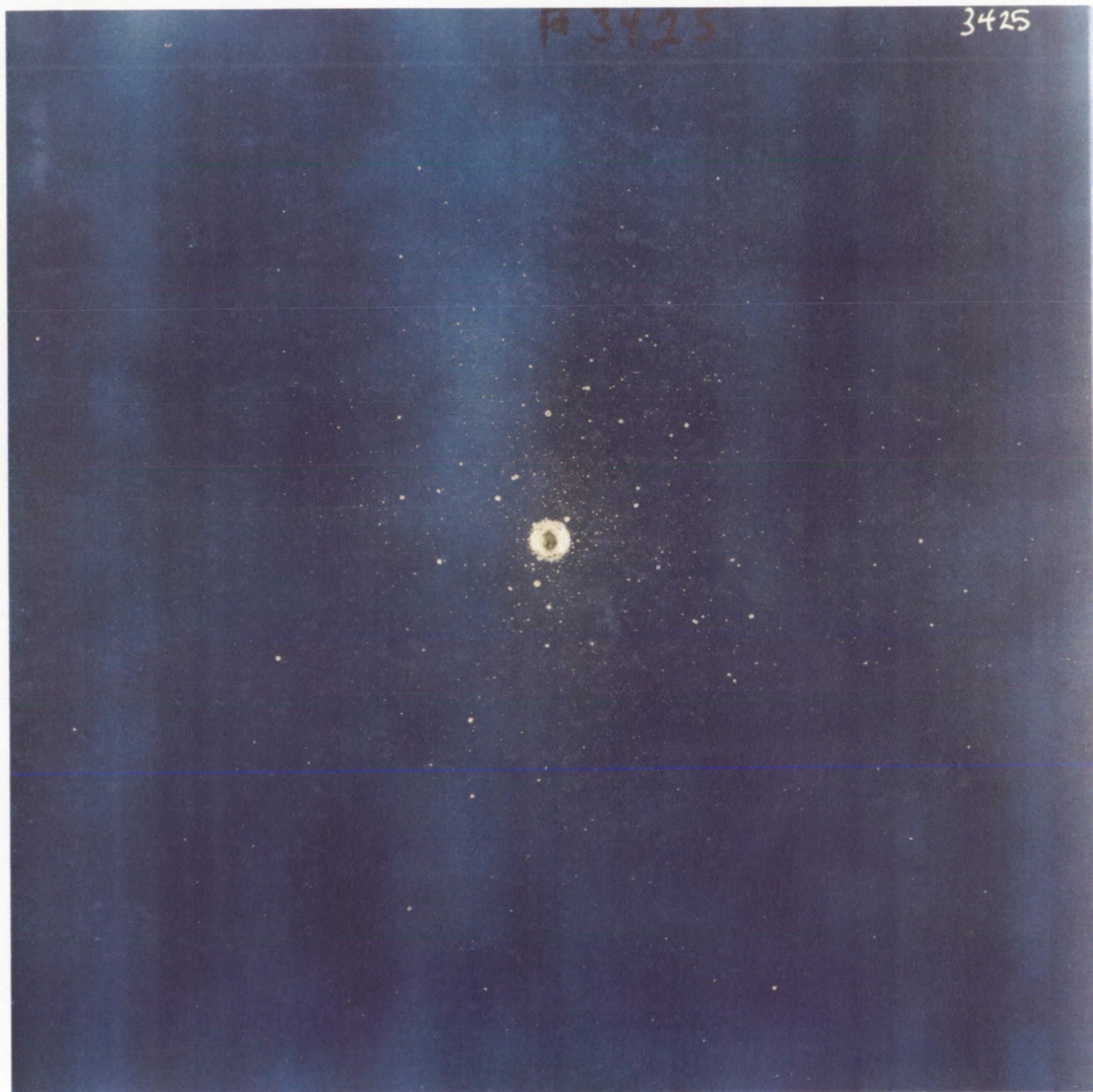
# Experiment: 3425

Projectile: Al  
 $D_p = 3.175 \text{ mm}$   
 $V = 1.95 \text{ km/s}$

Target:  
 $M = 1.590 \text{ mm}$   
 $T = 0.254 \text{ mm}$   
 $N = 10$   
 $S = 50.8 \text{ mm}$   
 $SM = 0.180 \text{ g/cm}^2$



ORIGINAL PAGE  
BLACK AND WHITE PHOTOGRAPH



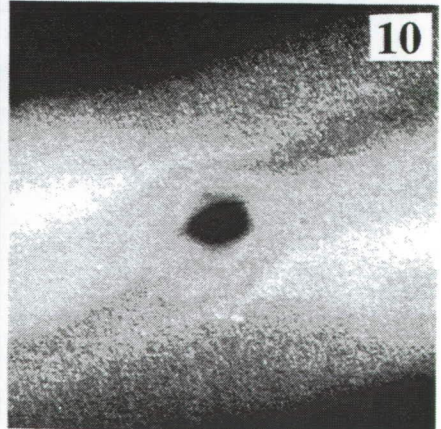
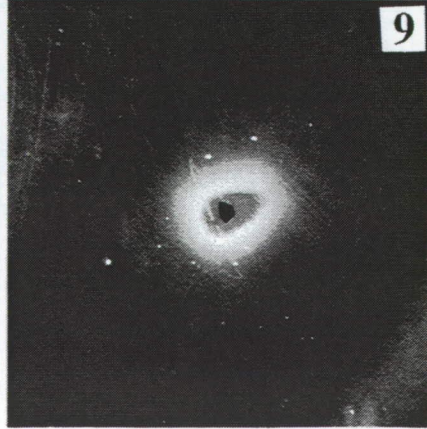
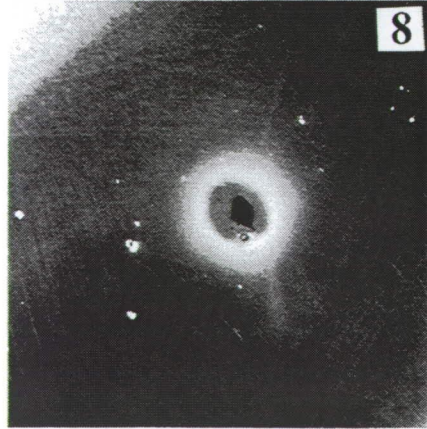
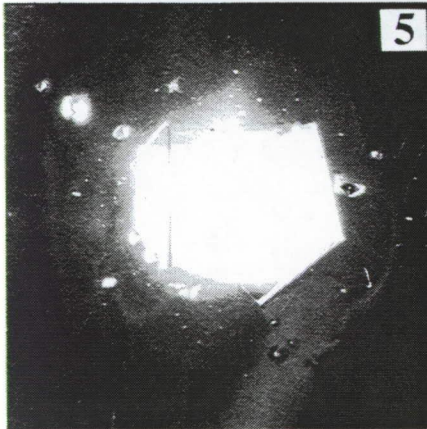
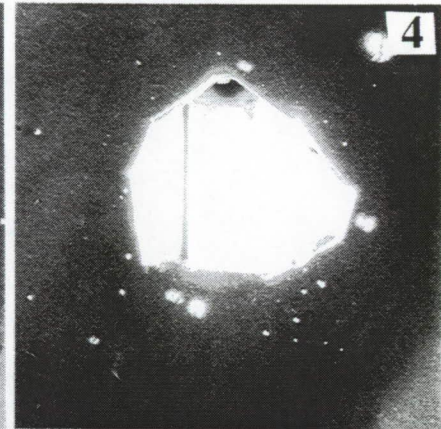
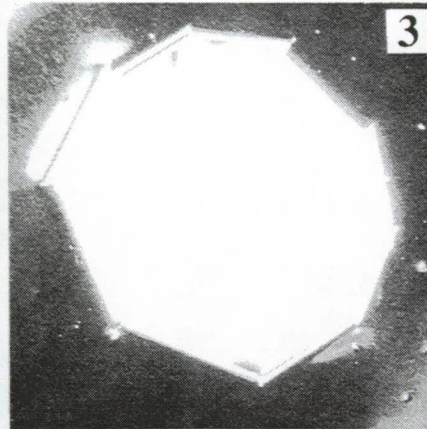
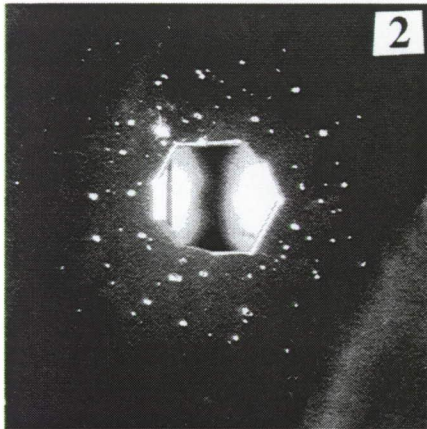
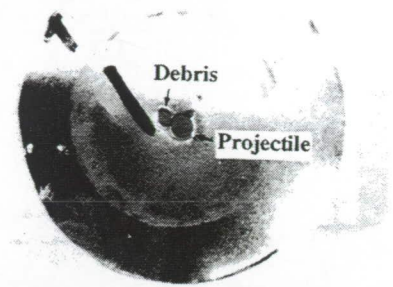


Experiment: 3426

Projectile: SL  
D<sub>p</sub> = 3.175 mm  
V = 2.00 km/s

Target: Foilstack  
T = .0762 mm  
N = 10  
S = 50.8 mm  
SM = 0.200 g/cm<sup>2</sup>

2 cm



F

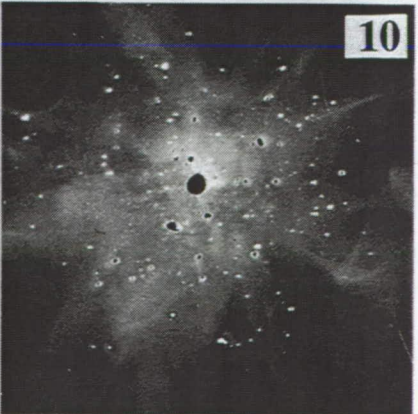
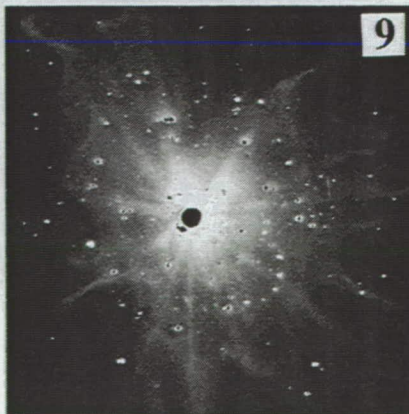
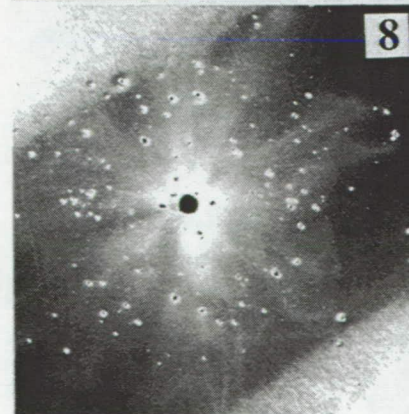
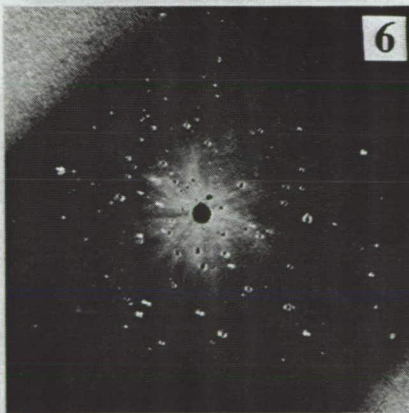
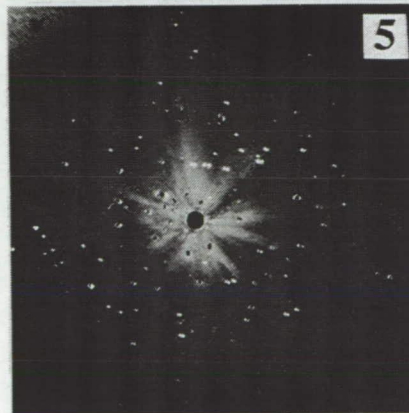
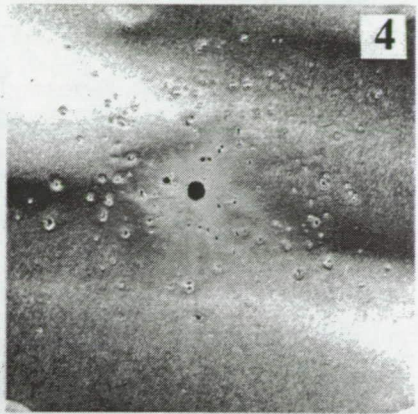
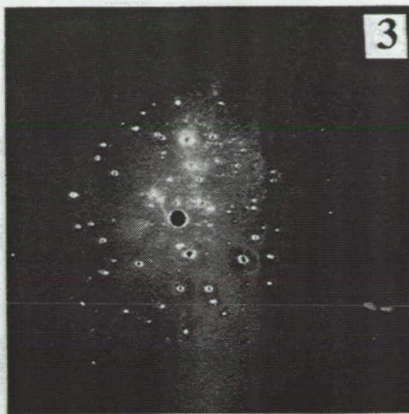
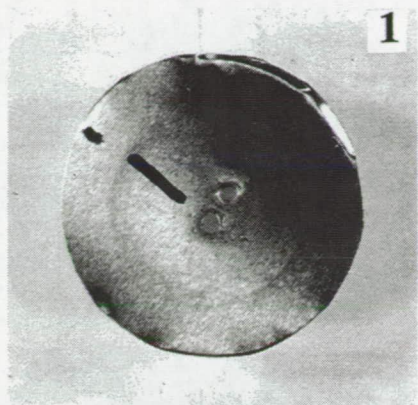


**Experiment: 3427**

Projectile: Al  
D<sub>p</sub> = 3.175 mm  
V = 1.97 km/s

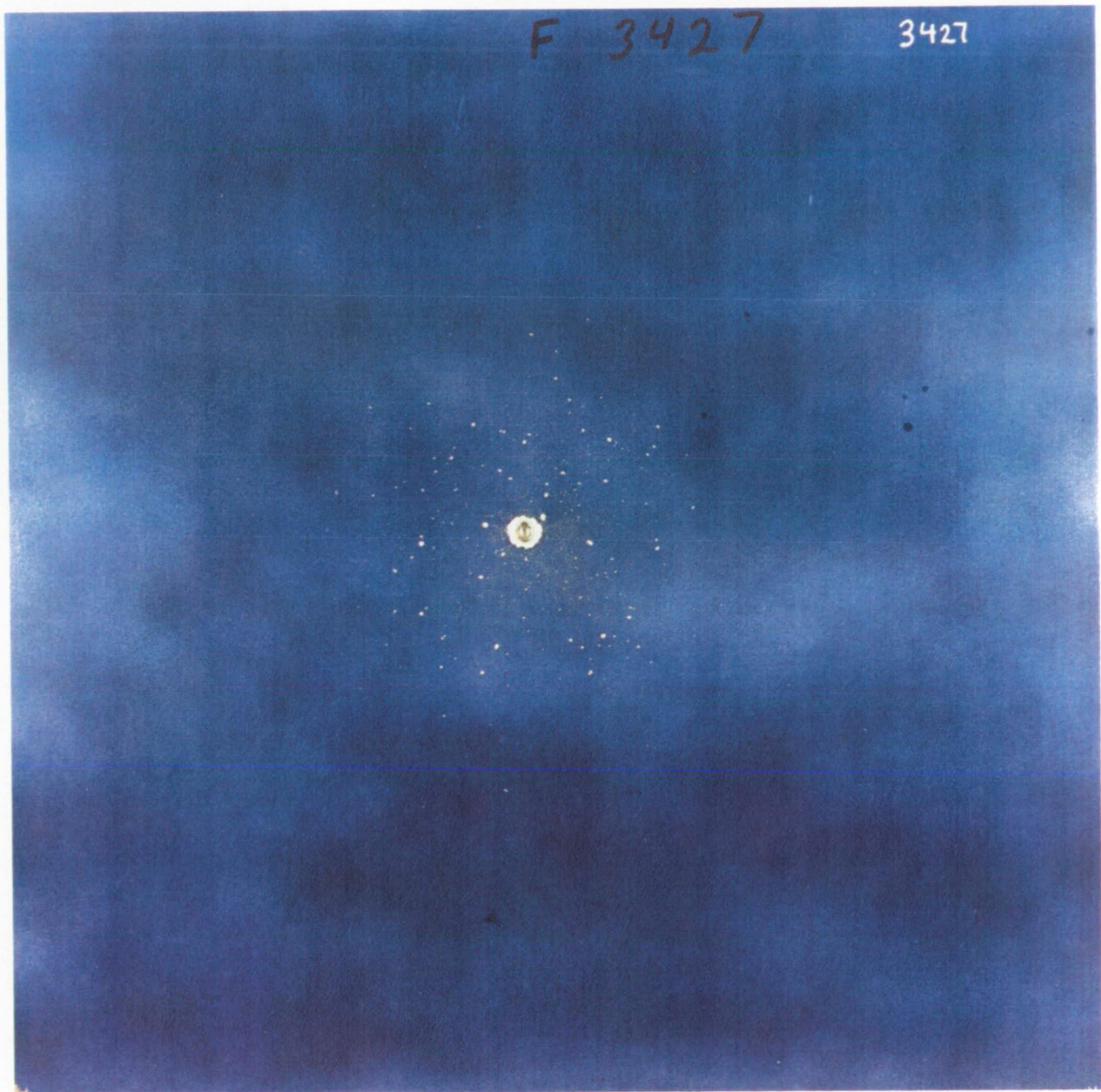
Target: Foilstack  
T = .0762 mm  
N = 10  
S = 50.8 mm  
SM = 0.200 g/cm<sup>2</sup>

2 cm



ORIGINAL PAGE  
BLACK AND WHITE PHOTOGRAPH

3427

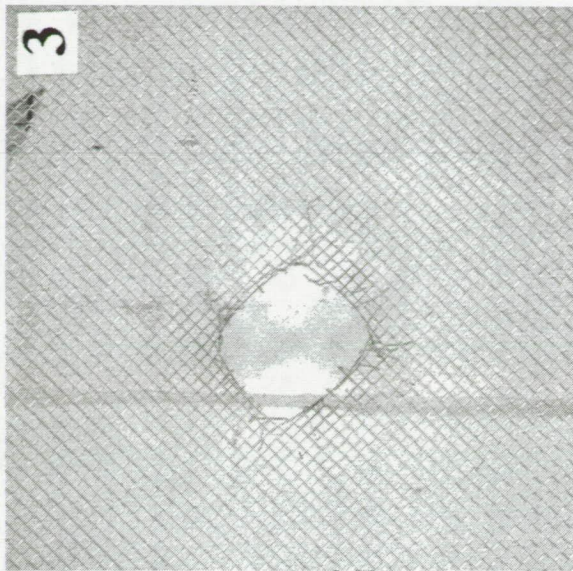
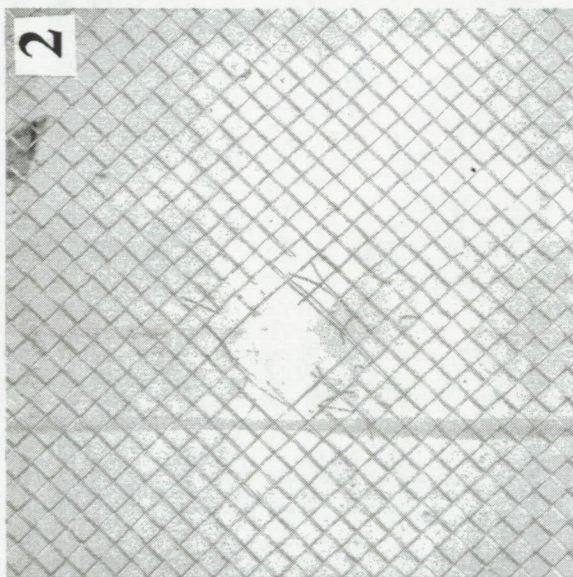
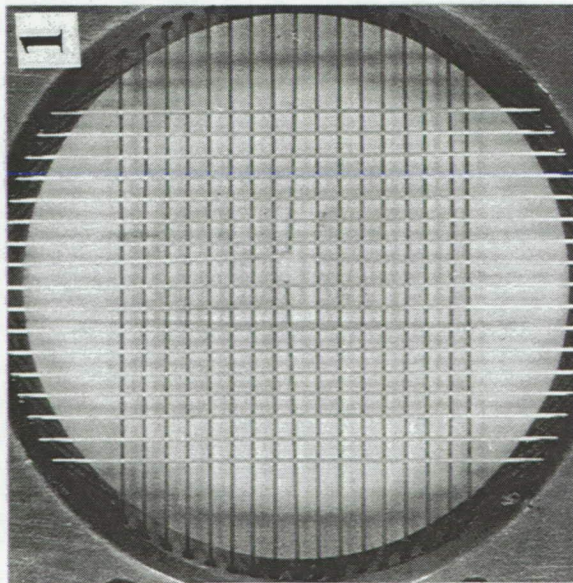


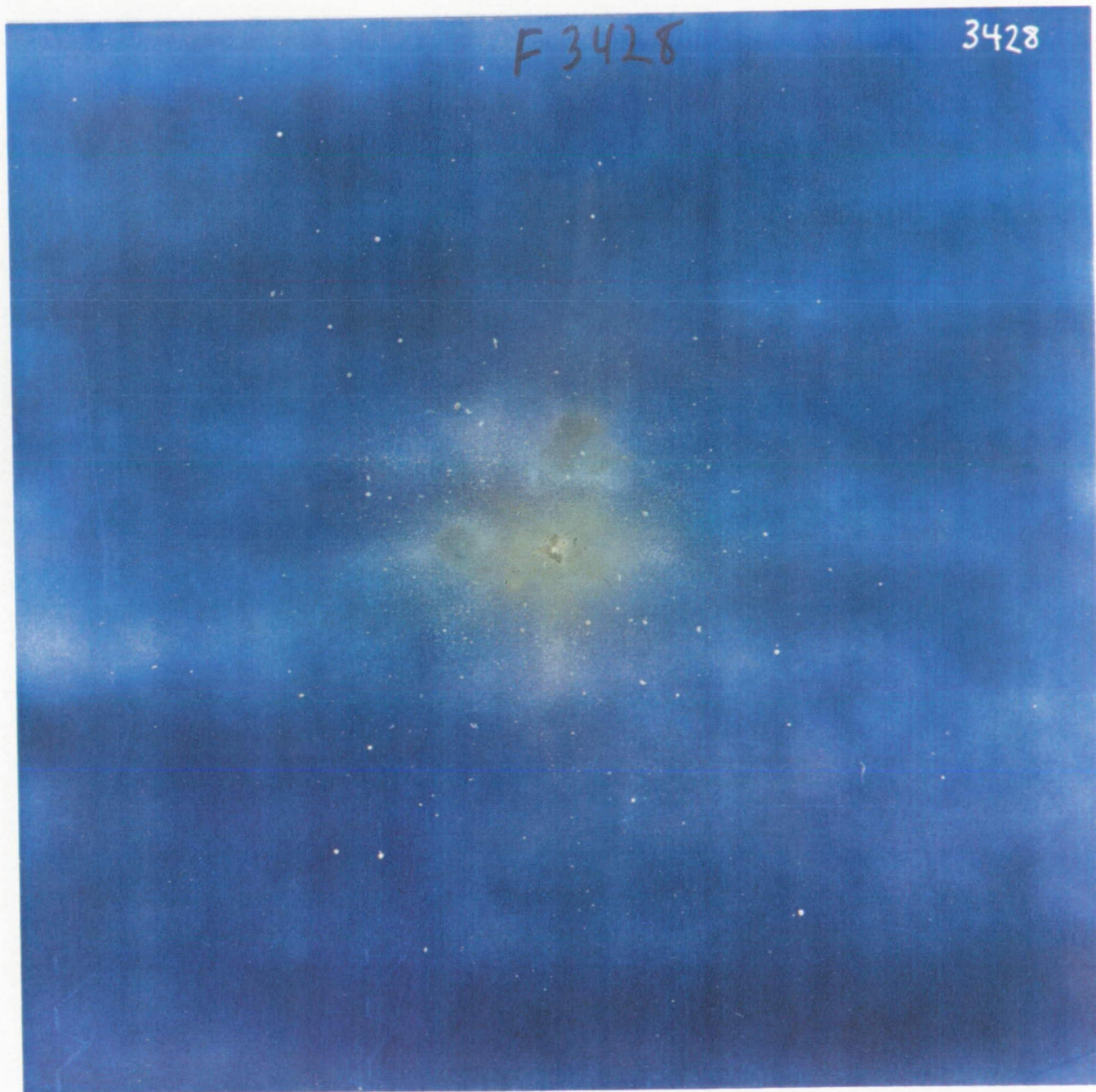
# Experiment: 3428

Projectile: SL  
Dp = 3.175 mm  
V = 1.94 km/s

Target: Mixed Meshes  
M = Variable  
T = Variable  
N = 3  
S = 25.4 mm  
SM = 0.080 g/cm<sup>2</sup>

SM  
1 ————— 0.046  
2 ————— 0.016  
3 ————— 0.018



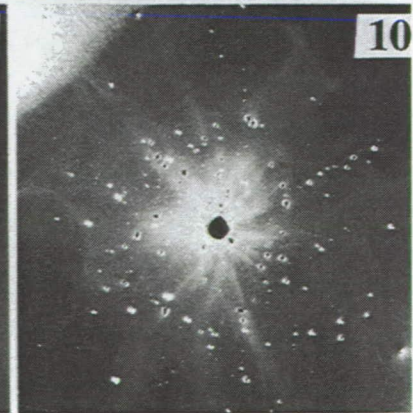
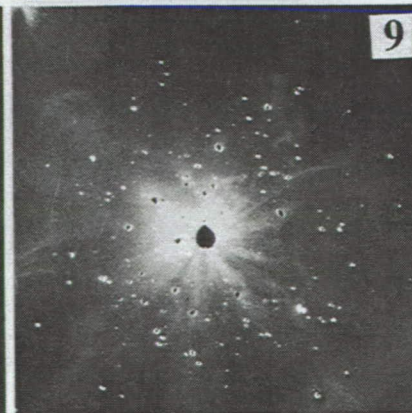
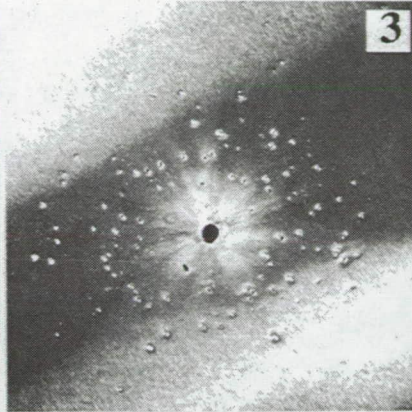
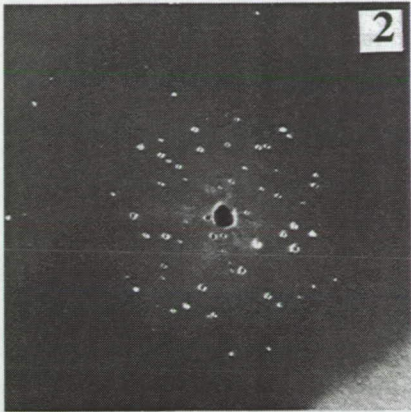
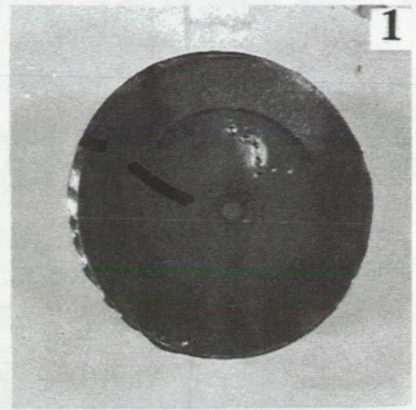


**Experiment: 3429**

Projectile: Al  
 $D_p = 3.175 \text{ mm}$   
 $V = 1.99 \text{ km/s}$

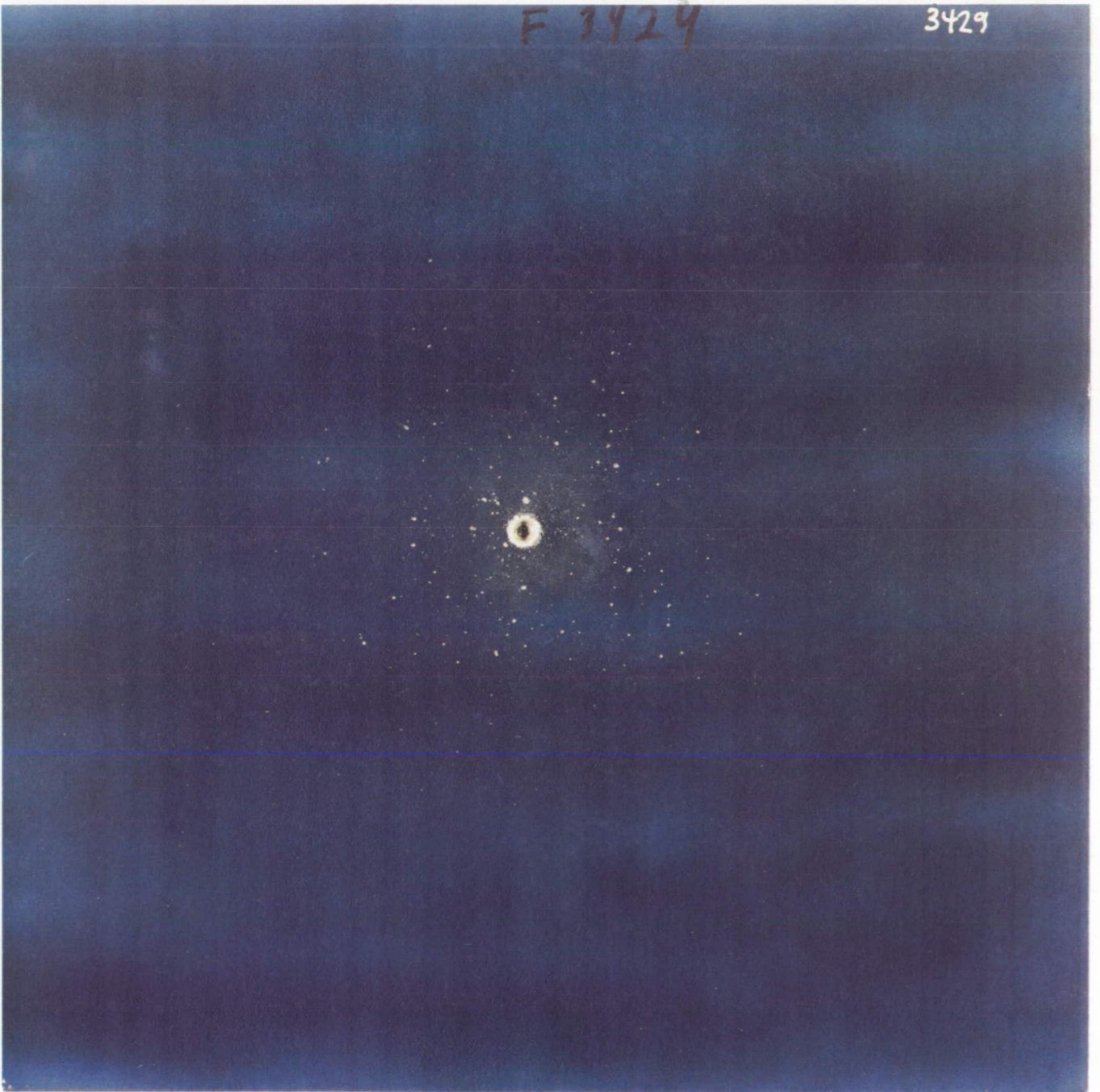
Target: Foilstack  
 $T = .0762 \text{ mm}$   
 $N = 10$   
 $S = 50.8 \text{ mm}$   
 $SM = 0.200 \text{ g/cm}^2$

2 cm



F 3424

3429

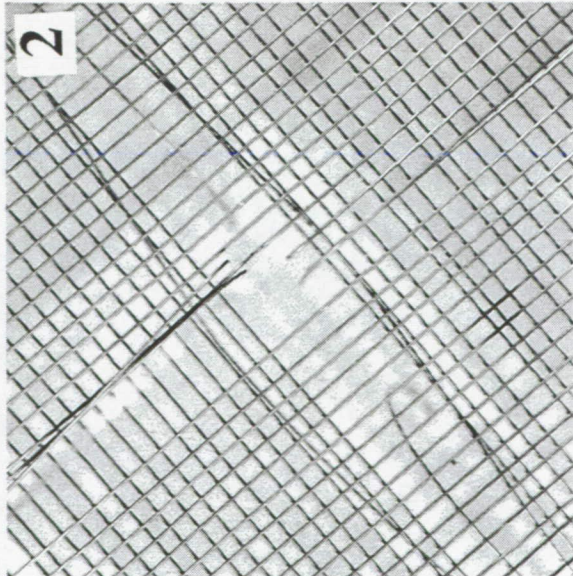
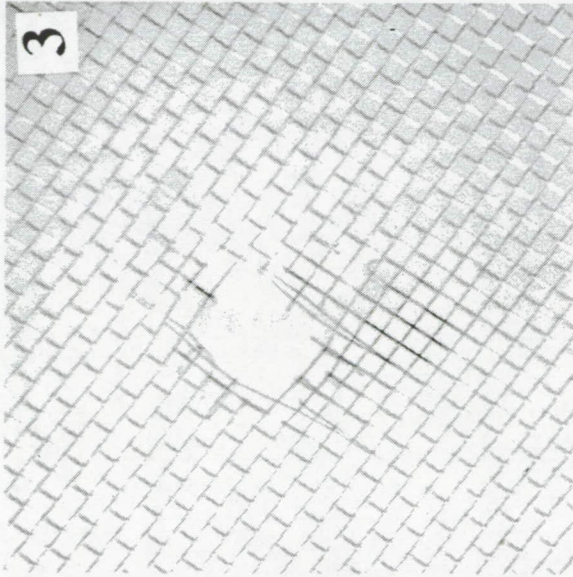
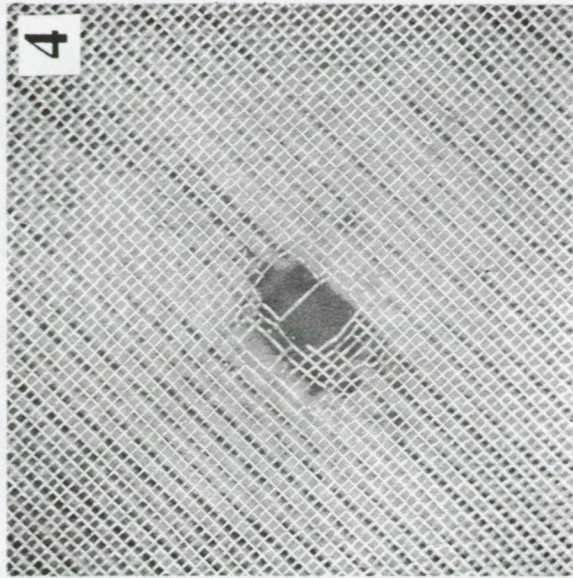
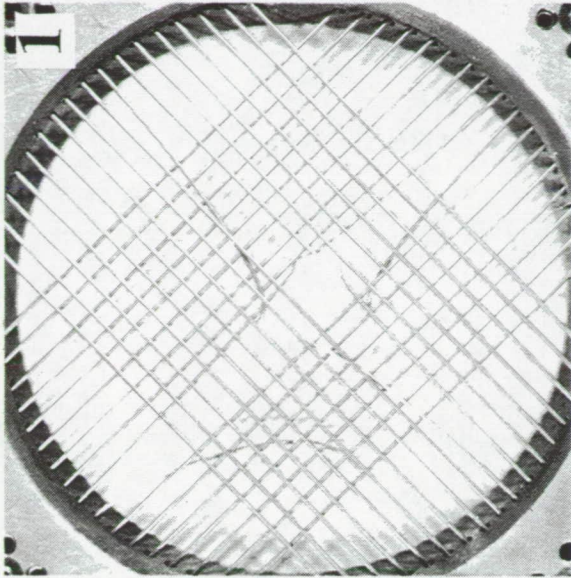


# Experiment: 3431

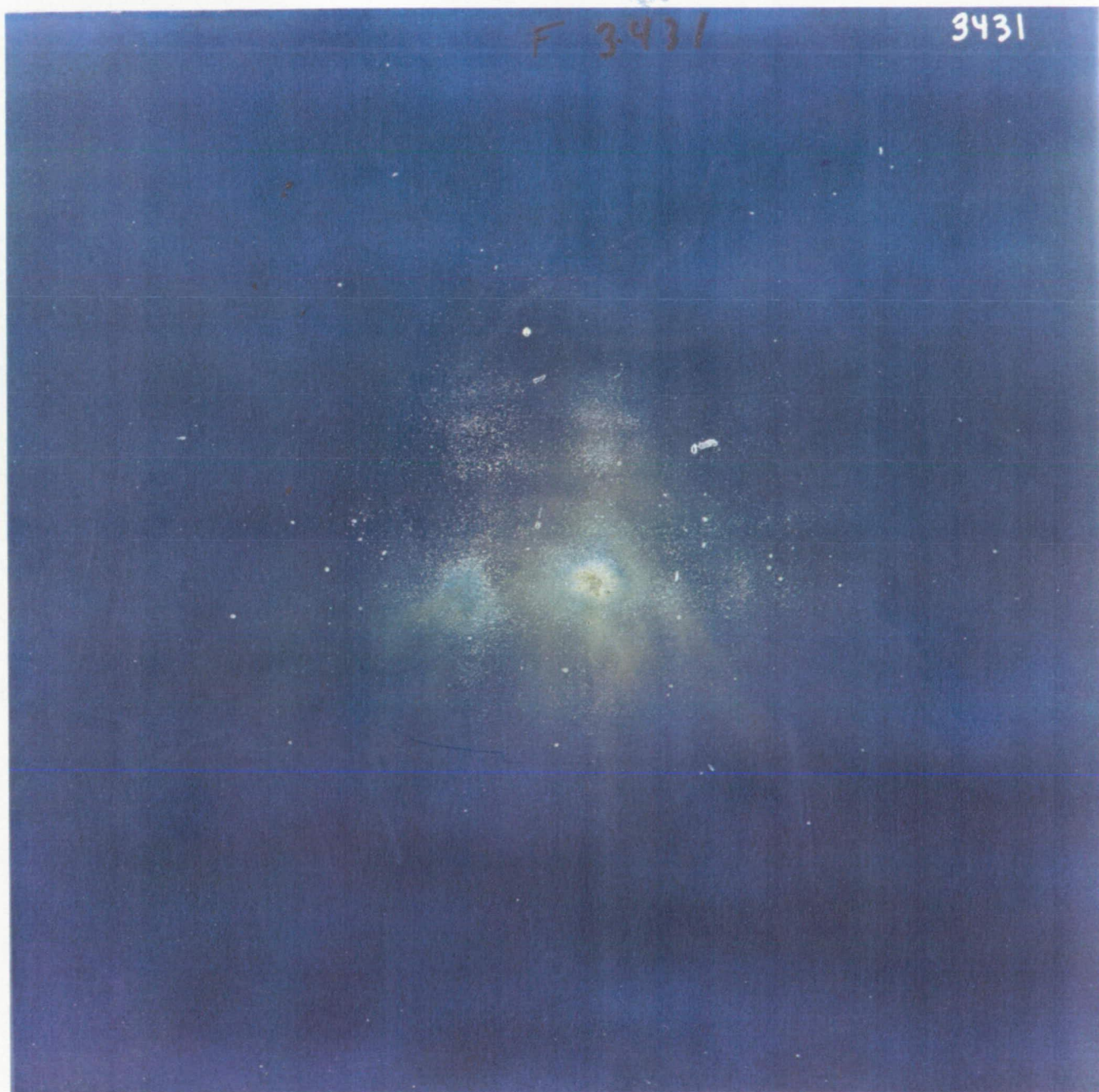
Projectile: SL = 3.175 mm  
 Dp = 1.95 km/s  
 V =

Target: Mixed Meshes  
 M = Variable  
 T = Variable  
 N = 4  
 S = 25.4 mm  
 SM = 0.158 g/cm<sup>2</sup>

	SM
1	_____ 0.078
2	_____ 0.046
3	_____ 0.016
4	_____ 0.018



3431



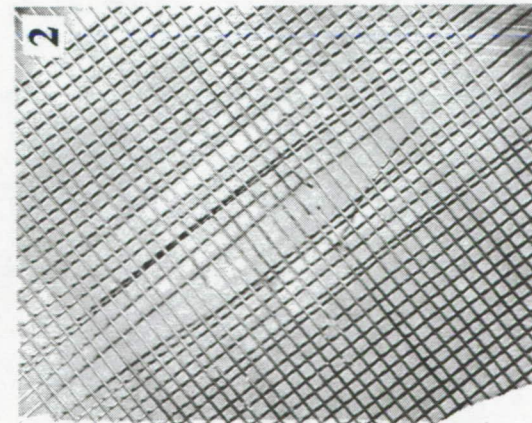
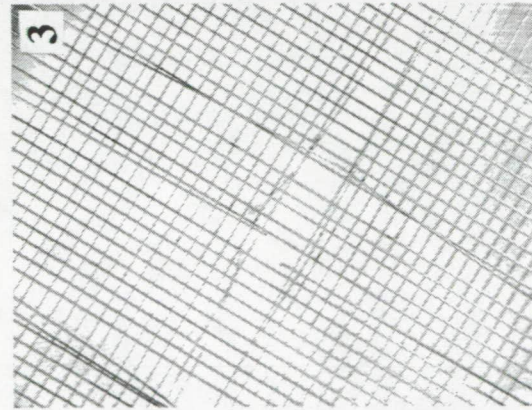
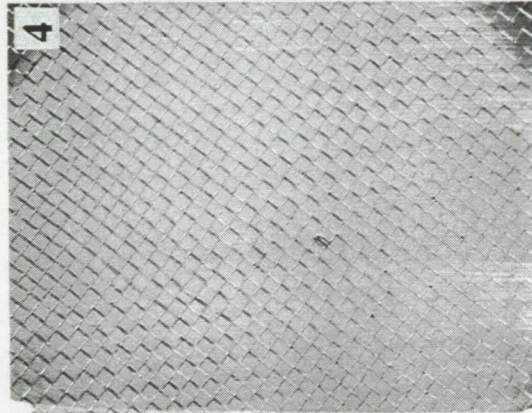
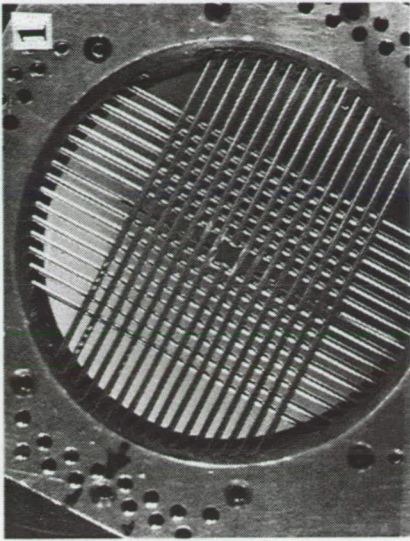


**Experiment: 3432**

Projectile: SL = 3.175 mm  
 Dp = 2.00 km/s  
 V =

Target: Mixed Meshes  
 M = Variable  
 T = Variable  
 N = 5  
 S = 25.4 mm  
 SM = 0.495 g/cm<sup>2</sup>

	SM
1	0.338
2	0.078
3	0.046
4	0.016
5	0.018



F 3432

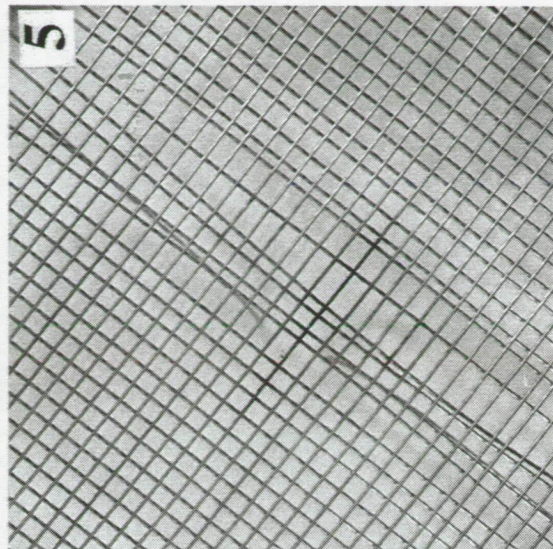
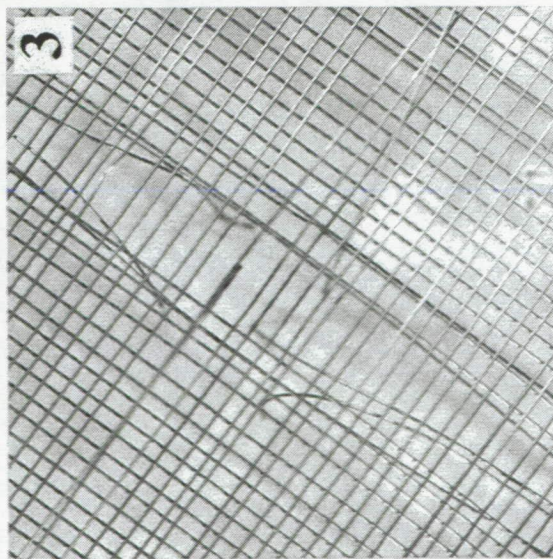
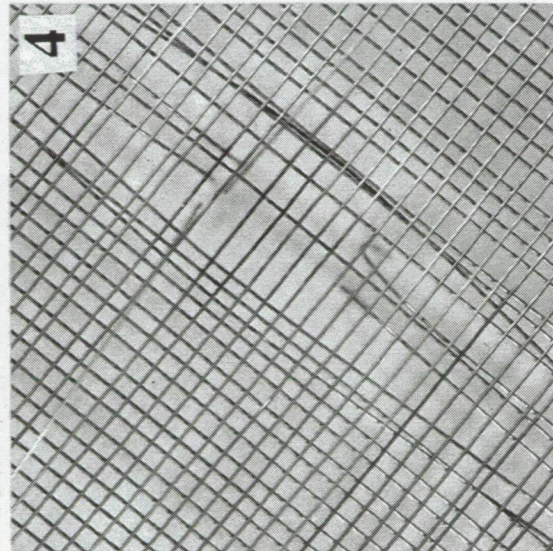
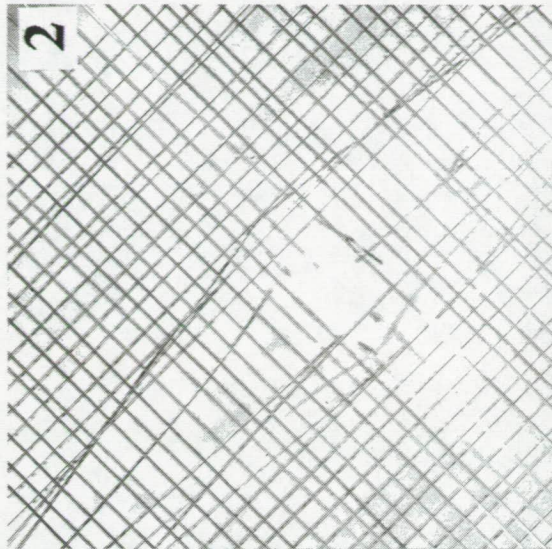
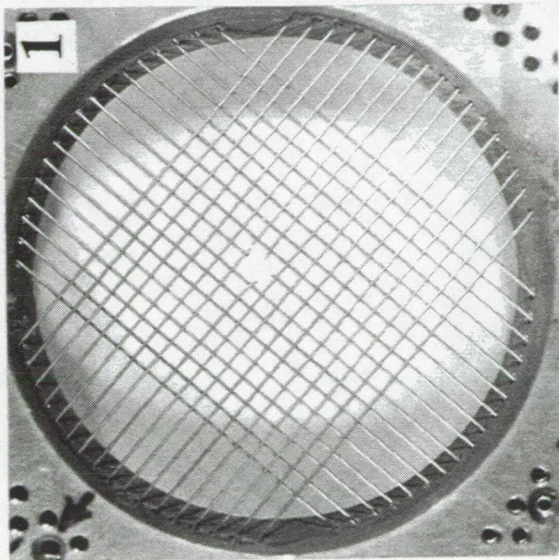
3432



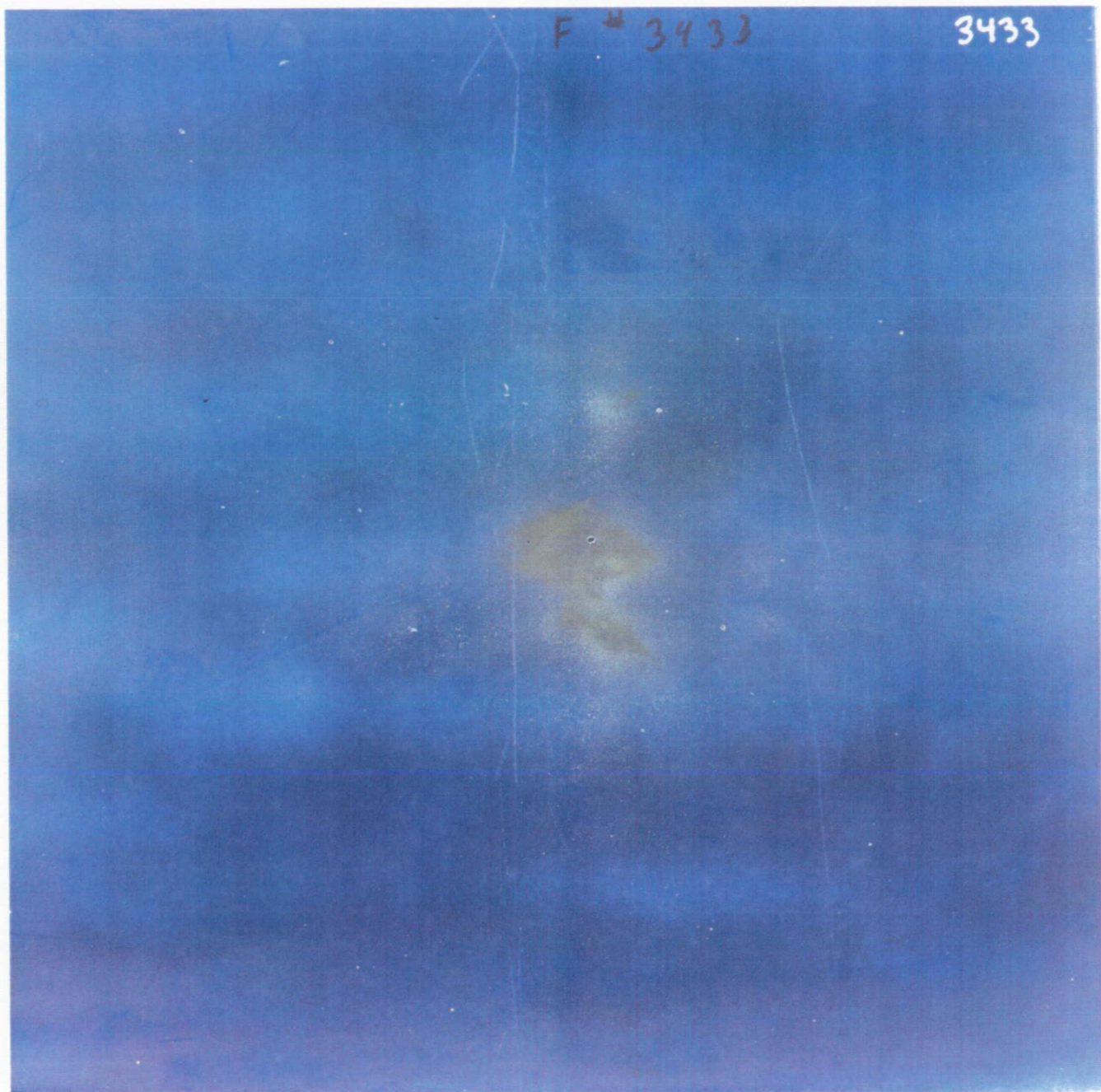
**Experiment: 3433**

Projectile: SL  
Dp = 3.175 mm  
V = 1.98 km/s

Target: M = 3.175 mm  
T = 0.584 mm  
N = 5  
S = 25.4 mm  
SM = 0.230 g/cm<sup>2</sup>



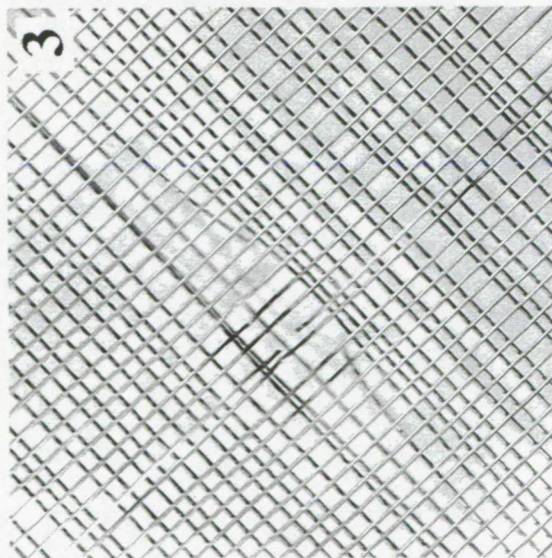
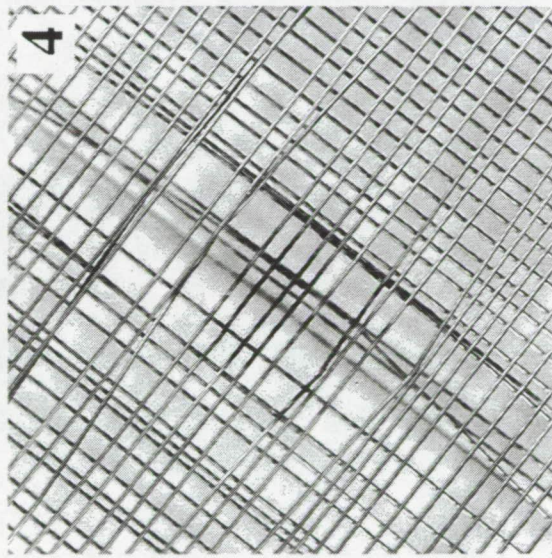
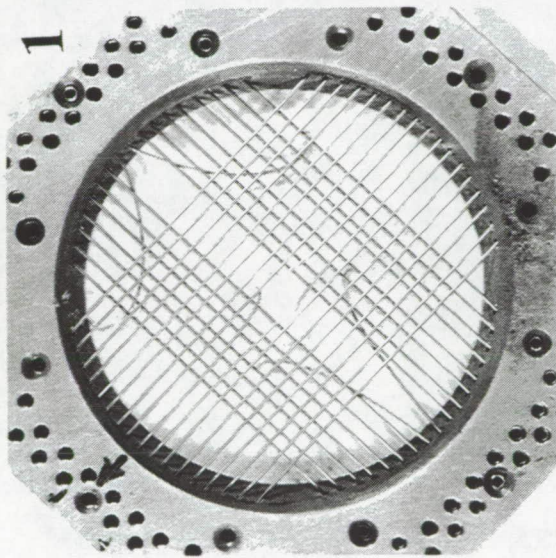
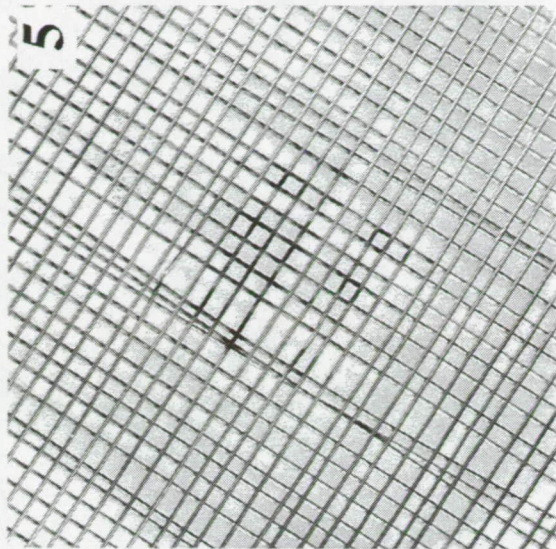
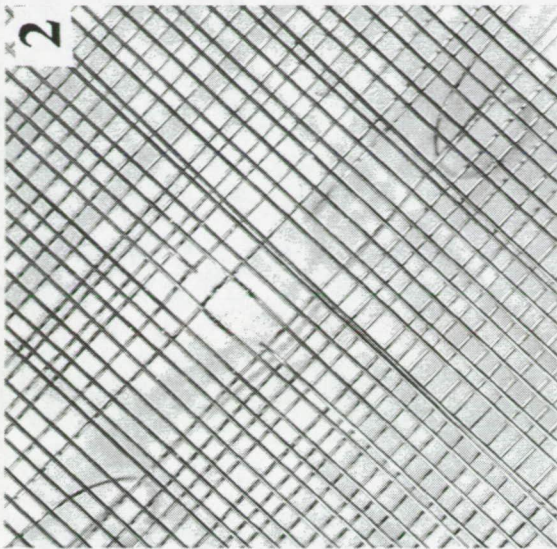
3433

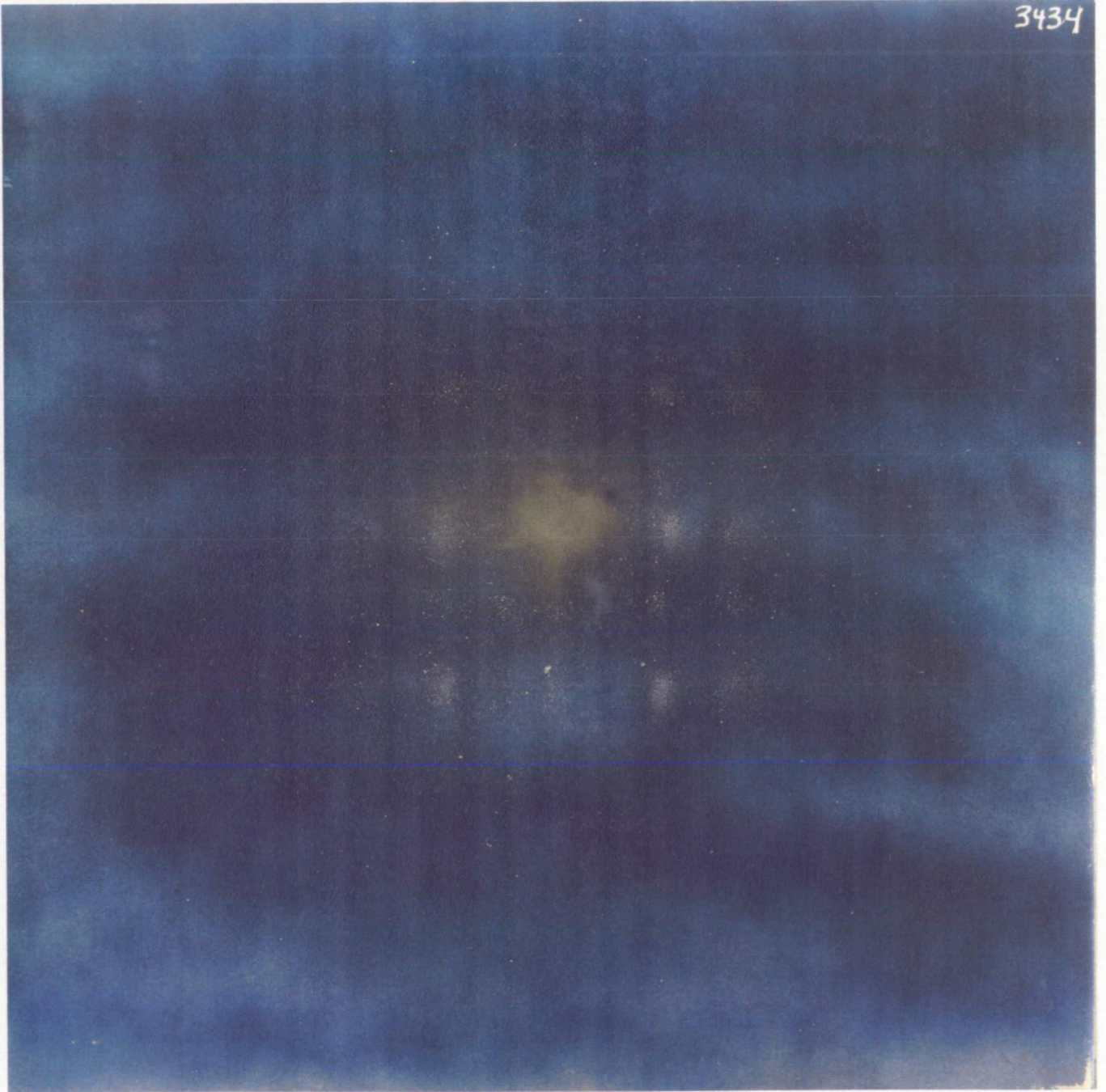


**Experiment: 3434**

Projectile: SL = 3.175 mm  
Dp = 2.00 km/s  
V =

Target: M = 3.175 mm  
T = 0.762 mm  
N = 5  
S = 25.4 mm  
SM = 0.388 g/cm<sup>2</sup>

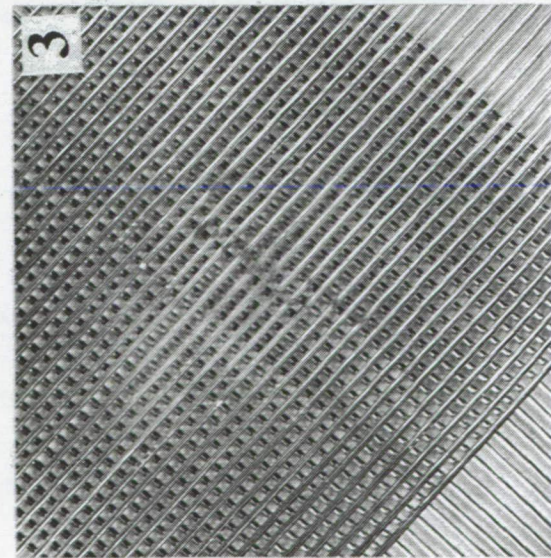
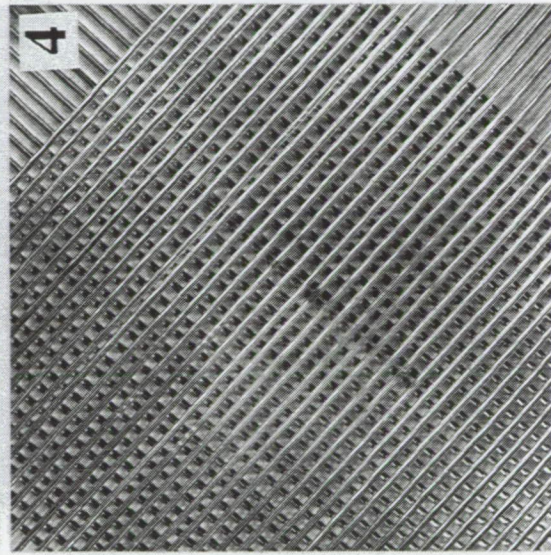
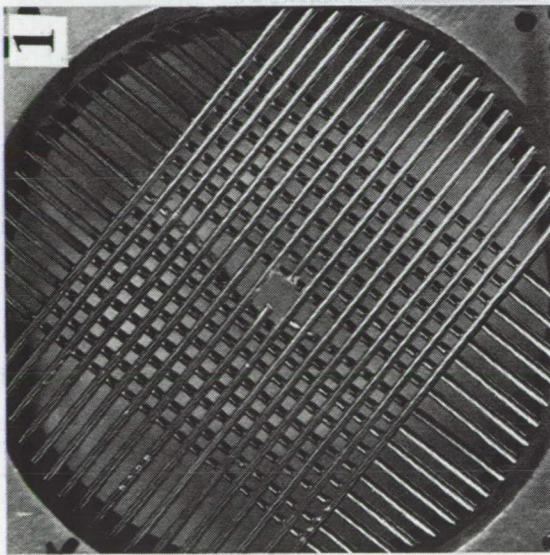
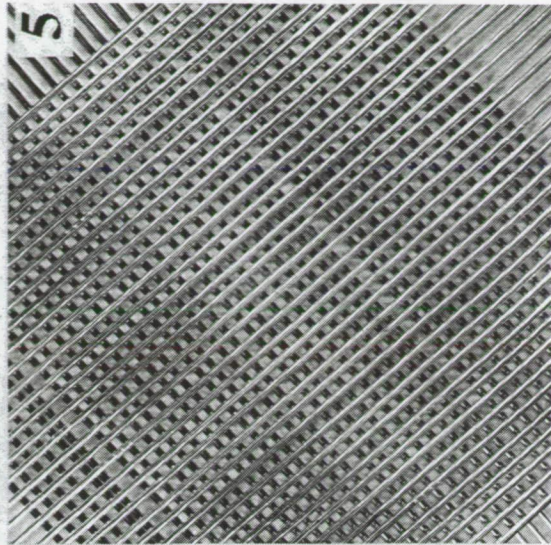
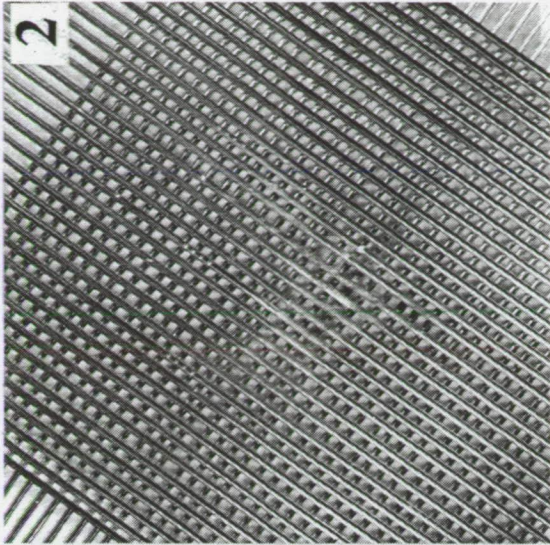


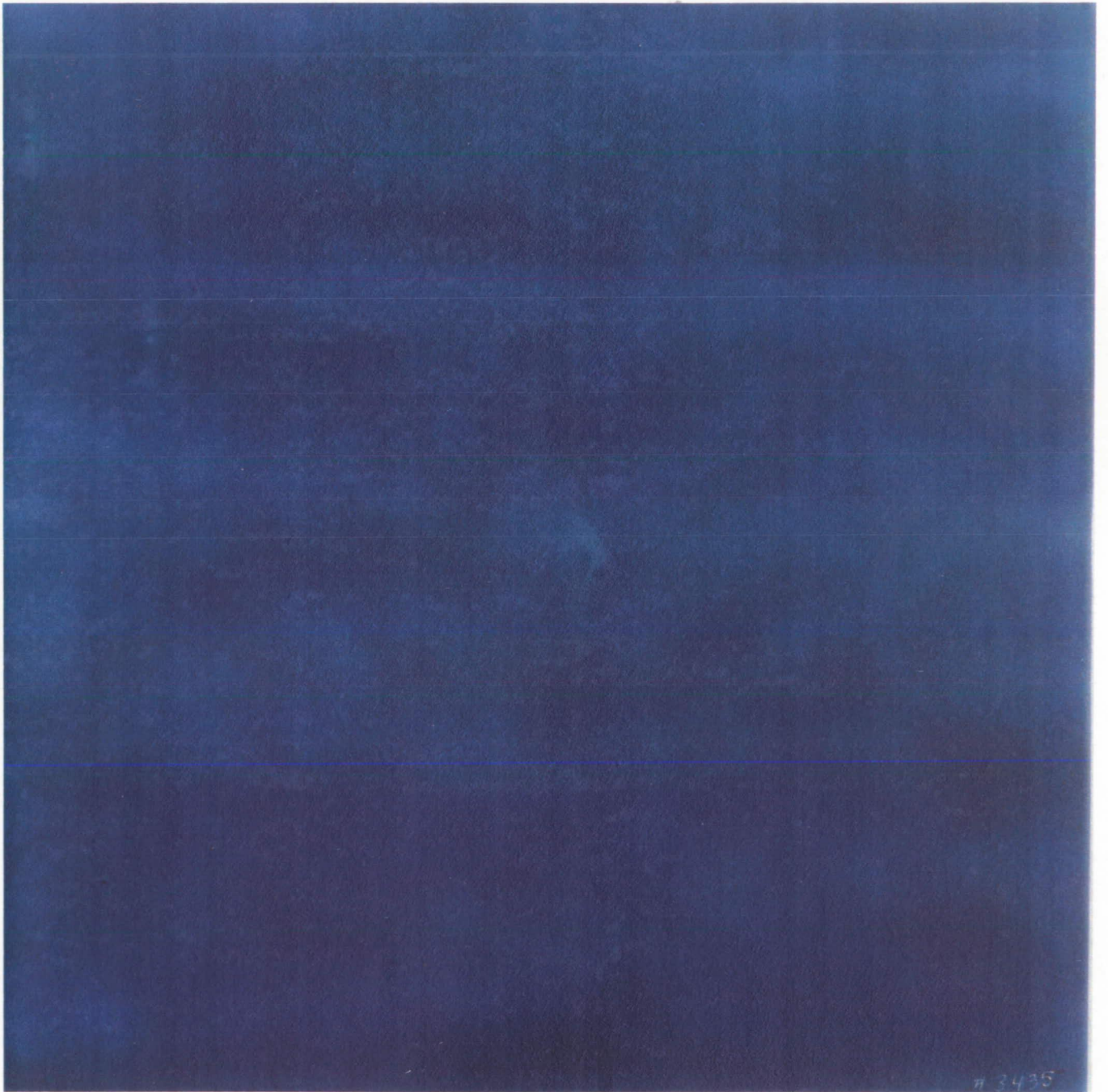


**Experiment: 3435**

Projectile: SL  
Dp = 3.175 mm  
V = 1.91 km/s

Target: M = 3.175 mm  
T = 1.590 mm  
N = 5  
S = 25.4 mm  
SM = 1.688 g/cm<sup>2</sup>







# REPORT DOCUMENTATION PAGE

Form Approved  
OMB No. 0704-0188

The reporting burden for this collection of information is estimated to average 1 hour per response, including the time for reviewing instructions, searching existing data sources, gathering and maintaining the data needed, and completing and reviewing the collection of information. Send comments regarding this burden estimate or any other aspect of this collection of information, including suggestions for reducing this burden, to Washington Headquarters Services, Directorate for Information Operations and Reports, 1215 Jefferson Davis Highway, Suite 1204, Arlington, VA 22202-4302, and to the Office of Management and Budget, Paperwork Reduction Project (0704-0188), Washington, DC 20503.

1. AGENCY USE ONLY (Leave blank)	2. REPORT DATE March 1993	3. REPORT TYPE AND DATES COVERED Technical Memorandum	
4. TITLE AND SUBTITLE Impact Experiments into Multiple-Mesh Targets: Concept Development of a Lightweight Collisional Bumper		5. FUNDING NUMBERS	
6. AUTHOR(S) Friedrich Horz*, Mark J. Cintala*, Ronald P. Bernhard**, Frank Cardenas**, William Davidson**, Gerald Haynes**, Thomas H. See**, Jerry Winkler**, Barry Gray***		8. PERFORMING ORGANIZATION REPORT NUMBER S-714	
7. PERFORMING ORGANIZATION NAME(S) AND ADDRESS(ES) Solar System Exploration Division NASA Johnson Space Center Houston, Texas 77058		10. SPONSORING / MONITORING AGENCY REPORT NUMBER NASA TM-104764	
9. SPONSORING / MONITORING AGENCY NAME(S) AND ADDRESS(ES) National Aeronautics and Space Administration Washington, D.C. 20546-001		11. SUPPLEMENTARY NOTES *NASA; **Lockheed Engineering and Sciences Company, Houston, Texas; ***Physics Dept., Clear Lake High School, Houston, Texas.	
12a. DISTRIBUTION / AVAILABILITY STATEMENT Unclassified/unlimited Subject Category 39		12b. DISTRIBUTION CODE	
13. ABSTRACT (Maximum 200 words) This study explores the utility of multiple-mesh targets as potential lightweight shields to protect spacecraft in low-Earth orbit against collisional damage. Earlier studies revealed that single meshes comminute hypervelocity impactors with efficiencies comparable to contiguous targets. Multiple interaction of projectile fragments with any number of meshes should lead to increased comminution, deceleration and dispersion of the projectile, such that all debris exiting the mesh stack possesses low specific energies (ergs/cm <sup>2</sup> ) that would be readily tolerated by many flight systems. The study is conceptual exploring the sensitivity of major variables such as impact velocity, the specific areal mass (g/cm <sup>2</sup> ) of the total mesh stack (SM), and the separation distance (S) between individual meshes. Most experiments employed five or ten meshes with total SM typically <0.5 the specific mass of the impactor, and silicate glass impactors rather than metal projectiles. While projectile comminution increases with increasing impact velocity due to progressively higher shock stresses, encounters with multiple-meshes at low velocity (1-2 km/s) already lead to significant disruption of the glass impactors, with the resulting fragments being additionally decelerated and dispersed by subsequent meshes, and unlike most contiguous single-plate bumpers, leading to respectable performance at low velocity.			
14. SUBJECT TERMS Impactors; impact tolerances; impact damage; impact tests; materials tests; impact loads impingement; penetration; shielding; attenuation; attenuators; spacecraft shielding; terminal ballistics; bumpers; protectors; space debris; mesh		15. NUMBER OF PAGES 225	16. PRICE CODE
17. SECURITY CLASSIFICATION OF REPORT unclassified	18. SECURITY CLASSIFICATION OF THIS PAGE unclassified	19. SECURITY CLASSIFICATION OF ABSTRACT unclassified	20. LIMITATION OF ABSTRACT UL